Nonlinear effects compensation for long-haul superchannel transmission system

Abdelkerim Amari

ParisTech
INSTITUT DES SCIENCES ET TECHNOLOGIES
PARIS INSTITUTE OF TECHNOLOGY

TELECOM ParisTech

2016-ENST-0031

EDITE - ED 130

Doctorat ParisTech

T H È S E

pour obtenir le grade de docteur délivré par

TELECOM ParisTech

Spécialité « Communications et Electronique »

présentée et soutenue publiquement par

Abdelkerim AMARI

le 07 juin 2016

Nonlinear effects compensation for long-haul superchannel transmission system

Directeur de thèse : **Yves JAOUEN et Philippe CIBLAT**

Jury

M. Stephan WABNITZ, Professeur, University of Brescia	Rapporteur
M. Charly POULLIAT, Professeur, INP - ENSEEIHT Toulouse	Rapporteur
M. Philippe GRAVEY, Directeur d'Études, Télécom Bretagne	Examinateur
M. Yann FRIGNAC, Maître de Conférences, Télécom SudParis	Examinateur
M. Erwan PINCEMIN, Ingénieur de Recherche,Orange Labs	Examinateur
M. Yves JAOUEN, Professeur, Télécom ParisTech	Directeur de thèse
M. Philippe CIBLAT, Professeur, Télécom ParisTech	Directeur de thèse

TELECOM ParisTech
école de l'Institut Mines-Télécom - membre de ParisTech
46 rue Barrault 75013 Paris - (+33) 1 45 81 77 77 - www.telecom-paristech.fr

T H È S E

Dédicaces

Je dédie ce travail
à mes chers parents
à toute ma famille

Remerciement

Je tiens à exprimer mes vifs remerciements envers tous ceux qui ont contribué au bon déroulement de ma thèse de doctorat.
Je commence par remercier tous les membres de jury pour avoir accepté d'évaluer mon travail de thèse. Je témoigne toute ma gratitude envers mes directeurs de thèse Yves Jaouën et Philippe Ciblat pour leur encadrement, leurs conseils précieux et le grand soutien qu'ils m'ont accordé.
Je remercie aussi tous les chercheurs du département Communications et Électronique de TELECOM ParisTech pour leurs conseils durant les réunions des groupes ainsi que toutes les personnes du service ressources humaines et de l'administration pour leur aide. J'exprime toute ma reconnaissance à tous mes amis thésards et post-doctorants pour leur encouragement et les bons moments vécus avec eux tout au long des années de ma thèse. Mes remerciements s'adressent aussi à toute ma famille pour leur soutien et encouragement.

Abstract

Optical communication systems have evolved since their deployment to meet the growing demand for high-speed communications. Over the past decades, the global demand for communication capacity has increased exponentially and the most of the growth has occurred in the last few years when data started dominating network traffic. In order to meet the increase of traffic demands fueled by the growth of internet services, an increase of access network capacity and consequently metro and long-haul network capacities is required.

Next generation of long-haul WDM transmission systems is expected to operate at 400Gbps or 1Tbps bit rate. Superchannel approaches, such as Nyquist WDM and multi-band OFDM, allow both high spectral efficiency and small guard-band which makes them promising candidates to generate these high bit rates in combination with multi-level modulations formats. Such transmission systems are strongly disturbed by fiber nonlinear effects which increase with the data rate and the small guard band. Therefore, fiber nonlinearities compensation is required to get the desired performance in terms of transmission reach. DSP based approaches such as digital back propagation (DBP) and third-order Volterra based nonlinear equalizer (VNLE) have been already proposed to deal with intra-channel or intra-band nonlinear effects.

In the context of superchannel systems, we have proposed a fifth-order inverse Volterra based nonlinear equalizer to compensate for fiber nonlinearities. The main contributions consist of deriving the corresponding fifth-order kernels and then finding a practical implementation scheme. Compared to the third-order VNLE, our proposed technique has significantly improved the performance in terms of Q factor and/or transmission distance in OFDM based superchannel system.

Multi-band OFDM and multi-subcarrier Nyquist WDM superchannels suffer also from inter-band/subcarrier nonlinear interference in addition to intra-band/subcarrier nonlinear effects. Thus, we have proposed an inter-band/subcarrier nonlinear interference canceler (INIC) to deal with nonlinear interference. This approach consists in detecting the adjacent bands/subcarriers, regenerating them thanks to the Volterra series model of optical fiber, and removing them from the band/subcarrier of interest. Different ways to implement the INIC are described and compared to the well-known nonlinear compensation techniques such as DBP and third-order VNLE in Nyquist WDM and super-nyquist WDM systems. Significant performance gain on either the Q factor or transmission distance is observed. In the context of 400Gbps scheme, the transmission distance gain is up to 500km compared to the DBP and VNLE. Similarly, a significant improvement of performance is observed when applying INIC in Multi-band OFDM superchannel.

Keywords : Optical fiber communications, Superchannel, MB-OFDM, Nyquist WDM, Volterra series, Nonlinear effects, Nonlinear interference, Digital signal processing

Résumé

Les systèmes de communications optiques jouent un rôle important pour satisfaire la demande incessante de trafics de données. Cette demande, induite par des applications gourmandes en termes de bande passante et débit, nécessite une augmentation de la capacité des réseaux optiques d'accès et par conséquent une augmentation des capacités de réseaux de transports métropolitains et longues distances. La prochaine génération de systèmes WDM longue distance devrait opérée à des débits de 400Gbps ou 1Tbps. Cette montée en débit s'appuiera sur des nouvelles formes d'ondes avancées de type mono-porteuse (Nyquist-WDM) ou multi-porteuse (OFDM multi-bande). Ces approches sont basées sur le multiplexage de plusieurs porteuses espacées par des intervalles de garde réduits. D'autre part, pour générer ces très hauts débits, des modulations multi-états sont utilisées pour chaque porteuse grâce à leur efficacité spectrale élevée. Ces types de systèmes, qui combinent à la fois les approches multi-bande et les modulations multi-états, sont extrêmement vulnérables aux effets nonlinéaires de la fibre optique. En fait, les effets nonlinéaires sont dépendants de la puissance de transmission et inversement proportionnels à l'intervalle de garde. Cela rend leur compensation indispensable pour maintenir des bonnes performances des systèmes en terme de distance de transmission. Grâce à l'emploi de récepteurs à détection cohérente, des techniques de traitement du signal numérique sont utilisées pour combattre les effets nonlinéaires comme la rétro-propagation numérique (DBP) et l'égaliseur basé sur les séries de Volterra (VNLE) de troisième ordre.

Dans cette thèse, nous avons proposé deux nouvelles techniques numériques pour compenser les effets nonlinéaires intra-bande et les interférences nonlinéaires inter-bande dans les systèmes de transmission super-canal. La première approche, nommé l'égaliseur nonlinéaire basé sur les séries de Volterra de cinquième ordre, compense les effets nonlinéaires intra-bande. Cette technique a significativement augmenté les performances en comparaison avec le VNLE de troisième ordre dans le contexte de transmission OFDM mono-bande. Cependant, dans le contexte de transmission super canal OFDM multi-bande, les performances des VNLEs de cinquième ordre et de troisième ordre sont affectées par les interférences nonlinéaires causées par les bandes adjacentes. Par conséquent, on a proposé l'annulateur des interférences nonlinéaires (INIC) pour combatte les effets nonlinéaires inter-bande. L'INIC a significativement augmenté les performances en comparaison avec les techniques classiques DBP et VNLE de troisième ordre dans le contexte de transmission super canals OFDM multi-bande et Nyquis WDM.

MOTS-CLEFS : Transmission optique cohérent, 400Gbps/1Tbps, effets nonlinéaires, séries de Volterra, traitement numérique du signal, interférences nonlinéaires, transmissions longues distances

CONTENTS

List of Figures

List of Tables

List of Acronyms

ADC	Analog to Digital Convertor
ASE	Amplified Spontaneous Noise
AWGN	Additive White Gaussian Noise
BER	Bit Error Rate
CD	Chromatic Dispersion
CFO	Carrier Frequency Offset
CMA	Constant Modulus Algorithm
CO	Coherent Optical
CP	Cyclic Prefix
CPE	Common Phase Error
DAC	Digital to Analog Convertor
DBP	Digital Back Propagation
DCF	Dispersion Compensation Fiber
DD	Decision Directed
DFE	Decision Feedback Equalizer
DGD	Differential Group Delay
DP	Dual-Polarization
DSF	Dispersion Shifted Fiber
DSP	Digital Signal Processing
EDFA	Erbuim-Doped Fiber Amplifier
ENOB	Effective Number Of Bits
FEC	Forward Error Correction
FFT	Fast Fourier Transform
FIR	Finite Impulse Response
FWM	Four Wave Mixing
GN	Gaussian Noise
GD	Group Delay
GVD	Group Velocity Dispersion
ICI	Inter-Carrier Interference
IFFT	Inverse Fast Fourier Transform
IM-DD	Intensity Modulated Direct Detection

INIC	Inter-band/subcarrier Nonlinear Interference Canceler
ISI	Inter-Symbol Interference
IVSTF	Inverse Volterra Series Transfer Function
LEAF	Large Effective Area Fiber
LED	Light-Emitting Diode
LO	Local Oscillator
LPF	Low Pass Filter
MB	Multi-Band
MDM	Mode Division Multiplexing
MIMO	Multiple Input Multiple Output
MZM	Mach-Zehnder Modulator
MZI	Mach-Zehnder interferometer
NF	Noise Figure
NLE	NonLinear Equalizer
NLSE	NonLinear Schrodinger Equation
NZDSF	Non-Zero Dispersion Shifted Fiber
NRZ-OOK	Non-Return-to-Zero On/Off Keying
OEO	Optical-to-Electrical-to-Optical
OFDM	Orthogonal Frequency Division Multiplexing
OOK	On/Off Keying
OSNR	Optical Signal to Noise Ratio
PBC	Polarization Beam Combiner
PBS	Polarization Beam Splitter
PDL	Polarization Dependent Loss
PDM	Polarization Division Multiplexing
PMD	Polarization Mode Dispersion
QAM	Quadrature Amplitude Modulation
QPSK	Quaternary Phase Shift Keying
RDE	Radius Directed Equalizer
ROADM	Reconfigurable Optical Add Drop Multiplexer
RRC	Root Raised-Cosine
SDM	Spacial Division Multiplexing
SNR	Signal to Noise Ratio
SOP	State of Polarization
SPM	Self-Phase Modulation
SMF	Single Mode Fiber
SSMF	Standard Single Mode Fiber
TDM	Time Division Multiplexing
VSTF	Volterra Series Transfer Function
VNLE	Volterra based NonLinear Equalizer

WDM	Wavelength Division Multiplexing
WSS	Wavelength Selective Switch
XPM	Cross-Phase Modulation
XPolM	Cross-Polarization Modulation
ZF	Zero Forcing

INTRODUCTION

Problem statement

Optical fiber communication systems have played an important role in the evolution and development of modern communications networks. Due to their low cost, low attenuation and high bandwidth, optical fibers have dominated the area of long-haul terrestrial and transoceanic transmission. In addition to access and metro networks, today Fiber-to-the-Home (FTTH) systems are also available. Since their deployment in the 1970's, optical communication systems have evolved to meet the continuous grow of global demand for communication capacity. The invention of EDFA and the deployment of WDM technology have been the first breakthrough that stimulate the use of optical communication systems. Different fiber technologies had used to deal with transmission impairments such as dispersion and attenuation. Then, fiber capacity evolution had slowed down because of the full exploitation of the amplifier bandwidth, before it was revived by the re-introduction of coherent detection based systems in the early 2000's. Coherent based technology allowed the increase of spectral efficiency by exploiting new degrees of freedom. Polarization and phase, in addition to amplitude used in direct detection based systems, are available in coherent systems and can be used to increase spectral efficiency and so that fiber capacity. As a result, optical transmission has migrated from the use of OOK to multi-level modulation formats. An other important point that characterizes coherent detection based systems is the possibility of combination with DSP techniques to combat fiber distortion.

Fiber capacity increase is still required to face the ever increase of traffic demands driven by the growth of mobile, video and cloud services and machine-to-machine communications. According to Cisco Visual Networking Index [1], metro and long-haul traffic will triple between 2014 and 2019. The next generation of long-haul WDM transmission systems are expected to operate at 400Gbps/1Tbps per WDM wavelength whereas the most recent commercial fiber operates at 100Gbps. Such high bit rate is difficult to achieve without finding new technological paths. Actually, the classic ways to increase data rate, by increasing the symbol rate and/or encoding more bits per symbol, face several challenges that make their practical implementations impossible. Increasing the symbol rate to generate 400Gbps/1Tbps requires a very high speed optical and electronic components which are not commercially available today and in

the near future. On the other hand, very high spectral efficiency modulation are needed to generate these high bit rates. Such modulation formats require very high optical signal to noise ratio (OSNR) which strongly increases the sensitivity to fiber nonlinear effects. Due to nonlinear effects, sending 400Gbps/1Tbps over a WDM wavelength can reach only few hundreds of kilometers if only linear processing is carried out at the receiver side which is not the desired transmission reach in the context of long-haul transmission. Therefore, nonlinear processing at the receiver side is crucial for the next generation of long-haul WDM transmission systems. In addition, new way for using a WDM wavelength has been proposed, called superchannel approach, which consists in split a WDM wavelength into several optical bands with small guard-band between them. This approach enables an easier practical implementation by sampling with respect to the band instead of the wavelength. Two kinds of superchannel based on Nyquist WDM and multi-band OFDM are now subject of research investigations to evaluate their performance. Superchannel systems combined with multi-level modulation formats can be considered as promising candidates in terms of practical implementation and performance. However, superchannel transmission is also vulnerable to fiber nonlinear effects. Kerr-induced nonlinear effects such as self-phase modulation (SPM), cross-phase modulation (XPM), cross-polarization modulation (XpolM) and four-wave mixing (FWM) depending on bite rate and interval guard, reduce the transmission performance and their mitigation is required.

Contributions of the thesis

Our work has been funded by the SASER-SIEGFRIED European program. Our contribution consists in developing new DSP algorithms for the next generation of long-haul WDM transmission systems. In the context of superchannel transmission systems, fiber nonlinear effects are considered as the major constraint and their mitigation is a hot topic to get the desired performance in terms of transmission reach. Many works on Digital Back Propagation and third-order Volterra series have been proposed. Nevertheless, gain in performance is still necessary. Therefore, we developed new techniques to compensate for nonlinear effects in optical fiber.

To deal with intra-band nonlinear effects in multi-band OFDM superchannel, we developed a fifth-order Volterra based nonlinear equalizer (VNLE). The main idea of this technique is increasing the order of Volterra based nonlinear equalizer. We first derived mathematically the fifth-order Volterra kernels which characterize the nonlinear equalizer. Then, we proposed a practical implementation scheme. The performance of the proposed technique are evaluated by simulation and a significant gain is observed in comparison with third-order VNLE in certain configurations.

We observed a reduction of performance of our proposed fifth-order VNLE and the classic approaches such as digital back-propagation (DBP) and third-order VNLE in case of multi-band transmission. As a result, we proposed a nonlinear interference canceler to compensate for nonlinear interference in the context of superchannels based on multi-band OFDM and multi-

subcarrier Nyquist WDM. The proposed inter-band/subcarrier nonlinear interference canceler (INIC) significantly improve the performance in comparison with the classic nonlinear effects mitigation techniques.

Thesis outline

The thesis is organized as follows: in chapter 1, we briefly review the evolution of optical fiber communication systems. We highlight the technological breakthrough that characterized the evolution of fiber capacity like the deployment of WDM systems and the revival of coherent detection. Then, we focus on optical fiber impairments. We describe linear distortions and then we detail nonlinear effects because of their important impact in superchannel systems.

In chapter 2, we briefly give the principle of high spectral efficiency modulation formats. The second part of this chapter is dedicated to the system models. We describe superchannel transmission systems for both multi-band OFDM and Nyquist WDM approaches. After that, we give the state of the art about nonlinear effects compensation techniques.

In chapter 3, we propose the fifth-order Volterra based nonlinear equalizer. A derivation of fifth-order Volterra operators and a practical implementation scheme are given for single-polarization and dual-polarization configurations. Then, simulations are done to evaluate the performance of the proposed technique in the context of OFDM based superchannel.

In chapter 4, we propose an inter-band nonlinear interference canceler. This approach combats nonlinear interference in multi-band OFDM and Nyquist WDM superchannels. Simulation results are given before introducing a complexity analysis of the proposed nonlinear interference canceler.

Publications

Journal Papers

J1 **A. Amari**, P. Ciblat, and Y. Jaouen, “Inter-subcarrier Nonlinear Interference Canceler for Long-Haul Nyquist-WDM Transmission,” *IEEE Photonics Technology Letters (PTL)*. vol. 28, no. 23, pp. 2760-2763, December 2016.

International Conferences

C1 **A. Amari**, P. Ciblat, and Y. Jaouen,“Fifth-order Volterra series based Nonlinear Equalizer for long-haul high data rate optical fiber communications," *Asilomar Conference on Signals, Systems, and Computer*, November 2014.

C2 V. Vgenopoulou,**A. Amari**, M. Song, E. Pincemin, I. Roudas, and Y. Jaouen,“Volterra-based Nonlinear Compensation in 400 Gb/s WDM Multiband Coherent Optical OFDM Systems," *Asia Communications and Photonics Conference (ACP)*, November 2014.

C3 **A. Amari**, P. Ciblat, and Y. Jaouen,“Inter-Band Nonlinear Interference Canceler for Long-Haul Coherent Optical OFDM Transmission,"*IEEE/OSA Tyrrhenian International Workshop on Digital Communications (TIWDC)*, October 2015.

CHAPTER 1

STATE OF THE ART ABOUT OPTICAL FIBER COMMUNICATION SYSTEM

In this chapter, we briefly describe the evolution of optical fiber communication systems. We emphasize the technological breakthroughs that stimulate the increase of fiber capacity such as the invention of EDFA and the deployment of coherent detection based systems. On the other hand we focus on fiber propagation impairments. We highlight fiber nonlinear effects because of their strong impact for the next generation of long-haul WDM systems.

1.1 Evolution of optical fiber transmission systems

Optical fiber communication uses light pulses to transmit information from a point to another. Semiconductor devices such as light-emitting diodes (LEDs) and laser diodes are used to generate light at the transmitter. The transmission medium consists of an optical fiber which is a dielectric cylindrical waveguide made from low-loss materials such as silica. Light pulses propagate inside the fiber due to the internal reflection between the core and the cladding [2]. Signal amplification is required to deal with fiber loss, especially for long-haul and transoceanic transmission. At the receiver side, photo-detectors ensure the conversion of the transmitted signal to the electrical domain. The advantages that stimulate the use of optical fiber for communication systems are its low attenuation and wide spectral bandwidth compared to other communication systems. Today, optical communication systems are widely used to meet the rapidly increasing demand for telecommunication capacity and internet services. Actually, optical communication is unchallenged for the high transmission capacity with low latency in long-haul and transoceanic transmission.

Optical fibers were first introduced in the early 1970's. Semiconductor AlGaAs was used as laser and transmission is carried out in the range of $800-850nm$ wavelength. The transmission performance were limited by material dispersion. The maximum transmission bit-rate-distance reached is about $1Gb-km.s^{-1}$ for multi-mode fibers [2]. In the early 1980's, single mode

fibers (SMF) with 1310nm wavelength, defined by the ITU-T as the standard G.652, were used to deal with fiber dispersion. In fact, the zero-dispersion wavelength is about 1268nm [3], and the fiber dispersion was reduced by adding waveguide dispersion material to shift the zero-dispersion to 1310nm [4]. SMF presented higher performance in terms of bandwidth and transmission reach in comparison with multi-mode fiber. Thus, it became the fiber of choice for long-haul transmission systems by 1984 [5]. The need of increasing transmission distance had pushed fiber transmission to 1550nm wavelength which presents the lowest fiber loss as shown in fig.1.1. The attenuation value at 1550nm is about $0.2dB.km^{-1}$, while the corresponding

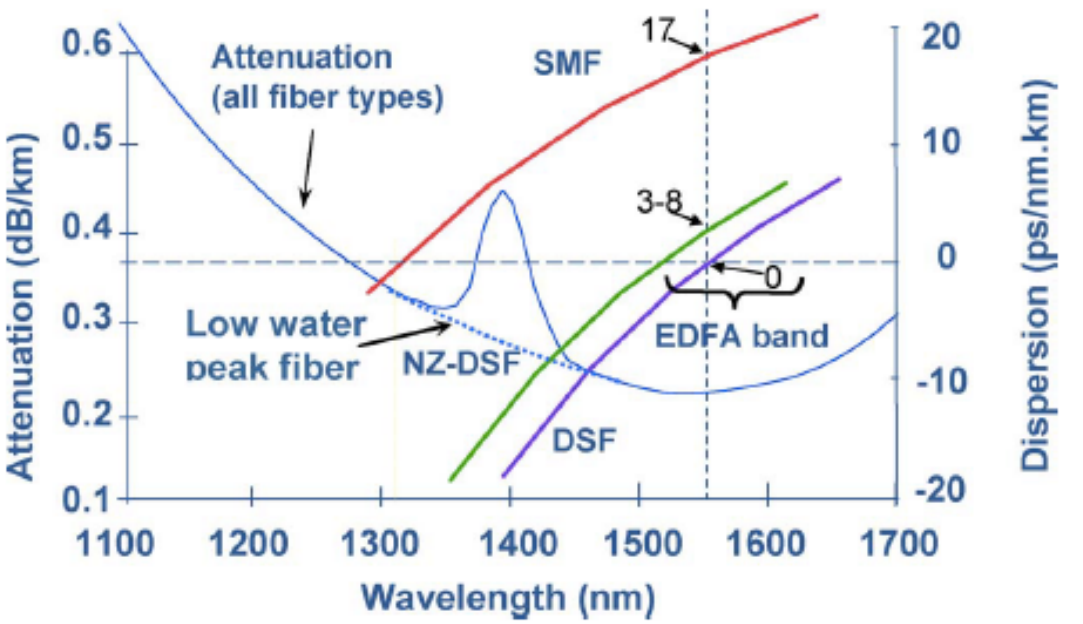

Figure 1.1: Fiber attenuation and dispersion for single-mode fibers [5]

attenuation at 1310nm is about $0.35dB.km^{-1}$. Then, transmission reach can be increased by 75% using 1550nm. At this value of wavelength, the fiber chromatic dispersion is about $17ps.nm^{-1}.km^{-1}$ as shown in fig.1.1. Therefore, dispersion shifted fibers (DSF) were used and optimized to combat fiber dispersion by shifting zero dispersion wavelength to 1550nm.

At the receiver, intensity modulation and direct detection (IM-DD) scheme was commonly employed in optical communication systems for long time and attracted more attention than coherent detection scheme. Actually, IM-DD based receiver sensitivity is independent of the carrier phase and the state of polarization (SOP) of the received signal which are randomly fluctuating in real systems. IM-DD allows only amplitude based modulation formats and the decision is related to the signal intensity. A photo-detector ensures the conversion of the optical signal to the electrical domain by creating a current proportional to the signal intensity. The expression of the generated current is given by:

$$I = R.E^2 \tag{1.1}$$

where R is the responsivity of the photo-detector and E is the amplitude of the optical field. The principle of direct detection based receiver is shown in fig.1.2.

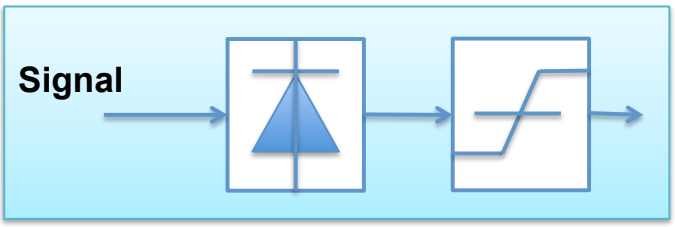

Figure 1.2: Direct detection

1.1.1 EDFA invention: Wavelength division multiplexing transmission

The first breakthrough in optical communications was the invention of the Erbium-Doped Fiber Amplifiers (EDFA) in the late 1980's. It avoids the expensive optical-to-electrical-to-optical (OEO) regeneration. It also allows the amplification of a multiplex of optical signals with different wavelength inside the amplifier bandwidth. EDFA band includes 1550nm wavelength as shown in fig. 1.1. A dramatic increase in system capacity was achieved through the aggregation of several wavelengths propagating simultaneously inside the SMF. This technique enabled by optical amplifiers is called wavelength division multiplexing (WDM). WDM technology was developed in the mid-1990's and it increased lightwave systems capacity to roughly 1Tbps by fiber around 2000 [6]. More precisely, this rate is obtained through 80 WDM wavelength, each of them with 10Gbps. It consists in transmitting independent signals using different wavelengths propagating simultaneously in the fiber. Wavelength aggregation is done using multiplexer at the transmitter, a demultiplexer at the receiver side splits them apart as presented in fig. B.1.

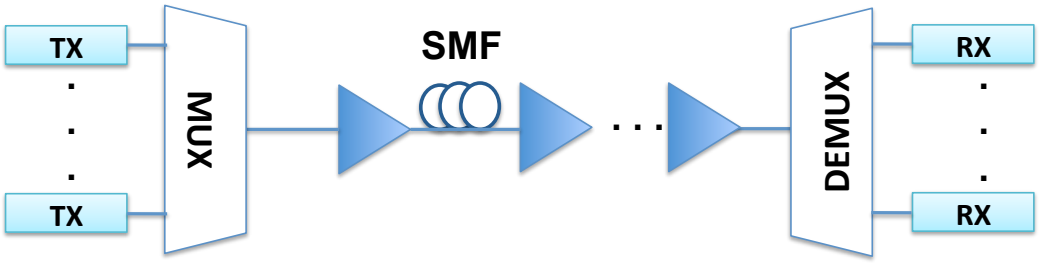

Figure 1.3: WDM transmission system

Fig.1.4 shows the evolution of system capacity for WDM system in comparison with single channel time-division multiplexing (TDM) system in research demonstrations. WDM transmission allowed a significant increase of data rate from gigabits per second to over than one terabit per second. It has strongly increased system capacity in comparison with TDM.

DSF fibers used for single-wavelength transmission at 1550nm are not convenient for WDM systems. In fact, interactions between WDM channels lead to the generation of new signals at

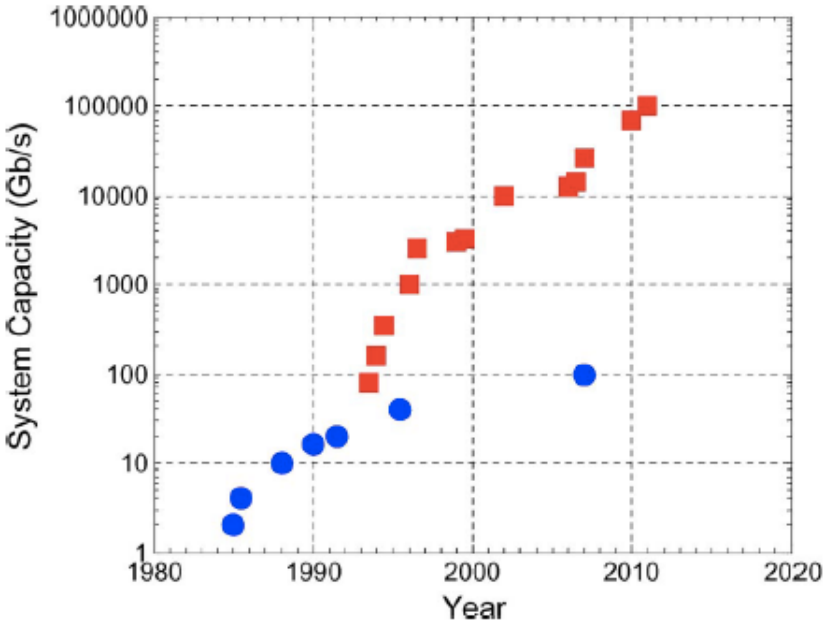

Figure 1.4: Evolution of capacity for WDM (square marker) and TDM (disk marker) systems [7]

new frequencies because of nonlinear effects named four-wave mixing (FWM). FWM, detailed in section 1.2.5-c, causes crosstalk between WDM channels and it is inversely proportional to the fiber dispersion. Then, non-zero dispersion shifted fibers (NZDSF) were developed for WDM transmission to combat FWM [8]. NZDSFs with larger effective area such as LEAF were widely used for long-haul WDM transmission.

1.1.2 From 2.5Gbps to 10Gbps (per wavelength) non-coherent detection based systems

WDM systems were deployed firstly with 40 wavelengths each of them with 2.5Gbps over 800km of standard SMF. Non-Return-to-Zero On/Off Keying (NRZ-OOK) was used as modulation formats. Accumulated chromatic dispersion (CD) was the major limitation to increase further the bit rate. Increasing data rate to 10Gbps per wavelength was made possible by using dispersion compensation fiber (DCF) in addition to forward error correction codes (FEC). DCF is used in concatenation with SMF as shown in fig.1.5. In order to compensate chromatic dispersion, DCF has an opposite sign of dispersion with respect to the already installed SMF [9]. FEC consists in adding redundancy to the transmitted signal in order to make possible detection and correction of errors at the receiver. The use of Reed-Solomon (RS) FEC codes, which provide about 6 dB gain in optical to signal noise ratio (OSNR), and Enhanced-FEC (EFEC) with 8.5 dB gain in OSNR had significantly increased the transmission performance[10].

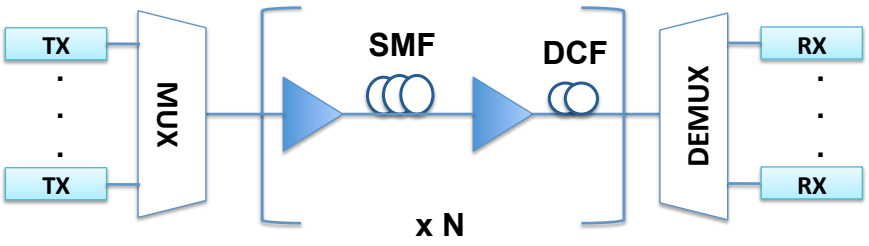

Figure 1.5: WDM system with dispersion compensation fiber (DCF)

1.1.3 40Gbps coherent detection based systems

The migration of direct detection based OOK systems from 10Gbps to 40Gbps per wavelength was challenged by different fiber impairments. In fact, polarization mode dispersion (PMD), which has negligible effect in 10Gbps, reduces drastically the transmission performance at 40Gbps. Indeed in non-coherent based communication (with OOK) passing from 10Gbps to 40Gbps leads to divide the bit period by 4 which decreases also the tolerance on the PMD by 4. In addition, CD tolerance is divided by a factor of 16 at 40Gbps and that requires an increase of OSNR by $6dB$ to get similar performance to OOK 10Gbps systems [11]. This high increase of OSNR leads to a strong nonlinear distortion. An other way to increase the rate was to increase the number of WDM wavelength, but this is a very limited option due to the optical amplifier bandwidth. These limitations oriented the researches to focus the possibility to increase the spectral efficiency and so to the use of coherent detection instead of direct detection. This is the second main breakthrough on the optical-fiber communications community.

1.1.3-a Coherent detection

Coherent detection was first introduced by DeLange in 1970 [12]. Its complexity of implementation and the high performance of IM-DD systems meeting the desired fiber capacity made its deployment unnecessary. However, the need of increasing capacity and spectral efficiency and the availability of high speed ADCs/DACs has led to a revival of the coherent detection.

The introduction of coherent detection permitted the use of multilevel modulations formats due to the ability to detect the signal phase and amplitude. Thus, higher spectral efficiency can be achieved compared to direct detection technique. An other major advantage of coherent detection is the possible combination with digital signal processing (DSP) algorithms. Therefore, fiber impairments can be mitigated efficiently in electrical domain and that avoids the use of DCF to combat CD. The principle of coherent detection is depicted in fig. 1.6. It consists in mixing the received signal with a continuous wave generated by a local oscillator (LO). LO produces a frequency very close to the frequency of the received signal and it serves as an absolute phase reference.

Phase diversity homodyne receiver and intradyne receiver are usually used to detect both in-phase and quadrature components of the optical signal simultaneously. This can be ensured

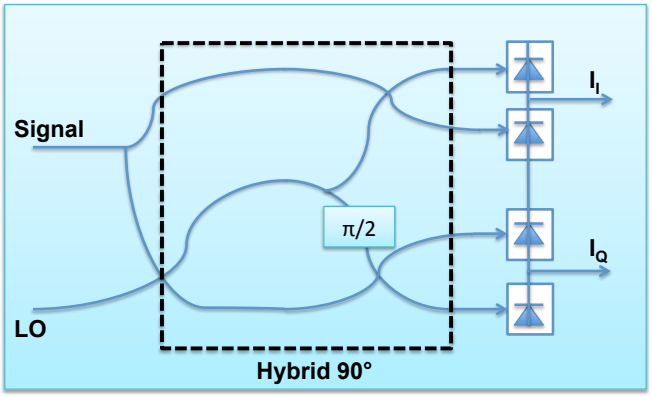

Figure 1.6: Coherent detection with Hybrid 90^o device

by using an 90° optical hybrid and the output photocurrents from the balanced photodiodes are then given by [13]:

$$I_I(t) = R\sqrt{P_s P_l}\cos(\theta_s(t) - \theta_l(t)) \tag{1.2}$$

$$I_Q(t) = R\sqrt{P_s P_l}\sin(\theta_s(t) - \theta_l(t)) \tag{1.3}$$

where P_s, P_l, θ_s and θ_l are the powers and phases of the received signal and the local oscillator respectively. Therefore, the complex amplitude or the baseband signal can be expressed as:

$$I_c(t) = I_I(t) + jI_Q(t) \tag{1.4}$$

$$= R\sqrt{P_s P_l}e^{[j(\theta_s(t)-\theta_l(t))]}. \tag{1.5}$$

After that, DSP techniques are used to deal with fiber impairments such as dispersion and nonlinear effects.

Coherent-based technology has been used instead of direct detection-based technology in the 40Gbps and the current 100Gbps standard technology for optical long-haul WDM systems. Thanks to coherent detection, in addition to the phase and the amplitude, polarization of the received signal is also available and it can be used to increase the spectral efficiency. In fact, due to polarization division multiplexing (PDM), transmission bit rate can be doubled easily. Therefore, PDM, known also as dual-polarization transmission, is widely used in coherent optical transmission systems.

1.1.3-b Polarization division multiplexing

Polarization division multiplexing allows more efficient use of the available bandwidth. It enables a factor of two increase in spectral efficiency since the data rate is twice without increasing the symbol rate. In PDM systems, both orthogonal polarization at the same wavelength are used to transmit independent data. A coherent phase and polarization diversity receiver is used to detect both polarizations as shown in fig. B.2.

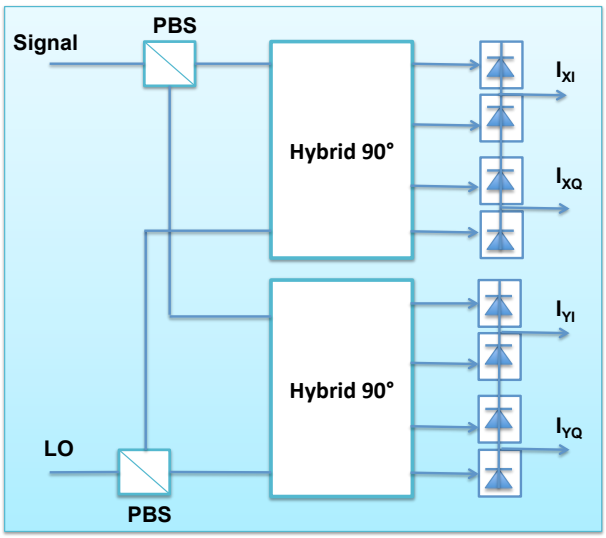

Figure 1.7: Block diagram of phase and polarization diversity coherent receiver

PDM technique has been used in $40Gbps$ long-haul WDM systems and beyond. However, dual-polarization transmission suffers from several impairments such as polarization mode dispersion (PMD) and nonlinear cross-polarization modulation (XPolM) which reduce the transmission performance.

1.1.3-c Digital signal processing algorithms

The deployment of coherent detection with DSP algorithms has enabled offline compensation for fiber impairments. DSP based fiber impairments compensation can be easily and efficiently implemented at the receiver to equalize the received signal after the analog to digital conversion (ADC). It can be also performed at the transmitter side to predistort the transmitted signal before the digital to analog conversion. The different stages of DSP at the receiver are shown in fig. 1.8.

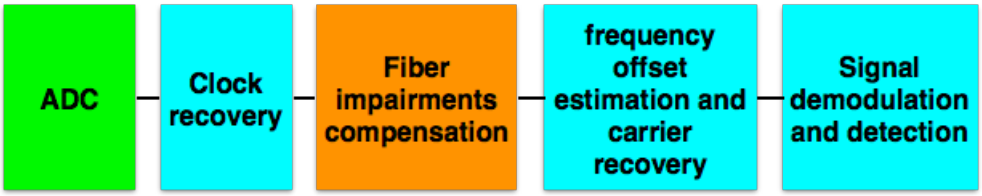

Figure 1.8: DSP blocks for coherent receiver

Several approaches have been proposed to combat CD and PMD. Research works are currently oriented to other fiber impairments such as polarization dependent loss (PDL) and nonlinear effects which their impacts become more and more important in high data rate systems.

Then, a frequency offset and carrier recovery are done before signal detection and decision. These DSP algorithms will be detailed in section 2.2.

1.1.4 100 Gbps coherent systems

After the commercialization of 40Gbps coherent technology in the mid of 2000s, 100Gbps (per wavelength) coherent system was chosen to be the next standard technology for optical transport network (OTN) to meet the growth of traffic demands [14]. Several approaches are proposed for 100Gbps coherent systems such as dual-polarization Quaternary phase-shift keying (DP-QPSK) systems and orthogonal frequency-division multiplexing (OFDM) based systems[15].

In fact, by placing 88 WDM channels at 50GHz-spaced grids, a total capacity of $8.8Tbps$ through a single fiber and a spectral efficiency of 2 can be achieved [7][13]. $8.8Tbps$ is commercialized today by *Alcatel-Lucent* for 100Gbps DP-QPSK per waverlength over a distance of 4000km. A $17.6Tbps$ ($88x200$Gbps DP-16-QAM) is also available for a transmission distance of 1000km. *PacketLight Networks* has proposed 100Gbps (DP-QPSK) coherent systems which can reach up to 2000km for ultra-long-haul networks. 100Gbps coherent systems for OTN are also commercialized by *ZTE Corporation*, *Ciena*, *Huawei* and *Infinera*...

1.1.5 Fiber capacity limit

The introduction of coherent detection and dual-polarization in WDM transmission systems have increased the spectral efficiency. Fig. 1.9 shows the spectral efficiency achieved in research demonstrations versus year [7].

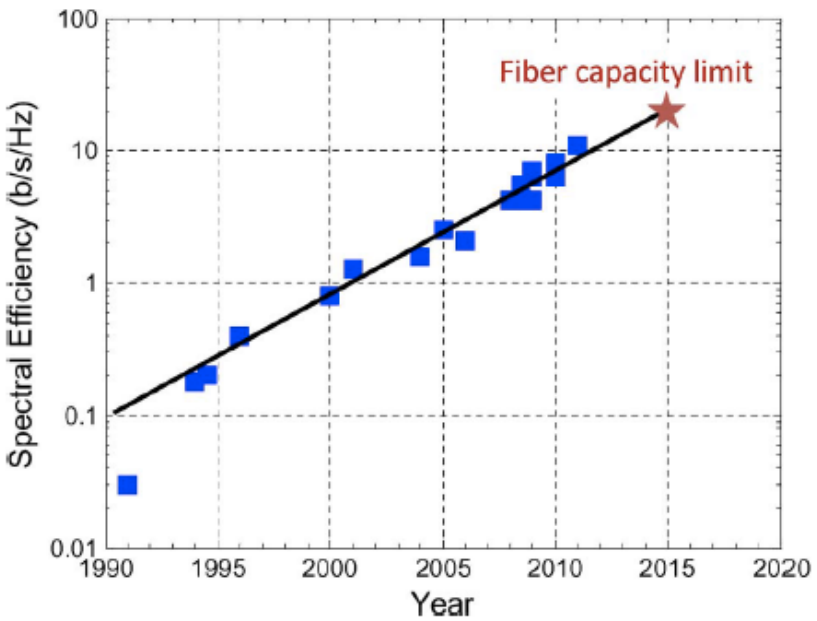

Figure 1.9: Spectral efficiency achieved in research testbeds versus year [7]

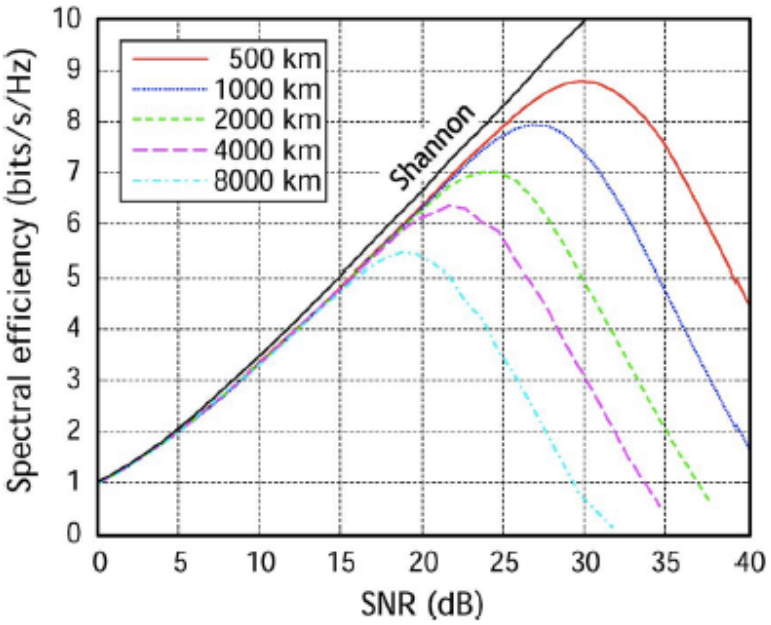

Figure 1.10: Nonlinear fiber (Gaussian) capacity limits for a range of transmission distance [7]

Spectral efficiency improvement has revived the increase of fiber capacity after it had slowed down because of the full exploitation of the amplifier bandwidth. The strong traffic demand increase requires a continuous improvement of system capacity. The next generation of long-haul WDM systems is expected to operate at 400Gbps or 1Tbps per wavelength. Such high bit rate is extremely difficult to achieve without finding new technological paths. The use of multi-level modulation formats faces a serious challenge which is fiber nonlinear effects. Advanced modulation formats require higher optical signal-to-noise ratio (OSNR) and so that higher input powers. Such input powers lead to the increase of sensitivity to fiber nonlinear effects, that significantly reduces the transmission reach. In fact, the optical fiber is a nonlinear transmission medium due to Kerr effect [16]. Fiber capacity is limited by noise at low power and by fiber nonlinearity (if the transmit waveform is not modified and adapted to nonlinearity) at high input power as shown in fig. 1.10.

Space-division multiplexing (SDM) (such as multi-core fibers (MCF) or mode-division multiplexing (MDM)) are proposed to meet the ever growth in traffic demands. The first one consists in inserting several independent cores per fiber and the total fiber capacity can thus be increased according to the number of cores [7]. MDM can be used in multi-mode fibers [17]. An increase of capacity can be realized according to the number of supported orthogonal modes. Transmission impairments can be mitigated using digital signal processing to increase system performance . SDM techniques are investigated in research demonstrations but they still do not meet the desired performance in terms of transmission reach in long-haul

transmission.

Thus, SMF is still the chosen fiber in long-haul transmission systems. To meet the increased demands in SMF capacity, researches are focused to find new approaches to increase system capacity and to achieve the expected high bit rate for the next generation of long-haul WDM systems. An aggregation of optical subcarriers with small guard-band is proposed [18]. This technique, called superchannel transmission, is a potential candidate for the next generation in combination with multi-level modulation formats. Researches now are concentrated in evaluating the performance of two types of superchannels based on OFDM and Nyquist-WDM systems.

1.2 Optical fiber transmission impairments

Long-haul transmission over SMF suffers from several limitations [2]. Fiber loss causes the attenuation of the propagating optical power and so that signal amplification is required periodically. Amplifier such as EDFA generates amplified spontaneous noise (ASE) and the accumulation of ASE noise reduces transmission performance. In addition, fiber dispersion such as chromatic dispersion (CD) and polarization mode dispersion (PMD) cause intersymbol interference (ISI). At high date rate transmission, nonlinear effects become more important and their compensation is necessary to maintain long transmission distance. These different kinds of optical fiber impairments are presented by the simplified version of the nonlinear Schrodinger equation (NLSE) that governs the wave propagation inside an SMF:

$$\frac{\partial E}{\partial z} + j\frac{\beta_2}{2}\frac{\partial^2 E}{\partial t^2} + \frac{\alpha}{2}E = j\gamma|E|^2E \tag{1.6}$$

where E is the electric field envelope of the optical signal, α is the fiber attenuation coefficient, β_2 is the second-order dispersion parameter and γ is the nonlinear coefficient of the fiber.

In followings subsections, we highlight the causes and the impacts of optical fiber impairments.

1.2.1 Attenuation

The optical power propagating along the fiber decreases exponentially with the transmission distance. The expression of attenuation is given by:

$$\alpha\,[dB.km^{-1}] = \frac{10}{L}\log_{10}\left(\frac{P_0}{P}\right) \tag{1.7}$$

where L is the fiber length or the span length in multi-span fiber. P_0 and P are the input and output optical power respectively. Fiber loss is induced by different mechanisms mainly: material absorption, Rayleigh scattering and bending losses.

Material absorption is the conversion of the electromagnetic wave energy into other forms such as vibration. It can be intrinsic caused by the fiber material silica and it occurs in infrared and ultraviolet bands. An other type of absorption is related to impurities in the fiber. The

most important impurities causing extrinsic absorption in the fiber is OH^- ions. The significant OH^- losses occur at 950nm, 1250nm and 1380nm. SMF standard G.652 has not an OH^- peak at 1380nm and that allows the transmission in the entire region located between 1300nm and 1700nm.

Rayleigh scattering is due the material inhomogeneities with a size smaller than wavelength. It depends on wavelength and the related loss is inversely proportional to the wavelength $\alpha_R \sim \frac{1}{\lambda^4}$. Thus, Rayleigh scattering loss is reduced at high wavelength. However, it restricts the use of fibers at short wavelength.

Macroscopic and microscopic bends cause also fiber loss. Macrobending losses appear when installing fibers and are negligible in practice. Microbending losses are due to the local distortions of fiber geometry.

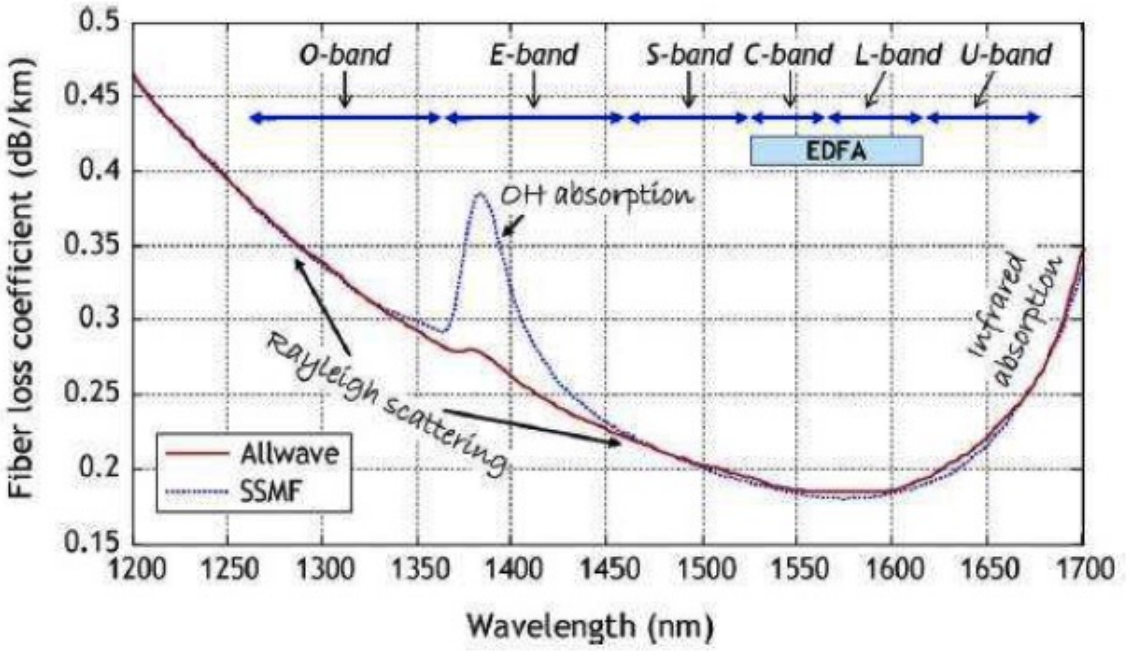

Figure 1.11: Attenuation of optical fiber [19]

Fig. 1.11 shows the different mechanisms responsible for fiber loss [19]. In standard SMF, the fiber loss is about $0.2dB.km^{-1}$ around the transmission wavelength 1550nm. In long-haul transmission system, multi-span fiber separated by amplifiers is used to deal with fiber loss. The typical distance between amplifiers is between 80 and 100km for a total transmission distance of $1500-3000$km.

1.2.2 Chromatic dispersion

In SMF, the energy of the injected pulse is transported by a single mode which is the fundamental mode. Thus, the advantage of SMF is the absence of intermodal dispersion but it is still affected by intramodal dispersion or chromatic dispersion. CD includes two types of dis-

persion: material dispersion and waveguide dispersion. the first one is due to the dependence of the refractive index of silica, the material used for fiber fabrication. The waveguide dispersion is caused by the structure and the geometric properties of the optical fibers. In eq.1.6, β_2 is the term responsible for CD in optical fiber. It is also known as the GVD parameter. The wavelength λ_D corresponding to $\beta_2 = 0$ is called zero dispersion wavelength. The value of the CD is characterized by the coefficient of chromatic dispersion D. The coefficient D is related to β_2 by the following expression:

$$D = -\frac{2\pi c}{\lambda^2}\beta_2 \tag{1.8}$$

It depends on wavelength λ. When $D < 0$, the fiber has normal dispersion and the lowest wavelength components of the optical pulse travel slower than the highest wavelength components. In the case of $D > 0$ (which is our case), the fiber is called with anomalous dispersion.

Figure 1.12: Inter-symbol interference due to chromatic dispersion

CD causes pulse broadening which leads to inter-symbol interference (ISI) as shown in fig.1.12. ISI reduce significantly the transmission performance and CD compensation is required. Several techniques are proposed to compensate CD such as the use of dispersion compensating fibers (DCFs) in concatenation with SMF [20]. However, this kind of approach increases the fiber sensitivity to nonlinear effects because of their reduced effective core area.

In SMF standard G.652 fiber used in our work, the value of the CD coefficient D is approximatively $17ps.nm^{-1}.km^{-1}$ at 1550nm wavelength.

1.2.3 Polarization mode dispersion

The fundamental mode of an SMF consists of two orthogonal components known as polarization states. Thus, in case of dual-polarization transmission, the injected optical pulse attacks the two polarization components and propagates inside the SMF in the two directions x and y. Unfortunately, because of manufacturing process, the optical fiber is not ideal circular and homogeneous, the core has not perfect symmetry and that leads to modal birefringence. In fact, because of core asymmetry, the refraction indexes of polarization x and y are different and the two polarizations travel inside the fiber with different velocities. The strength of modal birefringence can be expressed as [2]:

$$B_m = \mid n_x - n_y \mid \tag{1.9}$$

where n_x and n_y are the modal refractive indexes for the two polarization states x and y respectively.

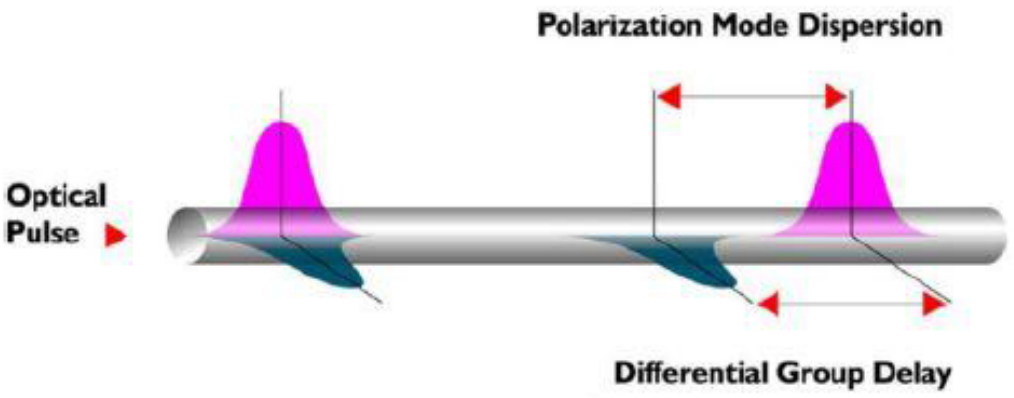

Figure 1.13: Illustration of polarization mode dispersion

As presented in fig. 1.13, birefringence causes a delay between the two orthogonal states of polarization during the propagation. This delay $\Delta\tau$ is known as differential group delay (DGD). DGD is not deterministic and it varies wildly with the wavelength and the time due to deployment conditions such as thermal and mechanical stresses. The average of DGD is referred to as PMD. The optical fiber can be modeled as a concatenation of birefringence segments with random axis variation. The concatenation of equal sections of birefringent fiber can be presented by the Jones matrix (given in hte frequency domain) as [21] :

$$T(\omega) = \prod_{n=1}^{N} B_n(\omega) R(\alpha_n) \tag{1.10}$$

$$= \prod_{n=1}^{N} \begin{pmatrix} e^{\sqrt{3\pi/8}b\omega\sqrt{h_n}/2+\phi_n} & 0 \\ 0 & e^{-\sqrt{3\pi/8}b\omega\sqrt{h_n}/2+\phi_n} \end{pmatrix} \begin{pmatrix} \cos\alpha_n & \sin\alpha_n \\ -\sin\alpha_n & \cos\alpha_n \end{pmatrix} \tag{1.11}$$

where N is the number of segment, B_n represents the birefringence matrix of n-th segment with h_n length, R is the matrix of a rotator that the random coupling angles between the segment axes, b is the PMD coefficient of the fiber and ω is the optical frequency. The phase ϕ_n accounts for the small temperature variation along the fiber. The DGD $\Delta\tau$ can be calculated based on the eigenvalues of the matrix $(\partial_\omega T(\omega))T^{-1}(\omega)$.

PMD is a potential source of pulse broadening which leads to strong ISI and it increases linearly with the data rate. In coherent transmission systems, MIMO processing techniques are used to mitigate PMD [22].

1.2.4 Optical amplification

In long-haul optical transmission, signal attenuation can be reduced by introducing optical amplifiers. Optical amplification presents two main advantages. It allows the use of WDM transmission system and it avoids optical to electrical to optical conversion which requires high-speed electronics. Rare earth doped fiber such as EDFA are mainly used as fiber amplifier for optical transmission systems. Currently, Raman amplification is also investigated to evaluate its performance. EDFA amplification process and its effect in optical fiber transmission systems are detailed in the following.

1.2.4-a EDFA

EDFA consists of Erbium doped Silica SMF pumped by semiconductor lasers at 980nm and 1480nm [23]. EDFA uses stimulated emission to amplify the transmitted optical signals and the principle is based on exciting Erbium ions Er^{3+} to higher energy level. At $980nm$, Erbium ions from ground level L_1 are excited into energy state L_3 [24]. The life time of Er^{3+} in L_3 is about $1\mu s$. After that, Erbium ions fall into metastable level L_2. Pump can also work at 1480nm to excite Er^{3+} ions directly to energy state L_2. This phenomena is called population inversion because the number of atoms at high energy level are higher than those of low energy level [25]. The optical signal passing through EDFA excites Er^{3+} ions to return to energy level L_1. This return is accompanied with photons emission at the range of 1520nm to 1570nm wavelength. This process is known as stimulated emission. Generated photons due to stimulated emission have the same properties as the signal and are responsible for signal amplification. Unfortunately, stimulated emission is accompanied by spontaneous emission. In fact, as the electrons have a finite excited state life time, some of the electrons return spontaneously to the ground state L_1 and emit photons with random phase. Some of these photons propagate in the direction of the signal as noisy photons and they are also amplified. This process is called amplified spontaneous emission (ASE). Fig. 1.14 details the principle of EDFA process with stimulated and spontaneous emission.

1.2.4-b Inline optical amplification

In long-haul transmission system, the transmission link consists of N spans equally spaced and separated by EDFAs. The use of EDFAs results in the generation of ASE noise. ASE noise reduces significantly the transmission performance. It is commonly considered as additive white Gaussian noise (AWGN). The power spectral density of ASE for a given polarization is expressed as:

$$N_{ASE} = (G-1)h\nu n_{sp} \tag{1.12}$$

where G is the EDFA gain, $h = 6,63\times10^{-34}m^2.kg.s^{-1}$ is Plank's constant and ν is the frequency of light. $h\nu$ corresponds to the photon energy and n_{sp} is the spontaneous emission factor (typically between 1 and 1.5).

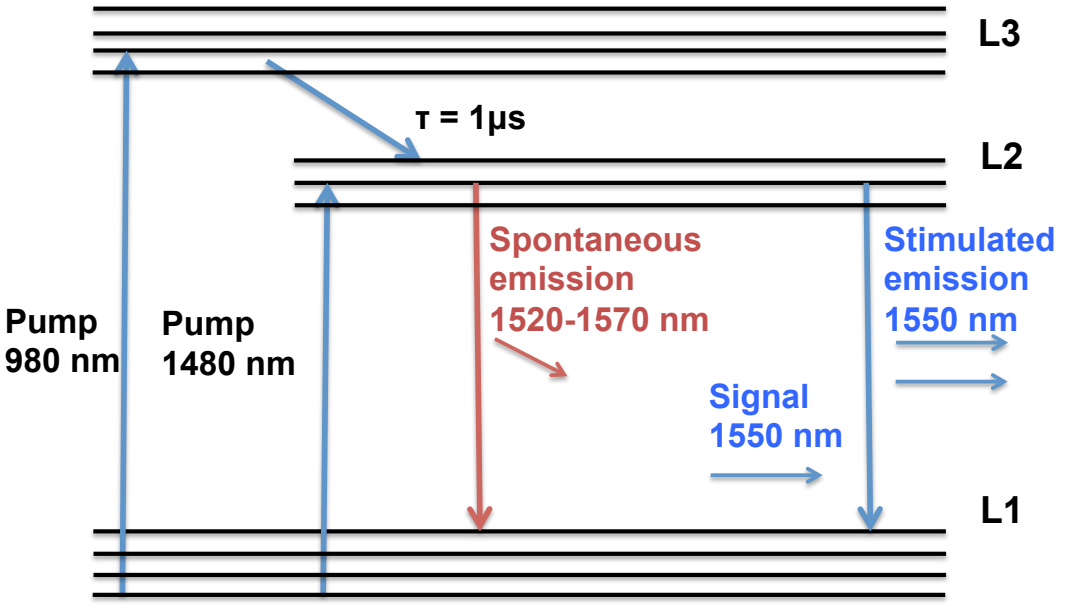

Figure 1.14: Principle of EDFA process

In case of N-span fiber transmission as shown in fig.1.15, the optical signal to noise ratio

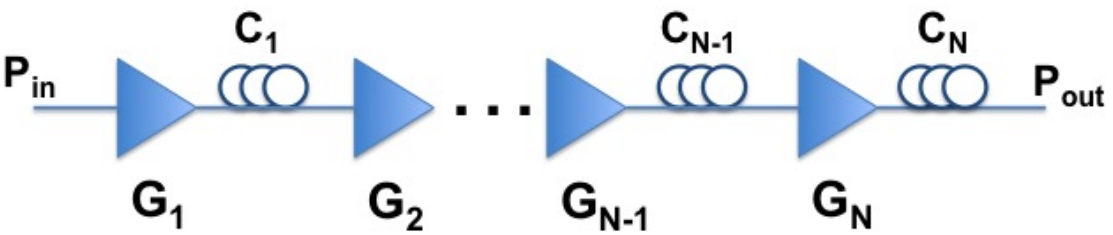

Figure 1.15: Multi-span SMF with EDFA amplifiers

(OSNR), for a reference optical bandwidth B_{ref}, is given by:

$$OSNR = \frac{P}{2NN_{ASE}B_{ref}} \tag{1.13}$$

where P is the total average signal power summed over the two states of polarization. The factor 2 corresponds to ASE power on two polarizations and B_{ref} is usually chosen $B_{ref} =$ 12.5GHz which correponds to a gap in wavelength equal to 0.1nm.

1.2.5 Nonlinear effects

The increase of fiber capacity and spectral efficiency in long-haul transmission systems give rise to nonlinear effects in the optical link. In fact, due to Kerr effect, the refractive index of the optical fiber depends on the intensity of the transmitted signal as [16]:

$$n(P) = n_0 + n_2 I(t) = n_0 + n_2 \frac{P(t)}{A_{eff}} \tag{1.14}$$

where n_0 and n_2 are the linear and nonlinear refractive index respectively, I is the signal intensity, P is the signal power and A_{eff} is the effective core area. The increase of the optical power or the decrease of the effective core area leads to the increase of nonlinear effects in the fiber.

In eq.1.6, nonlinear effects are presented by the nonlinear coefficient γ given by:

$$\gamma = \frac{2\pi n_2}{\lambda A_{eff}} \tag{1.15}$$

Kerr effect induces different kinds of nonlinear effects depending in the optical signal power and the channel spacing in case of multi-channel transmission such as Self-phase modulation (SPM), Cross-phase modulation (XPM), Four wave mixing (FWM) and Cross-polarization modulation (XPolM).

Nonlinear effects can be also caused by inelastic scattering like Stimulated Brillouin Scattering (SBS) and Stimulated Raman Scattering (SRS). Raman and Brillouin scattering are inelastic processes in which part of the optical wave power is absorbed by the optical medium. These effects can be neglected because they manifest only at input powers higher than the typical value used in optical transmission system.

Kerr-induced nonlinear effects are detailed in the following subsections. Notice that other classifications such as those given in [26] exist especially for multi-band systems where the non-linear interference comes from three different origins : the self channel interference (SCI) where the signal of the band of interest creates its own interference, the cross-channel interference (XCI) where the interference corresponds to a term where the signal of the band of interest and the other bands are, and the multi-channel interference (MCI) where a terme depending only on the other bands disturbs the band of interest.

1.2.5-a Self-phase modulation (SPM)

SPM consists in signal phase change due to interactions between the propagating signal and the optical fiber. In fact, the variation of signal intensity during the propagation inside the fiber induces the variations of the refractive index, and that leads to the modification of signal phase. Thus, the nonlinear phase variation is self-induced and the related phenomena is called SPM. SPM causes spectral broadening of the optical pulse. It increases in transmssion system with high input power because the chirping effect is proportional to the transmitted power.

The optical field propagating over an SMF with length L introduces a nonlinear phase ϕ_{NL} expressed as:

$$\phi_{NL}(t) = \frac{2\pi}{\lambda} n_2 I(t) L = \gamma L_{eff} P(t) \tag{1.16}$$

where L_{eff} is the effective length given by:

$$L_{eff} = \frac{1 - e^{-\alpha L}}{\alpha} \tag{1.17}$$

SPM-induced spectral broadening degrade the performance of long-haul optical transmission system. Next generation of long-haul WDM system requires the use of high spectral efficiency modulation formats which necessitate the injection of high input power. The effect of SPM becomes more important with high transmitted power. Several DSP techniques have been proposed to deal with SPM and nonlinear effects in general such as digital back propagation and Volterra based-nonlinear equalizer and that will be detailed later in section 2.3.

1.2.5-b Cross-phase modulation (XPM)

Transmission systems are currently not limited to single-channel systems. Multi-channel transmission used in WDM systems and subcarrier multiplexing used in superchannel approaches for the next generation system generate an other type of nonlinear phase modulation called XPM. In fact, the fiber refractive index depends not only on the intensity of its related optical signal but also on the intensity of other copropagating signals. XPM occurs when two or more optical signals with different wavelength copropagate inside the fiber. As a result, the nonlinear phase shift of a channel with wavelength λ_j depends on its power P_j and also on the power of other copropagating channel due to XPM. The expression of the nonlinear phase shift is given by:

$$\phi_{NL}^{j}(t) = \gamma L_{eff} \left[P_j(t) + 2 \sum_{m \neq j}^{N} P_m(t) \right] \tag{1.18}$$

The first term of the above equation corresponds to the SPM contribution in the nonlinear phase shift while the second term refers to the nonlinear phase shift induced by XPM and related to adjacent propagating channels. The factor 2 indicates that XPM is twice more effective than SPM for the same amount of power [16]. XPM is effective only when the interacting signals are overlapped.

As SPM, XPM reduces the transmission performance by chirping frequency and chromatic dispersion. It does not engender energy transfer between copropagating optical fields. In the presence of CD, XPM can be reduced by increasing the wavelength spacing. In this case, the propagation constants of these channels become sufficiently different. So, copropagating pulses walk away from each other. This walk-off phenomenon limits the interaction time between channels and the XPM effect is reduced.

XPM effect is inversely proportional to the channel spacing and it increases with the number of channels or subcarriers in the context of superchannel transmission. Superchannel approaches are expected to be used for the next generation of long-haul WDM transmission system due their high spectral efficiency. They consist on subcarrier multiplexing with small guard-band. In this context, XPM is more important and its compensation is a hot topic to maintain high system performance.

1.2.5-c Four-wave mixing (FWM)

Unlike SPM and XPM which result in nonlinear phase shift in the optical field, FWM process leads to energy transfer between copropagating channels. Physically, the origin of FWM process lies on nonlinear response of material bound electrons to the applied optical field. In fact, the magnitude of the polarization induced in the medium, which contains linear and nonlinear terms, is governed by the nonlinear susceptibilities. Second order nonlinear susceptibility vanishes due to the isotropic property of silica used for SMF, while the third order nonlinear susceptibility $\chi^{(3)}$ is responsible for generation of FWM process [16]. The induced nonlinear polarization is related to $\chi^{(3)}$ in case of monochromatic plane waves such as WDM signal as :

$$P_{NL} = \epsilon_0 \chi^{(3)}.E^3 \tag{1.19}$$

The derivation of eq.1.19 shows that for carrier frequencies ω_p, ω_q and ω_r, FWM generates new signals at frequency ω_{pqr} by combining these frequencies and it is given by [27]:

$$\omega_{pqr} = \omega_p + \omega_q - \omega_r \tag{1.20}$$

In multi-channel system with N wavelengths, the number of FWM-generated signals M is expressed as :

$$M = \frac{N^2(N-1)}{2} \tag{1.21}$$

FWM process results in power transfer between copropagating channels. That leads to power depletion which degrades the performance of channels. In addition, FWM can be an inter-channel crosstalk if the generated signal fall into other copropagating channels. That results in significant system performance degradation due to crosstalk among the channels. FWM depends on fiber dispersion and channel spacing. Fiber dispersion varies with wavelength, that means FWM-generated signal has different velocity than the original signals. Thus, increasing the fiber dispersion limits interactions between signals and reduces the power transfer to the new generated signals. Increasing the channel spacing decreases also FWM effect.

SPM and XPM are mainly related to the signal power and become more significant at high bit rate system. However, FWM effect is independent of the bit rate and is critically related to fiber dispersion and channel spacing. Therefore, FWM will be a serious limitation in the next generation long-haul WDM system due to the use of superchannel transmission with small guard-band.

1.2.5-d Cross-polarization modulation (XPolM)

Polarization division multiplexing is adopted today in optical transmission system due to its improvement in spectral efficiency. It consists in transmitting the signal in both orthogonal State of Polarization (SOP) of the wavelength. In multi-wavelength transmission system, XPolM occurs when the SOP of a transmitted channel depends on the SOP of other copropagating

channels which have random propagation inside the optical fiber because of PMD. The variation of the SOP can be expressed in Stokes space as [16]:

$$\frac{\partial S_j}{\partial z} = \gamma S_0 S_j \tag{1.22}$$

where S_j is the Stokes vector of the considered channel j and S_0 is the sum of all Stokes vectors of N copropagating channels and given by:

$$S_0 = \sum_{i=1}^{N} S_i \tag{1.23}$$

XPolM effect consists in rotating the SOP of the considered channel j around the instantaneous sum S_0 of Stokes vectors of the copropagating channels. It results in depolarization of the transmitted signal and that causes fading and channel crosstalk for dual polarization transmission systems[28]. XpolM can dominate XPM effect and it can be approximated as additive Gaussian noise [29].

1.3 Conclusion

In this chapter, we described the evolution of optical fiber communication systems. Then, we gave the main fiber propagation impairments. We highlight fiber nonlinear effects because of their strong impact for the next generation of long-haul WDM systems. Next generation of long-haul WDM systems is expected to operate at $400Gbps/1Tbps$ bit rate. Such high bit rate can be reached by using advanced modulation formats and superchannel systems. However, nonlinear effects compensation is mandatory to get the desired performance in terms of transmission reach. High spectral efficiency modulation formats, superchannel approaches and the state of the art about nonlinear effects mitigation will be detailed in the next chapter.

CHAPTER 2

400GBPS/1TBPS SUPERCHANNEL TRANSMISSION SYSTEM

Two main methods are expected to be used for next generation of long-haul WDM transmission systems in order to increase single-mode fibers capacity. The first one is the use of multi-level modulation formats allowed by coherent detection. The second approach exploits the benefits of parallel processing. Multiples optical carriers are generated by different transmitters and then combined with small guard band to deliver the desired bit rate. This approach is known as superchannel transmission. Superchannel systems are strongly affected by fiber nonlinear effects. Thus, fiber nonlinearity mitigation is required. The principle of multi-level modulation formats and superchannel approach are highlighted in the following. After that, a state of the art about nonlinear effects compensation is given.

2.1 High spectral efficiency modulation formats

Modulation can be defined as the process of encoding bits of information from a message source in a manner suitable for transmission. It can be in amplitude (amplitude shift-keying), phase (phase shift-keying), polarization (polarization shift-keying) or a combination of some of them such as multi-level modulation formats.

Multi-level modulation formats were introduced with coherent optical transmission systems. Coherent detection allowed the detection of amplitude and phase simultaneously. These two degrees of freedom are efficiently used in multi-level modulation format. This kind of modulation encodes multiple bits per transmitted symbol and it is a promising approach to increase spectral efficiency. In fact, while the spectral efficiency of binary modulation formats is limited to 1 bit/s/Hz/polarization. Multi-level modulation formats with m_0 bits of information per symbol can achieve a spectral efficiency up to m_0 bit/s/Hz/polarization, m_0 is given in function of number of constellation states M as:

$$m_0 = \log_2(M) \tag{2.1}$$

The modulated symbols are mapped to analog waveforms before being transmitted over the optical channel. They are sequentially transmitted at a rate R_s. The symbol period is $T_s = \frac{1}{R_s}$. The bit rate is related to R_s by [30]:

$$R_b = d.\log_2(M).R_s \tag{2.2}$$

where d is the degree of freedom (typically, number of polarizations or of modes or of cores).

Modulation is also characterized by the minimum distance between the closest points in the constellation and the average energy per symbol E_s.

QPSK modulation was used in the standard 100Gbps optical long-haul WDM systems. Higher order modulation formats such as (16-QAM) are expected to be used for the next generation of long-haul WDM systems. M-QAM modulation consists in varying both amplitude and phase of the signal. It can be considered as generalization of QPSK, which known also as 4-QAM. M-QAM modulation combines two carriers occupying the same frequency band and differ by a $\frac{\pi}{2}$ phase shift. These two carriers are amplitude-modulated and called in-phase (I) signal and quadrature-phase (Q) signal. However, QAM modulation with higher M requires higher OSNR which leads to higher sensitivity to nonlinear effects in optical fiber. Fiber nonlinearity, such as SPM and XPM, strongly affects QAM transmission and causes power-dependent phase rotation. That can strongly reduce the transmission performance and in particular the transmission distance. Fig.2.1 shows the constellations of respectively 16-QAM, 32-QAM and 64-QAM. Minimum distance between constellation points is inversely proportional to M while the spectral efficiency increases with M. 16-QAM modulation is a potential candidate to be

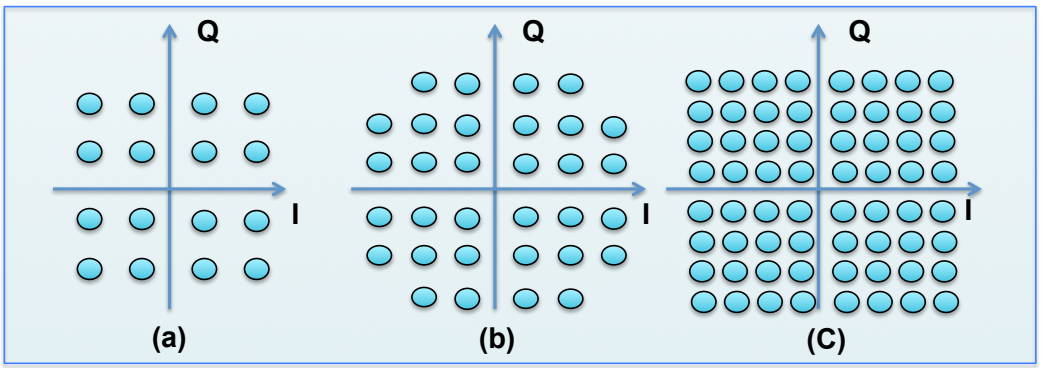

Figure 2.1: (a) 16-QAM, (b) 32-QAM, (c) 64-QAM

used in the next generation of long-haul WDM systems. It increases the spectral efficiency by a factor two compared to QPSK. In the other hand, It increases the sensitivity to fiber nonlinear effects but it still relatively reduced compared to higher order modulation such as 32-QAM and 64-QAM. Thus, 16-QAM meets the demand in higher data rates and it can be used for the next generation systems in combination with DSP-based nonlinearity mitigation techniques.

16-QAM increases also transmitter and receiver complexity in comparison with QPSK modulation. QAM signal can be generated with IQ modulator consisting of Mach-Zehnder Modu-

lator (MZM) with $\frac{\pi}{2}$ phase shift. Several techniques are proposed to generate 16-QAM signal electrically [31] [32], it can be also generated optically by combining two optical QPSK signals with different amplitude levels.

2.2 Superchannel transmission systems

The steadily growing need for transmission capacity in future optical fiber communication networks requires an increased transmitted data rate per fiber. Our works focus on increasing data rates of standard single-mode fibers. For this kind of fibers, a way to split the wavelength (which is too wide to be treat entirely) is to consider a superchannel approach. Superchannel systems based on multi-band OFDM and Nyquist-WDM are detailed in the following.

2.2.1 OFDM based superchannel transmission system

OFDM modulation is a multi-carrier technique. It was introduced in wireless communication systems to deal with inter-symbol interference in a multi-path channels. Thanks to coherent detection, coherent optical OFDM was proposed for 100Gbps transmission systems [33]. CO-OFDM was shown also extreme robustness against chromatic dispersion and polarization mode dispersion thanks to its cyclic prefix. The principle of OFDM modulation and superchannel based on multi-band CO-OFDM are detailed hereafter.

2.2.1-a OFDM principle

It consists in splitting a high data rate stream into several low-rate streams. These low-rate streams are transmitted simultaneously over orthogonal subcarriers. Each subcarrier is separately modulated in frequency, phase or amplitude. Multi-level modulation formats can be also used to modulate OFDM subcarriers. Mathematically, the baseband signal of N_{sc} OFDM subcarriers can be expressed as [34]:

$$s(t) = \sum_{j=0}^{+\infty} \sum_{k=0}^{+N_{sc}-1} c_{kj} \Pi(t - jT_s) e^{2i\pi f_k t} \tag{2.3}$$

where c_{kj} is the j-th information symbol at the k-th subcarrier with frequency f_k, T_s is the length of the OFDM frame, and $\Pi(t)$ is the pulse shaping function.

To satisfy the condition of orthogonality, subcarriers must be spaced at multiples of the inverse of the frame as given by [34]:

$$f_k - f_l = \frac{k-l}{T_s} \tag{2.4}$$

if the pulse shaping function is the rectangular one of duration T_s.

Due to orthogonality condition, the information transmitted over the subcarriers can still be separated despite strong signal spectral overlap as shown in fig. 2.2.

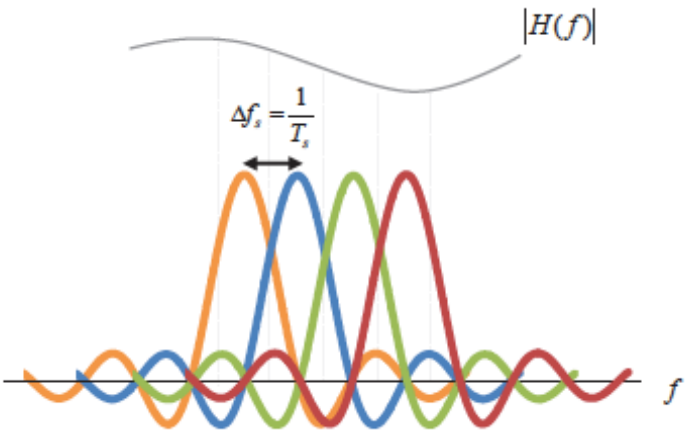

Figure 2.2: OFDM spectrum for a random channel frequency response [35]

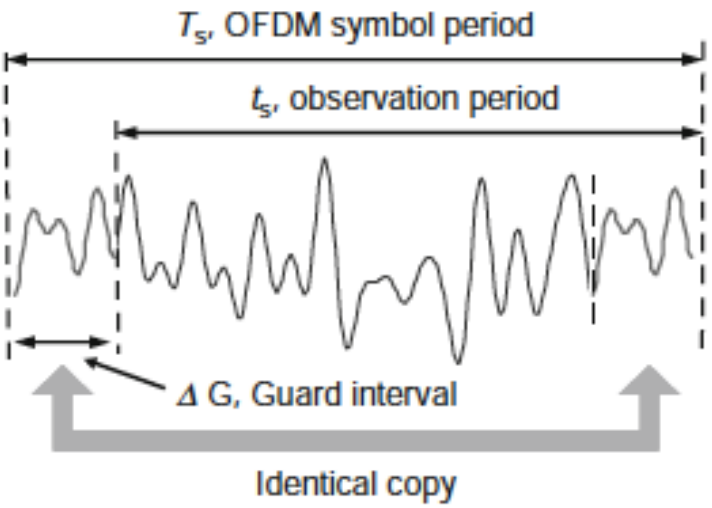

Figure 2.3: Time domain OFDM signal for one OFDM symbol [34]

However, in frequency selective channel, orthogonality is not ensured due multi-path interference or dispersion in case of optical transmission. That leads to intercarrier interference (ICI) which reduce the transmission performance. To avoid ICI, a guard interval, known as cyclic prefix (CP), is inserted between OFDM subcarriers. CP contains a copy of small part of the end of the OFDM symbol as shown in fig.2.3. CP avoids interference and it is chosen to be greater than the maximum delay spread of the channel. OFDM modulation and demodulation can be done based on IFFT and FFT as it will be detailed later in this section.

2.2.1-b Coherent optical OFDM system

CO-OFDM has inherited the advantages of OFDM modulation in wireless systems in terms of robustness against dispersion. However, as the optical fiber is a nonlinear medium, CO-OFDM suffers from fiber nonlinear effects. In fact, nonlinearity in wireless system are caused by am-

plifiers, while EDFA does not generate nonlinearity and nonlinear effects are generated mainly by the fiber itself. These effects are proportional to the data rate and inversely proportional to the guard-band, which means that fiber nonlinear effects will significantly increase in the context of OFDM based superchannel transmission. The principle of multi-band approach and the transmitter and receiver architectures of multi-band and dual-polarization CO-OFDM are given in the following.

Multi-band approach Given a predefined bandwidth (typically the WDM wavelength), it has been proposed to split the bandwith into several bands in order to work slowly on each band. Indeed, the generation of single-band OFDM on an entire WDM wavelength (of order 100GHz) requires a 200Gsamples/s ADC/DAC which are not commercially available yet. Notice that in low data rate old transmission systems, only a part of the WDM wavelength was occupied and a large guard band was present which led to low-speed ADC/DAC. Now wasting such a guard band is not possible at all if we would like to satisfy the data rate constraints.

When OFDM is used, this leads to the so-called multi-band OFDM (MB-OFDM) which has been considered for the next generation of long-haul WDM systems. Then the net bit rate can be expressed as [36]:

$$R = R_s.N_b.N_{pol}.\log_2(M) \tag{2.5}$$

where R_s is the symbol rate (of one band), N_b is the number of bands, $N_{pol} = 2$ is case of dual-polarization transmission and M is the number of constellation points of modulation.

In fig.2.4, we depict MB-OFDM spectrum for one polarization where the super-channel is a more generic name for the WDM wavelength. Notice that these OFDM based sub-bands are generated by different transmitters and decoded separately at the receiver side. A the

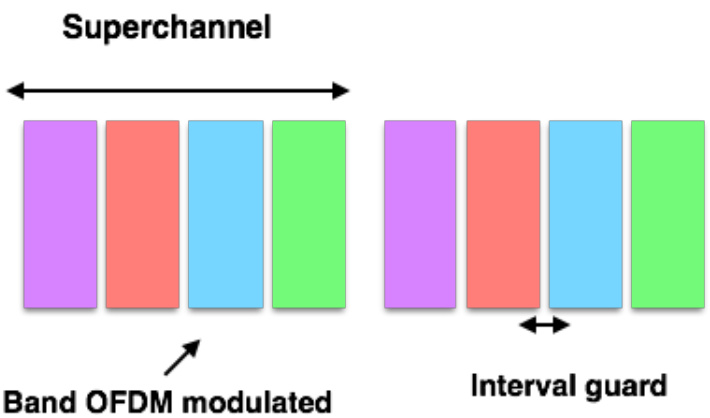

Figure 2.4: Multi-band OFDM spectrum

receiver, a band selection is done using a filter with a bandwidth slightly larger than the sub-band bandwidth. After that, each band is digitally processed and then detected separately.

MB-OFDM transmitter In MB-OFDM system, the CO-OFDM sub-bands can be generated using different transmitters at different wavelengths. A combiner is used to aggregate the generated sub-bands and the total transmitted signal X on polarization x or y can be written as

$$X_{x/y} = \sum_{n=1}^{N_b} X_{x/y,n} \tag{2.6}$$

where N_b is the number of sub-bands. The transmitter set-up for each sub-band is shown in fig.B.5.

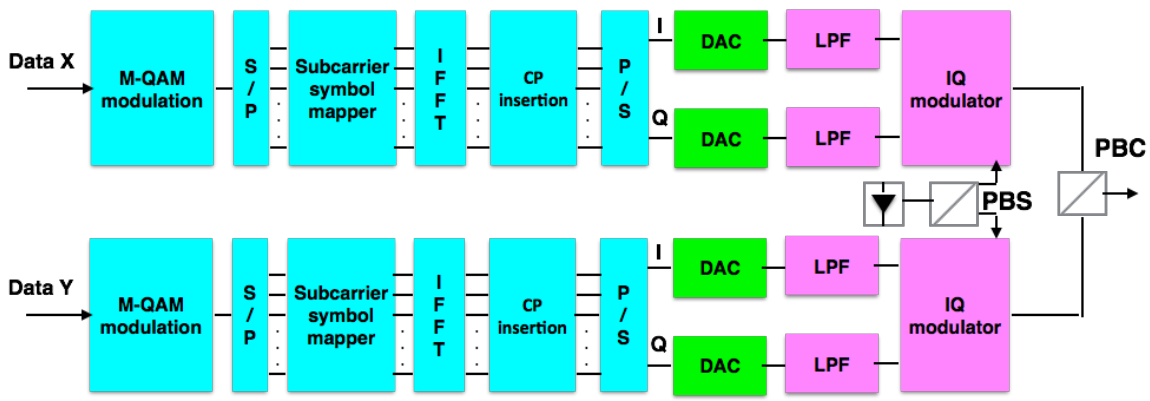

Figure 2.5: Transmitter set-up for the generation and processing of one OFDM band

First of all, the generated binary data are mapped onto M-QAM symbols. The N_{sc} M-QAM symbols are passed through serial to parallel conversion. Training sequence and pilot symbols are added to the useful data to be used for channel estimation and carrier phase recovery at the receiver. Synchronization sequence can be added also to ensure frequency and time synchronization. In MB-OFDM system, a guard band is inserted between sub-bands to avoid interference. This can be done by forcing lateral subcarriers to be null. After that, the information symbols are simultaneously modulated into N_{sc} orthogonal subcarriers using an IFFT of size N_{sc}. The output corresponds to the time domain OFDM signal.

Optical fiber transmission is vulnerable to chromatic dispersion and polarization mode dispersion which leads to ICI. Thus, cyclic prefix is added to deal with ICI and it should be larger than the total amount of dispersion to efficiently remove the interference. This condition is given by [37]:

$$\tau_{cp} \geqslant \tau_{maxCD} + \tau_{maxDGD} \tag{2.7}$$

Then, OFDM signal is passed by parallel to serial conversion and the digital output real(I) and imaginary (Q) parts are converted to analog domain using two DACs. Low-pass filters are used to remove the aliasing replicas before the up-conversion of the signal to the optical domain. The up-conversion is performed by IQ modulator composed by two MZM and a $\frac{\pi}{2}$ phase shift.

An identical process is done for the second polarization. The two polarization signal are then combined to get DP-CO-OFDM signal for each sub-bands. The final step before the transmission over the optical fiber is the OFDM modulated sub-bands aggregation. The MB-OFDM signal processing and detection at the receiver is detailed in the following.

MB-OFDM receiver The received signal is passed firstly by a dual-polarization receiver based on coherent detection. A polarization beam splitter separates the signal into two orthogonal polarization states. In MB-OFDM transmission system, the receiver processes band by band. So, a band selection and optical filtering is done to get the signal of each band separately. Then, an ADC performs the analog to digital conversion.

In superchannel transmission, the use of advanced modulation formats and multi-band approach with small guard-band strongly increase fiber nonlinear effects. Thus, nonlinear effects compensation is necessary to get high spectral efficiency without loss in system performance such as transmission reach. A nonlinear equalizer based on digital signal processing is used to compensate nonlinear effects. Several techniques are proposed such as digital back-propagation(DBP) and volterra series based equalizer and they will be detailed in the section 2.3. Finally, OFDM demodulation and signal detection is done. Fig.2.6 shows the MB-DP-CO-OFDM receiver set-up. Fig.2.7 emphasizes DP-CO-OFDM signal demodulation and signal detection.

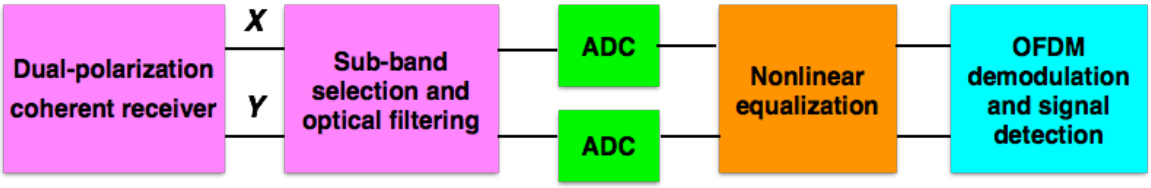

Figure 2.6: MB-DP-CO-OFDM receiver set-up

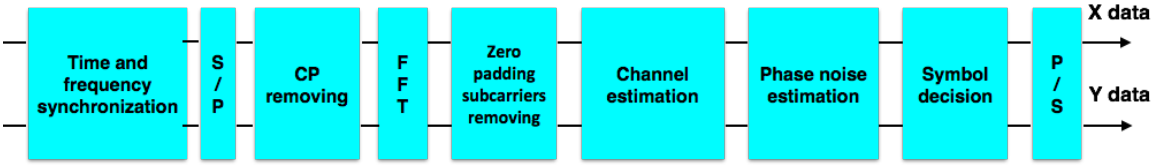

Figure 2.7: DP-OFDM demodulation and signal detection

Time and frequency synchronizations are required in OFDM system. In fact, an incorrect estimation of the beginning of the OFDM frame and the location of OFDM subcarriers results in loss of orthogonality. That leads to strong reduction of performance because of inter-symbol interference (ISI) and inter-carrier interference (ICI) [38]. Different algorithms are proposed for time synchronization such as Schmidl and Cox [39] method and Shi and Seepedin [40].

Frequency synchronization consists in compensating the relative carrier frequency offset (CFO) between lasers used in transmission and reception. CFO leads to ICI and SNR penalty [34] and it can be quantified by the normalized CFO with respect to the subcarrier spacing Δf given by $\epsilon = \frac{\Delta_{CFO}}{\Delta f}$. The main idea for CFO estimation and correction is firstly computing the integer and fractional parts of ϵ and then correcting the phase shift in time domain. It can be also done in frequency domain by shifting the spectrum circularly.

After that, cyclic prefix is removed before passing to frequency domain by applying FFT. Null subcarriers, used to insert guard-band between sub-bands, are suppressed and then channel estimation is performed based on training sequence. Channel estimation is required to separate the two polarizations and to compensate phase rotation and attenuation on subcarriers. The most popular estimation technique is suggested in [41] and it is based on least square estimation. To reduce the computational complexity, time-interleaved training sequences are used. The main idea is transmitting training sequence s_1 on polarization x for the first time slot t_1 and training sequence s_2 on polarization y in the second time slot t_2. The received signal Y_k for the k-th subcarrier can be written as:

$$Y_k = H_k . \begin{pmatrix} s_{1,t_1}(k) & 0 \\ 0 & s_{2,t_2}(k) \end{pmatrix} + \begin{pmatrix} n_{t_1}(k) \\ n_{t_2}(k) \end{pmatrix} \tag{2.8}$$

where H_k is channel matrix and $[n_{t_1}(k) n_{t_2}(k)]^{\mathrm{T}}$ represents the frequency-domain noise within subcarrier k. Then the estimation of channel matrix $\hat{H}_k$ is computed by:

$$\hat{H}_k = Y_k . S_k^{\#} \tag{2.9}$$

here S_k is the 2×2 matrix of training sequence. $S_k^{\#} = (S_k^{\mathrm{H}} S_k)^{-1} S_k^{\mathrm{H}}$ and the superscript H denote the conjugate transpose.

After channel estimation and equalization, phase noise compensation is performed using pilots tones. Phase noise affects OFDM signal by creating ICI and a common phase error (CPE) to all the subcarriers of the same OFDM symbol. Mainly, two methods are used for CPE estimation and correction. The first one, firstly developed for wireless systems, uses known data at certain subcarriers as pilot tones to estimate the common phase rotation of all subcarriers without taking into accounts ICI [42]. The second one consists in inserting RF pilot in the middle of the OFDM signal spectrum [43]. This pilot, which experiences the same phase noise as the OFDM signal, is extracted at the receiver using low-pass filter and conjugated. Then, CPE is removed by multipiling the OFDM signal by the RF pilot. This method reduces also ICI caused by the phase noise.

Finally, symbol detection is done based on zero-forcing (ZF) equalizer. The detected symbol is obtained by applying a threshold detector on the following signal:

$$Z_k = \hat{H}_k^{\#} . Y_k . \tag{2.10}$$

ZF equalization is used due to its low-complex implementation, and is optimal for CD and PMD impairments since they are represented by an unitary matrix.

2.2.2 Nyquist-WDM superchannel transmission system

Until its deployment in the mid-1990's, WDM system has evolved in terms of density of channels in the EDFA bandwidth to meet the demands on fiber capacity. From low density such as in coarse WDM (CWDM) to very high density, WDM systems can be classified based on channel spacing. Let Δf be the channel/band spacing. We define $\delta = \frac{\Delta f}{R_s}$ as the channel/band spacing factor. The following table 4.1 summarizes the different classes of WDM system in function of the channel spacing factor.

Table 2.1: WDM system classes

Definition	channel spacing factor δ
Coarse WDM	$\delta > 50$
WDM	$\delta > 5$
Dense WDM	$1.2 < \delta \leq 5$
Quasi-Nyquist WDM	$1 < \delta \leq 1.2$
Nyquist WDM	$\delta = 1$
Super-Nyquist WDM	$\delta < 1$

The deployment of coherent detection and multi-level modulation formats allowed the reduction of symbol rate and the increase of spectral efficiency. That results in WDM systems more and more dense in terms of number of channels. Quasi-Nyquist WDM, Nyquist WDM and super-Nyquist WDM are known as superchannel systems and they are expected to be implemented for the next generation of long-haul transmission systems.

2.2.2-a Nyquist-WDM superchannel concept

The principle of Nyquist WDM approach consists in the aggregation of multiple channels, also called subcarriers in the state-of-the-art (Be careful : these subcarriers correspond to a band –and not to a subcarrier– in a multi-band OFDM), with channel spacing equal to the Nyquist limit for transmission without inter-symbol interference. The multiple subcarriers have a almost rectangular spectrum –typically obtained thanks to Root Raised-Cosine (RRC) with a low roll-off– and construct a so-called superchannel. They are routed through optical add-drop mulitplexers(OADMs) and wavelength selective switches (WSSs) as a single entity.

Two configurations of reduced guard-band WDM system are also subject of research demonstrations to evaluate their performance. The first one is called quasi-Nyquist WDM, in this case the subcarrier spacing is slightly higher than symbol rates [44]. The second approach is known as super-Nyquist WDM and it allows an overlap between optical subcarriers [45]. Fig.B.4 shows the spectrum of Nyquist WDM signal. The transmitter and receiver set-up of Nyquist-WDM tranmission system are given in the following.

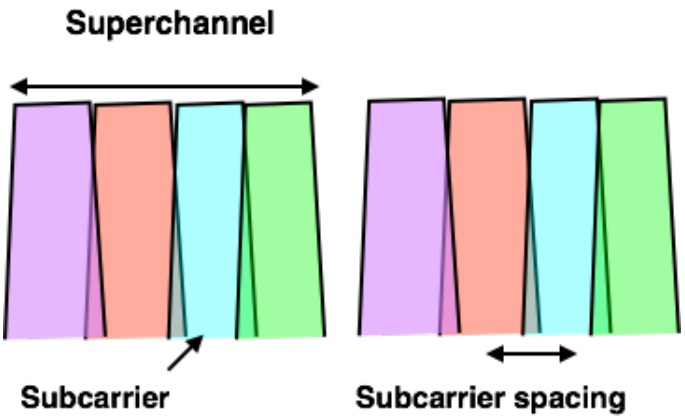

Figure 2.8: Nyquist WDM superchannel system

2.2.2-b Nyquist WDM transmitter

As the case of MB-OFDM transmitter, the desired number of optical subcarriers are generated by different transmitter with different wavelengths. After that, these subcarriers are combined with spacing equal to symbol rate and then transmitted over the optical link. The transmitted signal is given by eq.2.6. For each subcarrier, the generated binary data for both polarizations are mapped onto M-QAM symbols. After digital-to-analog conversion, a IQ-modulator is used for up-conversion of the analog signal to the optical domain.

The transmitter structure of each subcarrier is depicted in fig.B.8. A root raised-cosine

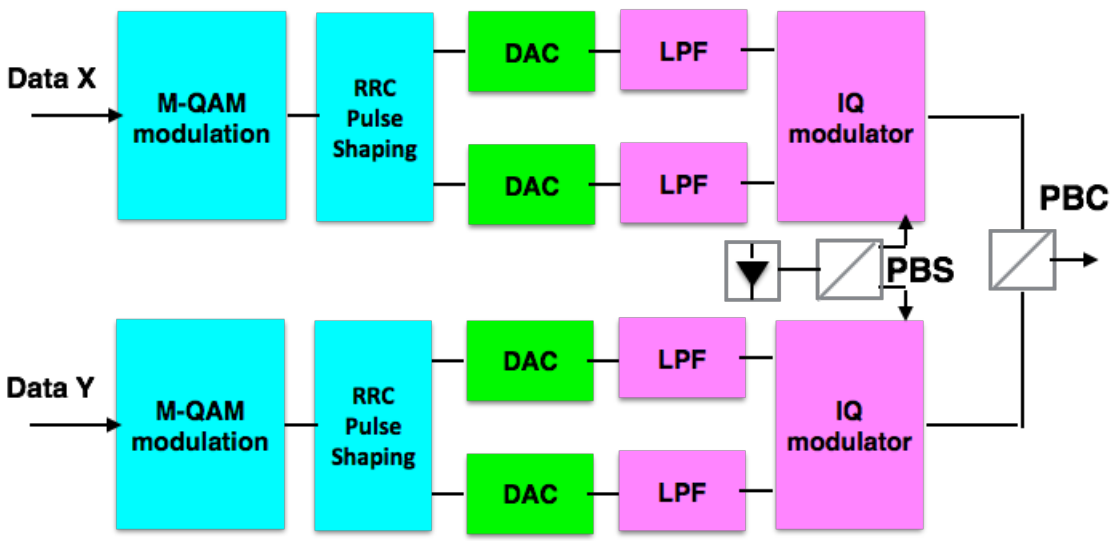

Figure 2.9: Nyquist WDM transmitter set-up

filter (RRC) is used to spectrally shape the optical subcarriers. RRC filter requires additional bandwidth expressed as a percentage of the symbol rate and called roll-off factor. RRC filter

satisfies Nyquist criterion of transmission without interference.

2.2.2-c Nyquist WDM receiver

At the receiver side, the received signal is passed first by a dual-polarization coherent receiver. A local oscillator (LO) is used to extract the amplitude and the phase for each polarization. Then, four balanced photodetectors (one for I, one for Q per polarization) ensure the detection of the signal components. Subcarrier selection is done by changing the frequency of the LO so that each subcarrier signal is DSP processed and detected separately. After that, the signal is filtered using low-pass filter and an ADC convert it to digital domain. Fig.B.9 shows the receiver set-up for Nyquist WDM transmission. Fiber impairments are fully mitigating by DSP.

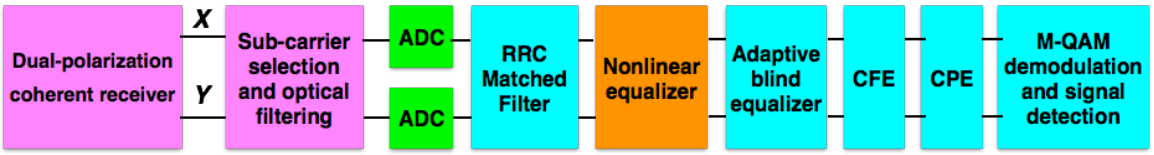

Figure 2.10: Nyquist WDM receiver set-up

The first step of DSP is nonlinear effects compensation. Nonlinear equalizer (NLE) is applied to combat fiber nonlinear effects which present a strong limitation for superchannel transmission systems. In fact, high bit rate transmission with Nyquist subcarrier spacing significantly increase nonlinearity such as SPM, XPM, XpolM and FWM. NLE compensates both nonlinear effects and the linear CD.

Then, an adaptive blind equalizers is used to compensate for dispersion like PMD and residual CD. Adaptive blind equalizers have simple implementation and avoid the decrease of spectral efficiency by using training sequence. Several equalizers have been used such as Constant Modulus Algorithms (CMA) mainly used for PSK modulation [46], Radius Directed Equalizer (RDE) which is an adaptation of CMA to QAM modulation [47], and Decision-Directed equalizer (DD) [48]. Generally, the principle of these equalizers consists in estimating FIR filter coefficients by minimizing the following cost function for each polarization:

$$J_{Eq}(w_{x/y}) = \mathbb{E}[J_{Eq,n}(w_{x/y})] \tag{2.11}$$

where $J_{Eq,n}(w_{x/y}) = (\mid z_{x/y}(n) \mid^2 - R_{Eq})^2$ with the equalizer $w_{x/y}$ for polarization either x or y and the equalizer output $z_{x/y}$ for polarization either x or y. R_{Eq} refers to the modulus of the constellation which is constant in case of CMA and variable for RDE. It corresponds to the decision symbol when DD equalizer is applied.

To avoid ISI, as described in MB-CO-OFDM receiver 2.2.1-b, carrier frequency estimator (CFE) is used to estimate and correct the CFO between lasers at the transmitter and receiver. After the compensation of fiber impairments, constant phase estimation is done based

on Viterbi-Viterbi algorithm. The basic idea of Viterbi-Viterbi algorithm is elevating the signal to the M-th power for M-PSK modulation [49] and to the 4-th power when the signal is M-QAM modulated [50]. Finally, symbol decision is performed by a threshold detector.

2.3 Nonlinear effects compensation techniques: State of the art

Nonlinear Kerr effect is a strong limitation factor for increasing fiber capacity. Kerr-induced nonlinear effects increase with the injected optical power and the decrease of channel spacing. Superchannel systems use multi-level modulation formats and subcarriers multiplexing at symbol rate. This kind of transmission systems is strongly vulnerable to fiber nonlinearity. Therefore, nonlinear effects mitigation is a hot topic currently for increasing fiber capacity without loss in system performance.

Several approaches have been proposed to compensate for fiber nonlinear effects [51]. Some of these techniques such as phase-conjugation, digital back-propagation (DBP) and Volterra based nonlinear equalizer (VNLE), have attracted more attention and they can be presented as promising methods to deal with fiber nonlinearity. Phase conjugation consists in inverting the spectrum of the data signal in the middle of the transmission link [52]. It can be implemented either in optical domain or electrical domain. However, it requires precise positioning and symmetric link design to get the desired performance.

Thanks to the introduction of coherent detection, DSP algorithms have been employed to combat fiber impairments and in particular nonlinear distortion. DBP and third-order VNLE have been suggested to deal with fiber nonlinearity in digital domain. These techniques provide an approximate numerical solution of the Manakov equation (NLSE in case of single-polarization transmission) given by:

$$\frac{\partial Y_{x/y}}{\partial z} + j\frac{\beta_2}{2}\frac{\partial^2 Y_{x/y}}{\partial t^2} + \frac{\alpha}{2}Y_{x/y} = j\gamma'(|Y_x|^2 + |Y_y|^2)Y_{x/y} \tag{2.12}$$

where $Y_{x/y}$ is complex field envelope for polarization x/y and $\gamma' = \frac{8}{9}\gamma$. The solution of the Manakov equation is not known analytically only for particular cases such as zero-dispersion transmission. Thus, numerical solution such as DBP and VNLE have been proposed.

2.3.1 Digital back propagation

DBP concept consists in transmitting the received signal through a fictitious fiber with inverse parameters. It is based on split-step Fourier method (SSFM). SSFM is an efficient technique and widely used to solve eq.B.2. SSFM divides the fiber link into several steps with small distance. For each step, the fiber link is modeled as a concatenation of linear and nonlinear operators.

By introducing the linear operator $\hat{D}$ and the nonlinear operator $\hat{N}$, eq.B.2 can be written as:

$$\frac{\partial Y_{x/y}}{\partial z} = (\hat{D} + \hat{N})Y_{x/y} \tag{2.13}$$

where $\hat{D} = -j\frac{\beta_2}{2}\frac{\partial^2}{\partial t^2} - \frac{\alpha}{2}$ and $\hat{N} = j\gamma'(|Y_x|^2 + |Y_y|^2)$. Then, the transmitted signal can be calculated from the inverse Manakov equation that governs the wave propagation inside the virtual fiber:

$$\frac{\partial Y_{x/y}}{\partial z} = (\hat{D}^{-1} + \hat{N}^{-1})Y_{x/y} \tag{2.14}$$

This equation can be solved using the noniterative asymmetric SSFM. Different ways of DBP implementation have been proposed depending on the implementation order of the linear and the nonlinear operators [53][54]. Preferably, the linear operator is applied in the first place because nonlinear effects are more important at high input power which is the case at the end of the virtual fiber.

The implementation of the linear operator is performed in frequency domain. the linear operator $\hat{D}$ compensate for the CD and its output is given by:

$$Z^{CD}_{x/y}(\omega, z) = Y_{x/y}(\omega, z)e^{-jh\left(\frac{\alpha}{2} + \frac{\beta_2}{2}\omega^2\right)} \tag{2.15}$$

After that, the nonlinear operator is applied in time domain to compensate for Kerr-induced

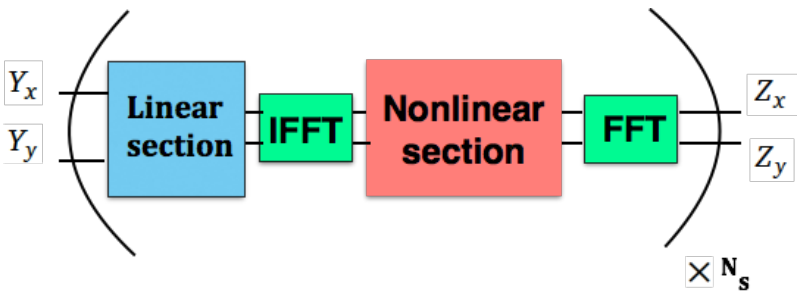

Figure 2.11: DBP principle for dual-polarization system

nonlinear effects. The output of the equalizer is expressed by:

$$Z_{x/y}(t, z) = Z^{CD}_{x/y}(t, z)e^{-j\varphi\gamma' h(|Z^{CD}_x|^2 + |Z^{CD}_y|^2)} \tag{2.16}$$

where $0 < \varphi < 1$ is a real-valued optimization parameter.

DBP technique has been assessed by simulation and experimental researches. As showed in fig.2.11 where N_s is the number of steps, DBP can be realized either in single-step per span or multi-step per span. It is a precise technique and it provides high performance at small step size. However, it has high computational load for real-time implementation as the number of steps per span increase. Some new approaches are proposed to reduce the complexity of DBP based on SSFM such as weighted SSMF [55].

In superchannel transmission system, DBP performance are affected by nonlinear effects depending on the copropagating bands such as FWM, XPM and XpolM.

2.3.2 Nonlinear effects compensation based on Volterra series

Fiber nonlinear effects can be modeled based on Volterra series transfer function (VSFT). In fact, VSTF is a powerful tool for solving the Manakov equation eq.B.2 (NLSE in case of single-polarization transmission) as shown in [56]. After modeling the optical channel based on VSTF, the p-th order theory developed by Schetzen [57] is used to derive the inverse (I)VSTF kernels in function of VSTF ones. IVSTF kernels characterize the nonlinear equalizer which compensate for fiber nonlinearity and CD. In the following, an overview about Volterra series is given. Then VSTF based fiber model is described before detailing Volterra NonLinear Equalizer (VNLE).

2.3.2-a Volterra Series overview

The Volterra series is a model for nonlinear behavior, it can be considered as Taylor series with memory. Whereas the usual Taylor series only represents systems that instantaneously map the input to the output, the Volterra series characterize systems in which the output also depends on past inputs. Mathematically, it is expressed as the following equation [58]:

$$y(t) = \sum_{N=1}^{\infty} \int_0^{\infty} \int_0^{\infty} \hbar_n(\tau_1, .., \tau_n) x(t-\tau_1)...x(t-\tau_n) d\tau_1 ... d\tau_n \tag{2.17}$$

where x is the input of the system, y is the output, and $\hbar_n(\tau_1, .., \tau_n)$ is called the n-th order Volterra kernel. This is equivalent to the following operator formulation :

$$y(t) = H[x(t)] = \sum_{n=1}^{\infty} H_n[x(t)] \tag{2.18}$$

where each H_n is called the n-th order Volterra operator given by:

$$H_n[x](t) = \int_{-\infty}^{\infty} ... \int_{-\infty}^{\infty} \hbar_n(\tau_1, .., \tau_n) x(t-\tau_1)...x(t-\tau_n) d\tau_1 ... d\tau_n \tag{2.19}$$

The first-order term is the convolution integral typical of linear dynamical systems with $\hbar_1$ being the impulse-response function. The higher order terms are multiple convolutions, involving products of the input values for different delay times.

For the optical fiber, because of the band pass nature, the even order terms in the Volterra transfer function will not generate in-band frequency components, thus the even order terms in the band pass Volterra series can be ignored.

2.3.2-b Fiber model based on Volterra series

We consider an SMF with N spans each of them with length L as transmission channel. Let X be the transmitted dual-polarization signal corresponding to the sequence S of information symbols and Y the fiber output of the N-th span. In the frequency domain, assuming a third-order Volterra approximation, the solution of eq.B.2 can be expanded as follows

$$Y_{x/y} = H_1[X_{x/y}] + H_3[X_x, X_y] \tag{2.20}$$

where H_1 and H_3 are the first-order and third-order VSTF operators. The corresponding expression based on VSTF kernels (in the frequency-domain) is given by:

$$Y_{x/y}(\omega) = h_1(\omega)X_{x/y}(\omega) + \iint h_3(\omega_1,\omega_2,\omega-\omega_1+\omega_2) \times [X_x(\omega_1)X_x^*(\omega_2)+X_y(\omega_1)X_y^*(\omega_2)]X_{x/y}(\omega-\omega_1+\omega_2)d\omega_1 d\omega_2 \tag{2.21}$$

where the superscript ()* stands for the complex conjugate. The kernels h_1 and h_3 are available in [59] and equal to

$$h_1(\omega) = e^{-j\omega^2\beta_2 NL/2} \tag{2.22}$$

$$h_3(\omega_1,\omega_2,\omega-\omega_1+\omega_2) = \frac{-jc'h_1(\omega)}{4\pi^2}\sum_{k=0}^{N-1} e^{-jk\beta_2\Delta\Omega L} \tag{2.23}$$

with $\Delta\Omega = (\omega_1-\omega)(\omega_1-\omega_2)$ is the spacing between the discrete frequencies in the sampling spectrum and $c' = \gamma' L_{eff}$ with L_{eff} the effective length defined in eq.1.17.

2.3.2-c Volterra based nonlinear equalizer

Like DBP, VNLE attempts to construct the inverse of the channel. Using p-th order theory, up to third-order inverse Volterra operator K_i can be computed from Volterra operators H_i as:

$$K_1 = H^{-1} \tag{2.24}$$

$$K_3 = K_1 H_3[K_1] \tag{2.25}$$

and then the IVSTF kernels can be expressed as the following [59]:

$$k_1(\omega) = e^{j\omega^2\beta_2 NL/2} \tag{2.26}$$

$$k_3(\omega_1,\omega_2,\omega-\omega_1+\omega_2) = \frac{jc'k_1(\omega)}{4\pi^2}\sum_{k=1}^{N} e^{jk\beta_2\Delta\Omega L} \tag{2.27}$$

where k_1 and k_3 are the first-order and third-order IVSTF kernels respectively. Thus, the VNLE output can be written in function of the received signal as:

$$Z_{x/y}(\omega) = k_1(\omega)Y_{x/y}(\omega) + \iint k_3(\omega_1,\omega_2,\omega-\omega_1+\omega_2) \times [Y_x(\omega_1)Y_x^*(\omega_2)+Y_y(\omega_1)Y_y^*(\omega_2)]Y_{x/y}(\omega-\omega_1+\omega_2)d\omega_1 d\omega_2 \tag{2.28}$$

The advantage of VNLE compared to other approaches is the possible implementation in parallel and that reduces the computational load. VNLE can be processed in frequency domain [60], in time domain [61], and in both frequency and time domain [59]. FFT and IFFT are used to pass from time domain to frequency domain and inversely. The principle of VNLE implementation based on both frequency and time domain is depicted in fig.2.12 . For each

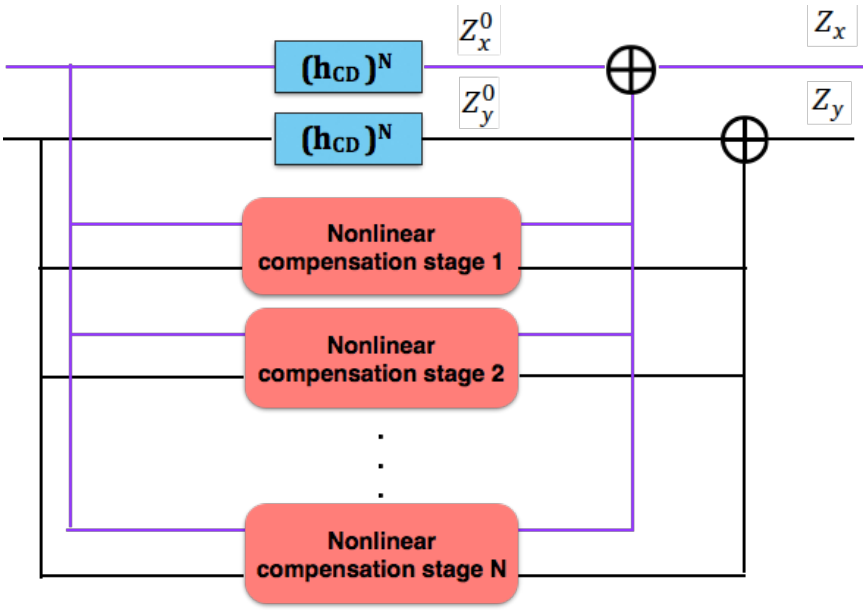

Figure 2.12: VNLE principle for dual-polarization system

polarization, the compensation can be divided into two parts processed in parallel. Linear part which consists in CD compensation and the output is given by:

$$Z^0_{x/y}(\omega) = k_1(\omega)Y_{x/y}(\omega) = h^N_{cd}(\omega)Y_{x/y}(\omega) \tag{2.29}$$

We define $h_{cd} = e^{j\omega^2\beta_2\frac{L}{2}}$ as the transfer function of CD compensation at each span. Concerning the nonlinear part of compensation, it is processed in parallel and it can be divided into N stages. For each span, the output $Z^k_{x/y}$ is derived firstly by passing the received signal through a CD compensation multiplied by those of the previous spans. After that, IFFT is used to pass to time domain and perform the nonlinear compensation. It consist in multiplying the signal by the total amount of power of the two polarizations and a constant jc'. Then, the output is converted to frequency domain by an FFT to perform the residual dispersion compensation. Fig.2.13 shows the principle of nonlinear equalization part for each span.

The output of the VNLE is got by combining the linear and nonlinear compensation:

$$Z_{x/y}(\omega) = Z^0_{x/y}(\omega) + \sum_{k=1}^{N} Z^k_{x/y}(\omega) \tag{2.30}$$

where the output of each span $Z^k_{x/y}$ is given by:

$$Z^k_{x/y}(\omega) = \frac{jc'}{4\pi^2}\iint e^{jk\beta_2\Delta\omega L}[Y_x(\omega_1)Y^*_x(\omega_2) + Y_y(\omega_1)Y^*_y(\omega_2)]Y_{x/y}(\omega-\omega_1+\omega_2)d\omega_1 d\omega_2 \tag{2.31}$$

VNLE has shown a high performance in combating nonlinear effects for signle-channel transmission systems. It has lower computational time compared to DBP. Some new approaches are

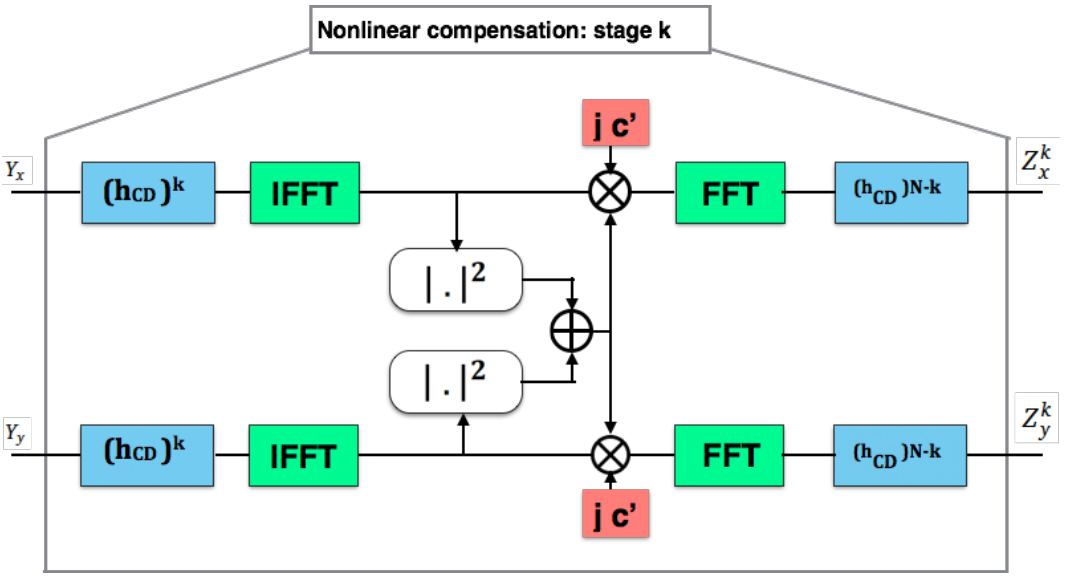

Figure 2.13: Realization of nonlinear equalization for stage k

proposed to reduce complexity such as weighted Volterra series nonlinear equalizer (W-VSNE) [62]. However, VNLE performance are decreased in superchannel transmission because of nonlinear effects depending on the adjacent bands such as FWM, XPM and XpolM.

2.3.3 Superchannel systems simulation results

2.3.3-a MB-OFDM simulation results

In this simulation part, the setup is inspired from the SASER European project whose the goal is to design a 400Gb/s system for long-haul communications [36]. We have four bands of bandwidth 20GHz each and spaced by 2GHz interval guard. On each band, we consider a dual-polarization 16-QAM OFDM with 512 subcarriers. The communication is done over 10 spans of 100km each, so 1000km. Each span is a standard SMF with $\alpha = 0.2$dB.km^{-1}, CD coefficient $D = 17$ps.nm^{-1}.km^{-1}, and $\gamma = 0.0014$m^{-1}.W^{-1}. The polarization mode dispersion (PMD) is 0.1ps.km$^{-1/2}$. We use Erbium-Doped Fiber Amplifier (EDFA) with a 5.5dB noise figure and a 22dB gain at each span.

The performance are given through the Q factor which relates to BER by

$$Q = 20\log_{10}[\sqrt{2}erfc^{-1}(2BER)] \tag{2.32}$$

Fig.B.10 shows Q factor versus input power for a single-band OFDM configuration. Single-step DBP and third-order VNLE outperform linear equalization and the gain is about $2dB$ and $1.2dB$ respectively. DBP has better performance than third-order VNLE in single-band configuration.

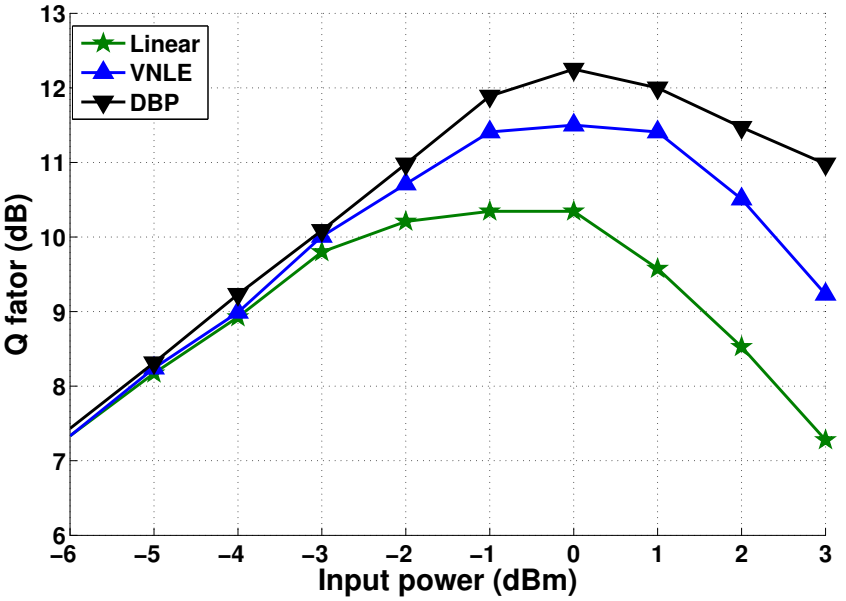

Figure 2.14: Input power vs. Q factor for single-band dual-polarization OFDM transmission

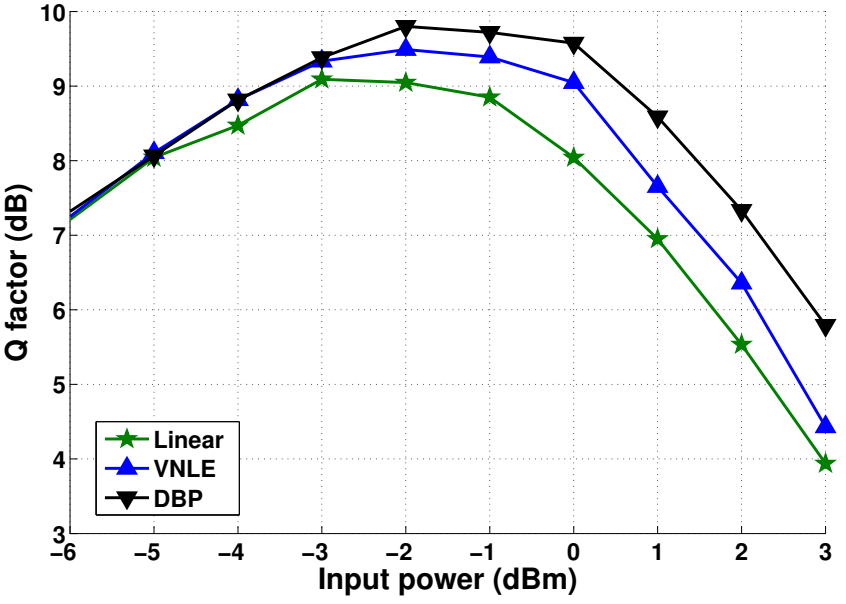

Figure 2.15: Input power vs. Q factor for four-band dual-polarization OFDM transmission

Fig.B.11 shows Q factor versus input power for a four-band OFDM based superchannel system. The gain is about 0.8 and 0.6, in comparsion with linear equalizer, for DBP and VNLE respectively. Thus, DBP and VNLE performance are strongly reduced in MB-OFDM configuration.

2.3.3-b Nyquist-WDM simulation results

We generate a dual-polarization 16QAM modulated Nyquist-WDM superchannel with 4 subcarriers. The bit rate is 448Gbps and the symbol rate per subcarrier and per polarization is $R_s = 14$Gbaud. As in MB-OFDM simulation, the transmission line consists of multi-span standard SMF with the same parameter. The shaping filter is a Root-Raised Cosine (RRC) with roll off $\rho = 0.01$. An Erbium-Doped Fiber Amplifier (EDFA) with a 5.5dB noise figure and a 20dB gain is used at each span of 100km. Notice that the analog to digital converter (ADC) works at twice the symbol rate.

We evaluate the performance Nyquist WDM in function of the subcarrier spacing factor δ. Fig.2.16 shows Q factor versus input power in Quasi-Nyquist WDM configuration with $\delta = 1.2$. In this case, the gain in terms of Q factor is about $0.5dB$ for third-order VNLE and $0.6dB$ for DBP compared with linear equalization.

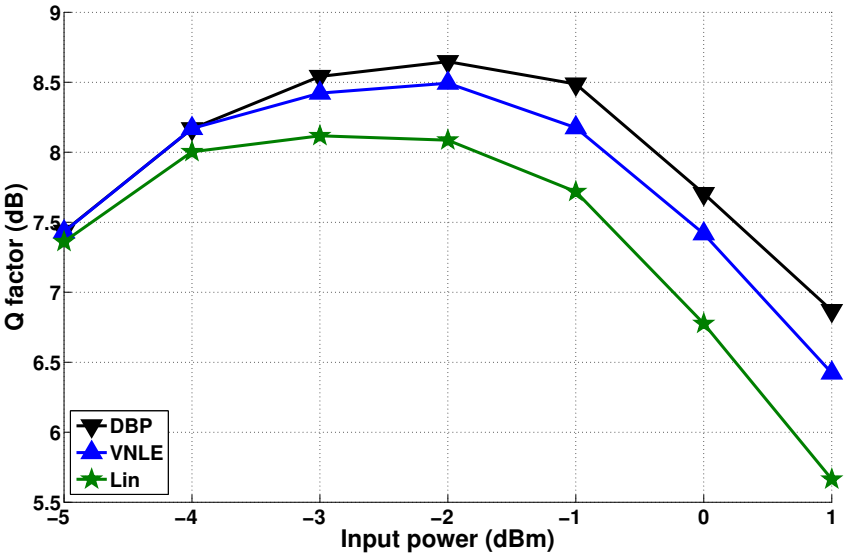

Figure 2.16: Input power vs. Q factor for four-band dual-polarization Quasi-Nyquist WDM transmission

When passing to Super-Nyquist WDM configuration with $\delta = 0.95$ in fig.2.17. The performance of DBP and third-order VNLE is reduced by about $1.8dB$ in comparison with Quasi-Nyquist WDM configuration. In addition, the gains of DBP and VNLE are about $0.4dB$ and $0.3dB$ respectively compared to linear case. Therefore, classic DBP and VNLE performance are reduced in superchannel systems.

2.4 Conclusion

In this chapter, we described the next generation of long-haul WDM transmission systems. It consists in the use of high spectral efficiency modulation formats and superchannel approaches.Then, superchannel systems based on MB-OFDM and Nyquist WDM are detailed.

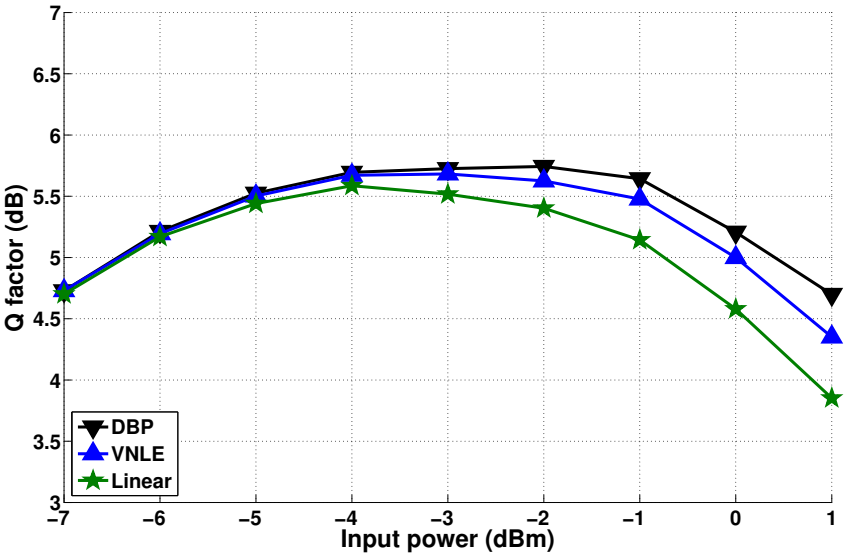

Figure 2.17: Input power vs. Q factor for four-band dual-polarization Super-Nyquist WDM transmission

The major constraint that faces this kind of transmission systems is the Kerr-induced nonlinear effects. Fiber nonlinearties increase with the input power and are inversely proportional to the band/subcarrier spacing. Thus, nonlinear effects compensation is required in superchannel systems. We gave the state of the art about nonlinear effects mitigation techniques. We also demonstrated by simulation that the performance of these techniques are reduced in such transmission systems. To increase the transmission performance in superchannel systems, we propose two new techniques

- We would like to push the VNLE for intra-band interference compensation. Therefore we propose a fifth-order VNLE in chapter 3.
- We would like to reduce the inter-band interference. Therefore we propose a Inter-band Nonlinear Interference Canceler (INIC) in chapter 4.

CHAPTER 3

FIFTH-ORDER VOLTERRA BASED-NONLINEAR EQUALIZER IN SUPERCHANNEL SYSTEM

Third-order Volterra based nonlinear equalization has been already considered to compensate for nonlinear effects in the optical fiber [59][60]. Because of the increase of nonlinear effects when considering superchannel transmission systems, improving nonlinear compensation performance is required. Our work idea to improve nonlinear mitigation consists in increasing the order of the nonlinear equalizer. We pass from third-order VNLE to fifth-order VNLE. Before evaluating the performance of this new equalizer by simulation, the main work is to derive mathematically the fifth-order inverse Volterra kernels and to find a practical implementation scheme.

In this chapter, we firstly give a brief description of p-th order inverse theory. After that, we derive fifth-order inverse Volterra kernels and we give an implementation scheme of the fifth-order VNLE in case of single-polarization and dual-polarization configuration. Finally, simulations are done to evaluate fifth-order VNLE performance.

3.1 P-th order inverse theory

P-th order inverse theory, developed by Schetzen [58], can be used to compute the inverse Volterra kernels that characterize the VNLE in function of the Volterra kernels that model the optical fiber. To do that, we pass first by the inverse Volterra operator, then the inverse kernels can be deduced using eq.2.19 in time domain or the equivalent expression in frequency domain. As described in Section 2.3.2-a, a physical nonlinear system, which is the optical fiber in our case, can be modeled based in Volterra series as:

$$y(t) = H[x(t)] = \sum_{n=1}^{\infty} H_n[x(t)] \tag{3.1}$$

where H is called the system operator and H_n is the n-th order Volterra operator. The p-th-order inverse model $K_{(p)}$, which corresponds to the output of the nonlinear equalizer, can be written when applied to a signal y as:

$$z(t) = K_{(p)}[y(t)] = \sum_{n=1}^{p} K_n[y(t)] \tag{3.2}$$

where K_n is n-th order Volterra inverse operator. The principle of p-th order inverse theory is the following. For a nonlinear systems H, the P-th order inverse $K_{(p)}$ is defined such that the resulting system Q have the first-order Volterra kernel equal to be the unit impulse response and the n-th order kernels (with $n < p+1$) are zero as shown in fig.3.1 [57].

$$Q[x(t)] = x(t) + \sum_{n=p+1}^{\infty} Q_n[x(t)] \tag{3.3}$$

After that, the expression of the inverse Volterra operators K_n can be determined as described

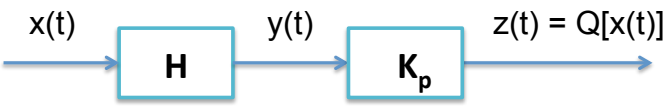

Figure 3.1: System Q formed by tandem connection of $K_{(p)}$ and H

in [58].

3.2 Kernels derivation and implementation

Our work consists in implementing fifth-order VNLE and comparing the simulation results to the third-order VNLE. Due to the property of the optical fiber, only odd-order kernels accounts for the fiber model and the nonlinear equalization. The output of fifth-order equalizer can be written based on inverse Volterra operators as:

$$Z = K_1[Y] + K_3[Y] + K_5[Y] \tag{3.4}$$

The expressions of the inverse Volterra operators K_1,K_3, and K_5 are given in [63]:

$$K_1 = H_1^{-1} \tag{3.5}$$

$$K_3 = -K_1 H_3 K_1 \tag{3.6}$$

$$\begin{aligned} K_5 &= K_1[-H_3[K_1 + K_1 H_3 K_1] - 3H_3 K_1] \\ &+ K_1[0.5H_3 K_1 H_3 K_1 + 0.5H_3[2K_1 + K_1 H_3 K_1]] \end{aligned} \tag{3.7}$$

In eq.B.5, we do not take into account the fifth-order IVSTF term related to fifth-order VSTF H_5 because of the complexity of implementation. Therefore, we consider third-order VSTF fiber model and fifth-order IVSTF nonlinear equalizer. An explicit expressions for $Z_1 = K_1[Y]$

and $Z_3 = K_3[Y]$ have been already developed and the IVSTF kernels k_1 and k_3 are given by eq.2.26 and eq.2.26 respectively.

Our main contribution is to exhibit a closed-form expression for the operator K_5 for which the input is Y and the output is denoted $Z_5 = K_5[Y]$. In the following, we detail the fifth-order IVSTF derivation and the fifth-order VNLE implementation in case of single-polarization and dual-polarization transmission.

3.2.1 Kernels derivation and implementation: single-polarization configuration

We consider an SMF with N spans, each of length L, attenuation coefficient α, second-order dispersion parameter β_2, and nonlinear coefficient γ. The solution of the NLSE (eq.1.6) that governs the wave propagation inside an SMF can be written based on VSTF as:

$$Y = H_1[X] + H_3[X] \tag{3.8}$$

where H_1 and H_3 are the first-order and third-order VSTF operators. The corresponding expression based on VSTF kernels is given by:

$$Y(\omega) = h_1(\omega)X(\omega) + \iint h_3(\omega_1,\omega_2,\omega-\omega_1+\omega_2)X(\omega_1)X^*(\omega_2)X(\omega-\omega_1+\omega_2)d\omega_1 d\omega_2 \tag{3.9}$$

In the following a general expression of K_5 and then Z_5 should be found before deriving a closed from expression for nonlinear compensation in optical fiber.

3.2.1-a Technical preliminaries

Eq.(B.5) corresponds to the fifth-order inverse Volterra operator without taking into accounts the fifth-order Volterra operator H_5 because of the complexity of implementation. This equation can be written easily as:

$$K_5 = -K_1H_3L_1 + 3K_3 + 0.5K_1H_3L_2 + 0.5K_1H_3L_3 \tag{3.10}$$

with $L_1 = K_1 - K_3$, $L_2 = -K_3$, and $L_3 = 2K_1 - K_3$. Then the output Z_5 can be decomposed into four terms defined as the following.

$$Z_5 = K_5[y] = z_1 + z_2 + z_3 + z_4$$

with

$$\begin{aligned} z_1 &= -K_1H_3[\ell_1] \\ z_2 &= 3K_3[Y] \\ z_3 &= 0.5K_1H_3[\ell_2] \\ z_4 &= 0.5K_1H_3[\ell_3] \end{aligned}$$

where $\ell_i = L_i[Y]$. In the following, each term z_i will be derived to find the corresponding kernels. Then a simplified version of Z_5 will be found.

Derivations of z_1

Using the integral form of the third-order Volterra operator which introduces the corresponding kernel, the expression of z_1 can be written as:

$$z_1(\omega) = -k_1(\omega) \int_{\omega_1} \int_{\omega_2} h_3(\omega_1, \omega_2, \omega - \omega_1 + \omega_2) \ell_1(\omega_1) \ell_1^*(\omega_2) \ell_1(\omega - \omega_1 + \omega_2) d\omega_1 d\omega_2 \tag{3.11}$$

Similarly, ℓ_1 is expressed based on the integral form by:

$$\ell_1(\omega) = k_1(\omega) y(\omega) - \int_{\omega_3} \int_{\omega_4} k_3(\omega_3, \omega_4, \omega - \omega_3 + \omega_4) Y(\omega_3) Y^*(\omega_4) Y(\omega - \omega_3 + \omega_4) d\omega_3 d\omega_4$$

Consequently, after replacing ℓ_1 in eq.3.11 by its expression we obtain,

$$\begin{aligned}
z_1(\omega) = -k_1(\omega) & \int_{\omega_1} \int_{\omega_2} h_3(\omega_1, \omega_2, \omega - \omega_1 + \omega_2) [k_1(\omega_1) Y(\omega_1) \\
& - \int_{\omega_3} \int_{\omega_4} k_3(\omega_3, \omega_4, \omega_1 - \omega_3 + \omega_4) Y(\omega_3) Y^*(\omega_4) Y(\omega_1 - \omega_3 + \omega_4) d\omega_3 d\omega_4] [k_1^*(\omega_2) Y^*(\omega_2) \\
& - \int_{\omega_5} \int_{\omega_6} k_3^*(\omega_5, \omega_6, \omega_2 - \omega_5 + \omega_6) Y^*(\omega_5) Y(\omega_6) Y^*(\omega_2 - \omega_5 + \omega_6) d\omega_5 d\omega_6] \\
& \times [k_1(\omega - \omega_1 + \omega_2) y(\omega - \omega_1 + \omega_2) - \int_{\omega_7} \int_{\omega_8} K_3(\omega_7, \omega_8, \omega - \omega_1 + \omega_2 - \omega_7 + \omega_8) \\
& \times y(\omega_7) y^*(\omega_8) y(\omega - \omega_1 + \omega_2 - \omega_7 + \omega_8) d\omega_7 d\omega_8] d\omega_1 d\omega_2
\end{aligned}$$

By developing the previous equation, we obviously obtain an expression of z_1 with a sum of eight terms t_i.

$$z_1(\omega) = -\sum_{i=1}^{8} k_1(\omega) \int_{\omega_1} \int_{\omega_2} h_3(\omega_1, \omega_2, \omega - \omega_1 + \omega_2) t_i(\omega_1, \omega_2) d\omega_1 d\omega_2 \tag{3.12}$$

with

$$t_1(\omega_1, \omega_2) = k_1(\omega_1) k_1^*(\omega_2) k_1(\omega - \omega_1 + \omega_2) Y(\omega_1) Y^*(\omega_2) Y(\omega - \omega_1 + \omega_2)$$

$$\begin{aligned}
t_2(\omega_1, \omega_2) = -k_1(\omega_1) k_1^*(\omega_2) Y(\omega_1) y^*(\omega_2) & \int_{\omega_7} \int_{\omega_8} k_3(\omega_7, \omega_8, \omega - \omega_1 + \omega_2 - \omega_7 + \omega_8) \\
& \times y(\omega_7) Y^*(\omega_8) Y(\omega - \omega_1 + \omega_2 - \omega_7 + \omega_8) d\omega_7 d\omega_8
\end{aligned}$$

$$\begin{aligned}
t_3(\omega_1, \omega_2) = -k_1(\omega_1) k_1(\omega - \omega_1 + \omega_2) Y(\omega_1) Y(\omega - \omega_1 + \omega_2) & \\
\times \int_{\omega_5} \int_{\omega_6} k_3^*(\omega_5, \omega_6, \omega_2 - \omega_5 + \omega_6) Y^*(\omega_5) Y(\omega_6) Y^*(\omega_2 - \omega_5 + \omega_6) d\omega_5 d\omega_6 &
\end{aligned}$$

$$t_4(\omega_1,\omega_2) = k_1(\omega_1)y(\omega_1)\int_{\omega_5}\int_{\omega_6} k_3^*(\omega_5,\omega_6,\omega_2-\omega_5+\omega_6)Y^*(\omega_5)Y(\omega_6)$$
$$\times Y^*(\omega_2-\omega_5+\omega_6)d\omega_5 d\omega_6 \int_{\omega_7}\int_{\omega_8} k_3(\omega_7,\omega_8,\omega-\omega_1+\omega_2-\omega_7+\omega_8)$$
$$\times Y(\omega_7)Y^*(\omega_8)Y(\omega-\omega_1+\omega_2-\omega_7+\omega_8)d\omega_7 d\omega_8$$

$$t_5(\omega_1,\omega_2) = -k_1^*(\omega_2)k_1(\omega-\omega_1+\omega_2)Y^*(\omega_2)Y(\omega-\omega_1+\omega_2)$$
$$\times \int_{\omega_3}\int_{\omega_4} k_3(\omega_3,\omega_4,\omega_1-\omega_3+\omega_4)Y(\omega_3)Y^*(\omega_4)Y(\omega_1-\omega_3+\omega_4)d\omega_3 d\omega_4$$

$$t_6(\omega_1,\omega_2) = k_1^*(\omega_2)Y^*(\omega_2)\int_{\omega_3}\int_{\omega_4} k_3(\omega_3,\omega_4,\omega_1-\omega_3+\omega_4)$$
$$\times Y(\omega_3)Y^*(\omega_4)Y(\omega_1-\omega_3+\omega_4)d\omega_3 d\omega_4 \int_{\omega_7}\int_{\omega_8} k_3(\omega_7,\omega_8,\omega-\omega_1+\omega_2-\omega_7+\omega_8)$$
$$\times Y(\omega_7)Y^*(\omega_8)Y(\omega-\omega_1+\omega_2-\omega_7+\omega_8)d\omega_7 d\omega_8$$

$$t_7(\omega_1,\omega_2) = k_1(\omega-\omega_1+\omega_2)Y(\omega-\omega_1+\omega_2)\int_{\omega_3}\int_{\omega_4} k_3(\omega_3,\omega_4,\omega_1-\omega_3+\omega_4)$$
$$\times Y(\omega_3)Y^*(\omega_4)Y(\omega_1-\omega_3+\omega_4)d\omega_3 d\omega_4 \int_{\omega_5}\int_{\omega_6} k_3^*(\omega_5,\omega_6,\omega_2-\omega_5+\omega_6)$$
$$\times Y^*(\omega_5)Y(\omega_6)Y^*(\omega_2-\omega_5+\omega_6)d\omega_5 d\omega_6$$

$$t_8(\omega_1,\omega_2) = -\int_{\omega_3}\int_{\omega_4} k_3(\omega_3,\omega_4,\omega_1-\omega_3+\omega_4)Y(\omega_3)Y^*(\omega_4)Y(\omega_1-\omega_3+\omega_4)d\omega_3 d\omega_4$$
$$\times \int_{\omega_5}\int_{\omega_6} k_3^*(\omega_5,\omega_6,\omega_2-\omega_5+\omega_6)Y^*(\omega_5)Y(\omega_6)Y^*(\omega_2-\omega_5+\omega_6)d\omega_5 d\omega_6$$
$$\times \int_{\omega_7}\int_{\omega_8} k_3(\omega_7,\omega_8,\omega-\omega_1+\omega_2-\omega_7+\omega_8)Y(\omega_7)Y^*(\omega_8)$$
$$\times Y(\omega-\omega_1+\omega_2-\omega_7+\omega_8)d\omega_7 d\omega_8$$

This notation will be used also for the derivation of the other terms z_i of the output Z_5. Some of t_is contain at most four integrals which is the maximal desired number of integrals for a fifth order kernel.

Derivations of z_2

The expression of z_2 is written using the integral form of the third-order inverse Volterra operator as the following:

$$z_2(\omega) = 3\int_{\omega_1}\int_{\omega_2} k_3(\omega_1,\omega_2,\omega-\omega_1+\omega_2)Y(\omega_1)Y^*(\omega_2)Y(\omega-\omega_1+\omega_2)d\omega_1 d\omega_2 \quad (3.13)$$

To obtain an expression of z_2 having the same notation used for z_1, we use eq.B.4 to express the third-order inverse Volterra operator in function of the corresponding Volterra operator H_3. Therefore, we are able to write z_2 as

$$z_2(\omega) = -3k_1(\omega)\int_{\omega_1}\int_{\omega_2} h_3(\omega_1,\omega_2,\omega-\omega_1+\omega_2)t_1(\omega_1,\omega_2)d\omega_1 d\omega_2 \quad (3.14)$$

Derivations of z_3

As the case of the previous terms, the expression of z_3 can be written using the integral form of the third-order Volterra operator as the following:

$$\begin{aligned} z_3(\omega) = 0.5k_1(\omega)\int_{\omega_1}\int_{\omega_2} & h_3(\omega_1,\omega_2,\omega-\omega_1+\omega_2) \\ & \times \ell_2(\omega_1)\ell_2^*(\omega_2)\ell_2(\omega-\omega_1+\omega_2)d\omega_1 d\omega_2 \end{aligned} \quad (3.15)$$

Using the integral form, ℓ_2 is given by:

$$\ell_2(\omega) = -\int_{\omega_3}\int_{\omega_4} k_3(\omega_3,\omega_4,\omega-\omega_3+\omega_4)Y(\omega_3)Y^*(\omega_4)Y(\omega-\omega_3+\omega_4)d\omega_3 d\omega_4$$

By introducing the same notation of previous terms, the final expression of z_3 can be written in function of t_i terms as the following:

$$z_3(\omega) = 0.5k_1(\omega)\int_{\omega_1}\int_{\omega_2} h_3(\omega_1,\omega_2,\omega-\omega_1+\omega_2)t_8(\omega_1,\omega_2)d\omega_1 d\omega_2 \quad (3.16)$$

Derivations of z_4

The last term z_4 should be expressed as the same way of the previous terms z_i to get a simplified version of Z_5. Using the integral form of the third-order Volterra operator, z_4 can be written as the following:

$$z_4(\omega) = 0.5k_1(\omega)\int_{\omega_1}\int_{\omega_2} h_3(\omega_1,\omega_2,\omega-\omega_1+\omega_2)\ell_3(\omega_1)\ell_3^*(\omega_2)\ell_3(\omega-\omega_1+\omega_2)d\omega_1 d\omega_2 \quad (3.17)$$

with

$$\ell_3(\omega) = 2k_1(\omega)y(\omega) - \int_{\omega_3}\int_{\omega_4} k_3(\omega_3,\omega_4,\omega-\omega_3+\omega_4)Y(\omega_3)Y^*(\omega_4)Y(\omega-\omega_3+\omega_4)d\omega_3 d\omega_4$$

By proceeding in the same manner, we obtain almost the same expression as for z_1, only some coefficients before t_i are different. We so have:

$$\begin{aligned} z_4(\omega) = k_1(\omega)\int_{\omega_1}\int_{\omega_2} & h_3(\omega_1,\omega_2,\omega-\omega_1+\omega_2) \\ & \times [4t_1(\omega_1,\omega_2)+2t_2(\omega_1,\omega_2)+2t_3(\omega_1,\omega_2)+t_4(\omega_1,\omega_2)+2t_5(\omega_1,\omega_2) \\ & + t_6(\omega_1,\omega_2)+t_7(\omega_1,\omega_2)+0.5t_8(\omega_1,\omega_2)]d\omega_1 d\omega_2 \end{aligned} \tag{3.18}$$

Final results

By combining the expressions of each term z_i, we now have that

$$\begin{aligned} Z_5(\omega) = k_1(\omega)\int_{\omega_1}\int_{\omega_2} & h_3(\omega_1,\omega_2,\omega-\omega_1+\omega_2) \\ & \times (t_2(\omega_1,\omega_2)+t_3(\omega_1,\omega_2)+t_5(\omega_1,\omega_2))d\omega_1 d\omega_2. \end{aligned} \tag{3.19}$$

Finally, we can write Z_5 as the following:

$$Z_5(\omega) = q_1(\omega) + q_2(\omega) + q_3(\omega) \tag{3.20}$$

with

$$\begin{aligned} q_1(\omega) = -k_1(\omega)\int_{\omega_1}\int_{\omega_2} & h_3(\omega_1,\omega_2,\omega-\omega_1+\omega_2)k_1(\omega_1)k_1^*(\omega_2)Y(\omega_1)Y^*(\omega_2) \\ & \times \int_{\omega_3}\int_{\omega_4} k_3(\omega_3,\omega_4,\omega-\omega_1+\omega_2-\omega_3+\omega_4)Y(\omega_3)Y^*(\omega_4) \\ & \times Y(\omega-\omega_1+\omega_2-\omega_3+\omega_4)d\omega_3 d\omega_4 d\omega_1 d\omega_2 \end{aligned} \tag{3.21}$$

$$q_2(\omega) = -k_1(\omega) \int_{\omega_1} \int_{\omega_2} h_3(\omega_1, \omega_2, \omega - \omega_1 + \omega_2) k_1(\omega_1) k_1(\omega - \omega_1 + \omega_2) \tag{3.22}$$
$$\times Y(\omega_1) Y(\omega - \omega_1 + \omega_2) \int_{\omega_3} \int_{\omega_4} k_3^*(\omega_3, \omega_4, \omega_2 - \omega_3 + \omega_4)$$
$$\times Y^*(\omega_3) Y(\omega_4) Y^*(\omega_2 - \omega_3 + \omega_4) d\omega_3 d\omega_4 d\omega_1 d\omega_2.$$

$$q_3(\omega) = -k_1(\omega) \int_{\omega_1} \int_{\omega_2} h_3(\omega_1, \omega_2, \omega - \omega_1 + \omega_2) k_1^*(\omega_2) k_1(\omega - \omega_1 + \omega_2) \tag{3.23}$$
$$\times Y^*(\omega_2) y(\omega - \omega_1 + \omega_2) \int_{\omega_3} \int_{\omega_4} k_3(\omega_3, \omega_4, \omega_1 - \omega_3 + \omega_4) Y(\omega_3) Y^*(\omega_4)$$
$$\times Y(\omega_1 - \omega_3 + \omega_4) d\omega_3 d\omega_4 d\omega_1 d\omega_2.$$

So far, no properties of optical fiber have been used for deriving the inverse Volterra series. In next Section, we will use closed-form expression for h_1 and h_3 in order to find the real operations to be done at the receiver side.

3.2.1-b Closed-form expression for fiber nonlinear effects compensation

In the previous section,we find a simplified version of Z_5 for any input Y. Z_5 is the output of the fifth-order inverse Volterra operator K_5 applied to an input signal Y. Now, we consider a real fiber transmission system, Y corresponds to the output of the optical fiber after passing it by a coherent receiver and an ADC to get an electrical signal. Thus, for an optical fiber transmission, the expression of Volterra kernels h_1 and h_3 are given by eq.2.22 and eq.2.23 respectively. Similarly, the inverse Volterra kernels k_1 and k_3 are given by eq.2.26 and eq.2.27 respectively. In case of single-polarization configuration, the parameter c' is replaced by $c = \gamma.L_{eff}$. Then, a closed-form expression of each term of eq.3.20 will be found in the following.

Derivations for q_1

According to Eq.(B.4), after using the integral form of the inverse Volterra operator K_3, we can derive the kernel k_3 and it takes the following form:

$$k_3(\omega_1, \omega_2, \omega - \omega_1 + \omega_2) = -k_1(\omega) h_3(\omega_1, \omega_2, \omega - \omega_1 + \omega_2) k_1(\omega_1) k_1^*(\omega_2) k_1(\omega - \omega_1 + \omega_2) \tag{3.24}$$

so, we can deduce easily the expression of the Volterra kernel h_3 in function of the inverse Volterra kernel k_3. This will be used to get more simplified expression of q_1.

$$h_3(\omega_1, \omega_2, \omega - \omega_1 + \omega_2) = -k_3(\omega_1, \omega_2, \omega - \omega_1 + \omega_2) k_1^*(\omega) k_1^*(\omega_1) k_1(\omega_2) k_1^*(\omega - \omega_1 + \omega_2) \tag{3.25}$$

By replacing h_3 with its previous expression, the term q_1 can be written in function of only inverse Volterra kernels as the following:

$$q_1(\omega) = \int_{\omega_1}\int_{\omega_2}\int_{\omega_3}\int_{\omega_4} k_3(\omega_1,\omega_2,\omega-\omega_1+\omega_2)k_3(\omega_3,\omega_4,\omega-\omega_1+\omega_2-\omega_3+\omega_4)$$
$$\times k_1^*(\omega-\omega_1+\omega_2)Y(\omega_1)Y^*(\omega_2)Y(\omega_3)Y^*(\omega_4)Y(\omega-\omega_1+\omega_2-\omega_3+\omega_4)d\omega_3 d\omega_4 d\omega_1 d\omega_2$$

Then, inverse Volterra kernels k_1 and k_3 are replaced by their optical transmission forms. Finally, after mathematical manipulations and factorizations we got the following form:

$$q_1(\omega) = -\frac{c^2}{(2\pi)^4} h_{cd}^N(\omega) \sum_{k,\ell=1}^{N} q_1^{(k,\ell)}(\omega) \tag{3.26}$$

with

$$q_1^{(k,\ell)}(\omega) = \int_{\omega_1}\int_{\omega_2}\int_{\omega_3}\int_{\omega_4} e^{j\beta_2 L(k\Delta\Omega+\ell\Delta\Omega_1)} \tag{3.27}$$
$$\times Y(\omega_1)Y^*(\omega_2)Y(\omega_3)Y^*(\omega_4)Y(\omega-\omega_1+\omega_2-\omega_3+\omega_4)d\omega_1 d\omega_2 d\omega_3 d\omega_4$$

where $\Delta\Omega_1 = (\omega_3-\omega+\omega_1-\omega_2)(\omega_3-\omega_4)$. h_{cd} corresponds to the transfer function of the CD compensation and given in Section 2.3.2-c.

Derivations for q_2

As the case of the derivation of q_1, the first step to do is replacing the Volterra kernel h_3 with respect to k_3. Thus, we obtain

$$q_2(\omega) = \int_{\omega_1}\int_{\omega_2}\int_{\omega_3}\int_{\omega_4} k_3(\omega_1,\omega_2,\omega-\omega_1+\omega_2)k_3^*(\omega_3,\omega_4,\omega_2-\omega_3+\omega_4)$$
$$\times k_1(\omega_2)Y(\omega_1)Y(\omega-\omega_1+\omega_2)Y^*(\omega_3)Y(\omega_4)Y^*(\omega_2-\omega_3+\omega_4)d\omega_1 d\omega_2 d\omega_3 d\omega_4.$$

The final form of q_2 is got by introducing the optical expressions of k_1 and k_3 which depend on the optical link parameter. h_{cd} contains the second order dispersion parameter β_2, the number of spans N and the length of each span L, while the attenuation coefficient α and the nonlinear coefficient γ are presented by the parameter c .

$$q_2(\omega) = \frac{c^2}{(2\pi)^4} h_{cd}^N(\omega) \sum_{k,\ell=1}^{N} q_2^{(k,\ell)}(\omega) \tag{3.28}$$

with

$$q_2^{(k,\ell)}(\omega) = \int_{\omega_1}\int_{\omega_2}\int_{\omega_3}\int_{\omega_4} e^{j\beta_2 L(k\Delta\Omega-\ell\Delta\Omega_2)} \times Y(\omega_1)Y(\omega-\omega_1+\omega_2)Y^*(\omega_3)Y(\omega_4)Y^*(\omega_2-\omega_3+\omega_4)d\omega_1 d\omega_2 d\omega_3 d\omega_4 \tag{3.29}$$

The factorization of the terms related to the double sum product leads to $\Delta\Omega_2 = (\omega_3 - \omega_2)(\omega_3 - \omega_4)$ and $\Delta\Omega$ given by Section 2.3.2-b

Derivations for q_3

Once again, we replace h_3 with its expression depending on k_3. We have

$$q_3(\omega) = \int_{\omega_1}\int_{\omega_2}\int_{\omega_3}\int_{\omega_4} k_3(\omega_1,\omega_2,\omega-\omega_1+\omega_2)k_3(\omega_3,\omega_4,\omega_1-\omega_3+\omega_4) \times k_1^*(\omega_1)Y^*(\omega_2)Y(\omega-\omega_1+\omega_2)Y(\omega_3)Y^*(\omega_4)Y(\omega_1-\omega_3+\omega_4)d\omega_1 d\omega_2 d\omega_3 d\omega_4$$

By doing the change of variable $\omega_1 \to \omega_1' = \omega - \omega_1 + \omega_2$, we have

$$q_3(\omega) = \int_{\omega_1'}\int_{\omega_2}\int_{\omega_3}\int_{\omega_4} k_3(\omega-\omega_1'+\omega_2,\omega_2,\omega_1')k_3(\omega_3,\omega_4,\omega-\omega_1'+\omega_2-\omega_3+\omega_4) \times k_1^*(\omega-\omega_1'+\omega_2)Y(\omega_1')Y^*(\omega_2)Y(\omega_3)Y^*(\omega_4)Y(\omega-\omega_1'+\omega_2-\omega_3+\omega_4)d\omega_1' d\omega_2 d\omega_3 d\omega_4$$

As the previous cases, we replace the inverse Volterra kernels by their optical expression. Using the permutation property, we check that:

$$q_3(\omega) = q_1(\omega) \tag{3.30}$$

Final results The final expression of Z_5 can be written as the following form

$$Z_5(\omega) = \frac{c^2}{(2\pi)^4} h_{cd}^N(\omega) \sum_{k,\ell=1}^{N} \left(-2q_1^{(k,\ell)}(\omega) + q_2^{(k,\ell)}(\omega)\right) \tag{3.31}$$

We remind Z_5 is the output of the fifth-order inverse Volterra Transfert Function.

3.2.1-c Practical implementation scheme

In this part, the objective is to find a practical implementation scheme for fifth-order inverse Volterra operator. Then, it will be combined with first and third-order to form the fifth-order VNLE as shown in fig.B.15

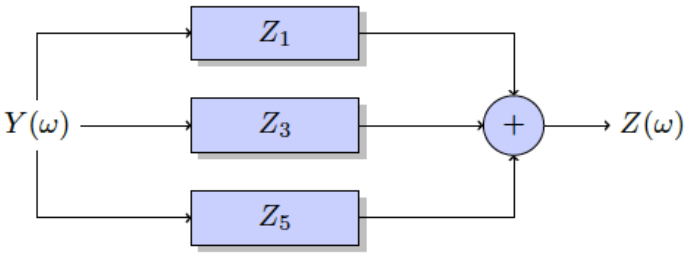

Figure 3.2: Realization of fifth-order VNLE for single polarization system

According to eq3.31, Z_5 can be decomposed into two main terms as follows:

$$Z_5(\omega) = \sum_{k,\ell=1}^{N} \left(S_1^{(k,\ell)}(\omega) + S_2^{(k,\ell)}(\omega) \right) \tag{3.32}$$

with

$$S_1^{(k,\ell)}(\omega) = -2\frac{c^2}{(2\pi)^4} h_{cd}^N(\omega) q_1^{(k,\ell)}(\omega) \tag{3.33}$$

$$S_2^{(k,\ell)}(\omega) = \frac{c^2}{(2\pi)^4} h_{cd}^N(\omega) q_2^{(k,\ell)}(\omega) \tag{3.34}$$

We now shall determine a practical scheme for implementing easily $s_1^{(k,\ell)}(\omega)$ and $s_2^{(k,\ell)}(\omega)$.

Scheme for $S_1^{(k,\ell)}(\omega)$

By doing a change of variable $\omega_1 \rightarrow \omega_1 = \omega - \omega_1 + \omega_2$, we obtain a more "symmetric" expression:

$$S_1^{(k,\ell)}(\omega) = -2\frac{c^2}{(2\pi)^4} h_{cd}^N(\omega) \int_{\omega_1}\int_{\omega_2}\int_{\omega_3}\int_{\omega_4} e^{j\beta_2 L\left(k(\omega_1-\omega)(\omega_1-\omega_2)+\ell(\omega_3-\omega_1)(\omega_3-\omega_4)\right)} \times Y(\omega-\omega_1+\omega_2)Y^*(\omega_2)Y(\omega_3)Y^*(\omega_4)Y(\omega_1-\omega_3+\omega_4)d\omega_1 d\omega_2 d\omega_3 d\omega_4.$$

We set $A_m(\omega) = h_{cd}^m(\omega)y(\omega)$ for any power m. Then by replacing the two first y with their expression with respect to A_k, and the three last y with their expression with respect to A_ℓ, we obtain

$$S_1^{(k,\ell)}(\omega) = -2\frac{c^2}{(2\pi)^4} h_{cd}^{N-k}(\omega) \int_{\omega_1}\int_{\omega_2}\int_{\omega_3}\int_{\omega_4} h_{cd}^{k-\ell}(\omega_1)A_k^*(\omega_2)A_k(\omega-\omega_1+\omega_2) \times A_\ell(\omega_3)A_\ell^*(\omega_4)A_\ell(\omega_1-\omega_3+\omega_4)d\omega_1 d\omega_2 d\omega_3 d\omega_4.$$

This fourfold integral seems to be impossible to implement in practice. Actually it is possible by mimicking the derivations done in [59] by introducing the time domain version of the signal $A_m(\omega)$. An important point to observe in the expression of $S_1^{(k,\ell)}$ is that the four integrals computation can be avoided by passing to time domain using fast Fourier transform.

Therefore the main idea to determine the implementation scheme is to perform the nonlinear compensation presented in $S_1^{(k,\ell)}$ in time domain. Let us define the Fourier Transform. We have:

$$A_m(\omega) = \int a_m(t) e^{-j\omega t} dt$$

and then the inverse Fourier transform which performs the frequency to time domain conversion is given by:

$$a_m(t) = \frac{1}{2\pi} \int A_m(\omega) e^{j\omega t} d\omega$$

By replacing $h_{cd}^{k-\ell}$, A_k and A_ℓ with their respective Fourier Transform, we firstly obtain that

$$\begin{aligned} S_1^{(k,\ell)}(\omega) = -2\frac{c^2}{(2\pi)^4} h_{cd}^{N-k}(\omega) \int \cdots \int g(t_1) a_k^*(t_2) a_k(t_3) a_\ell(t_4) a_\ell^*(t_5 a_\ell(t_6) \\ \times e^{j\omega_1(-t_1+t_3-t_6)+j\omega_2(t_2-t_3)+j\omega_3(t_6-t_4)+j\omega_4(t_5-t_6)-j\omega t_3} \\ \times d\omega_1 d\omega_2 d\omega_3 d\omega_4 dt_1 dt_2 dt_3 dt_4 dt_5 dt_6. \end{aligned}$$

where the function $g(t)$ is the inverse Fourier Transform of the CD transfer function $h_{cd}^{k-\ell}(\omega)$.

Now, we have two kinds of integrals in the expression of $s_1^{(k,\ell)}$. Some of the integrals are with respect to the time while the other ones are with respect to the frequency. Actually, integrals with respect to the frequencies ω_i can be avoided by introducing the Dirac delta function given by the following:

$$\int e^{j\omega t} d\omega = 2\pi\delta(t),$$

Thus, we obtain an expression of $s_1^{(k,\ell)}$ with only time domain integrations.

$$S_1^{(k,\ell)}(\omega) = \quad -2c^2 h_{cd}^{N-k}(\omega) \int \int g(t-t') |a_k(t)|^2 |a_\ell(t')|^2 a_\ell(t') e^{-j\omega t} dt dt'. \tag{3.35}$$

Then, we introduce new notations to show convolution products. In fact, convolution products in time domain become simple multiplications in frequency domain by using Fourier transforms. Therefore, the objective of this process is to perform signal multiplications in time domain and after that re-passing to frequency domain to multiply the signal by the transfer function of residual dispersion h_{cd}^{N-k}. We set:

$$x_1(t) = \sqrt{2}c|a_k(t)|^2 \quad \text{and} \quad x_2(t) = \sqrt{2}c|a_\ell(t)|^2 a_\ell(t).$$

Then, the expression of $s_1^{(k,\ell)}$ can be written now as the following:

$$S_1^{(k,\ell)}(\omega) = -h_{cd}^{N-k}(\omega) \int_t x_1(t) \left[\int_{t'} g(t-t') x_2(t') dt' \right] e^{-j\omega t} dt.$$

In addition, we set $x_3(t) = g(t) \star x_2(t)$ where $\star$ stands for the convolution product. We obtain

$$S_1^{(k,\ell)}(\omega) = -h_{cd}^{N-k}(\omega) \int_t x_1(t) x_3(t) e^{-j\omega t} dt.$$

Finally, we also set $x_4(t) = x_1(t)x_3(t)$ and $X_4(\omega)$ its Fourier Transform. After passing to frequency domain using Fourier transform, we get an implementable scheme given by:

$$S_1^{(k,\ell)}(\omega) = -h_{cd}^{N-k}(\omega)X_4(\omega) \tag{3.36}$$

Scheme for $S_2^{(k,\ell)}(\omega)$

We proceed in the same manner to determine a practical implementation scheme for the second term of output Z_5 of the fifth-order inverse Volterra operator when applied to the signal Y. We remind the expression for $S_2^{(k,\ell)}$.

$$\begin{aligned} S_2^{(k,\ell)}(\omega) = \frac{c^2}{(2\pi)^4} h_{cd}^{N}(\omega) \int_{\omega_1}\int_{\omega_2}\int_{\omega_3}\int_{\omega_4} e^{j\beta_2 L(k\Delta\Omega - \ell\Delta\Omega_2)} \\ \times Y(\omega_1)Y(\omega-\omega_1+\omega_2)Y^*(\omega_3)Y(\omega_4)Y^*(\omega_2-\omega_3+\omega_4)d\omega_1 d\omega_2 d\omega_3 d\omega_4 \end{aligned}$$

and $\Delta\Omega_2 = (\omega_3 - \omega_2)(\omega_3 - \omega_4)$.

First of all, we write the integral with respect to A_k and A_ℓ rather than y. Thus, we obtain

$$\begin{aligned} S_2^{(k,\ell)}(\omega) = \frac{c^2}{(2\pi)^4} h_{cd}^{N-k}(\omega) \int_{\omega_1}\int_{\omega_2}\int_{\omega_3}\int_{\omega_4} h_{cd}^{*k-\ell}(\omega_2) \\ \times A_k(\omega_1)A_k(\omega-\omega_1+\omega_2)A_\ell^*(\omega_3)A_\ell(\omega_4)A_\ell^*(\omega_2-\omega_3+\omega_4)d\omega_1 d\omega_2 d\omega_3 d\omega_4 \end{aligned}$$

By introducing $a_m(t)$ and $\tilde{g}(t) = g^*(-t)$ the inverse Fourier Transform of $h_{cd}^{*k-\ell}$, we have

$$\begin{aligned} S_2^{(k,\ell)}(\omega) = \frac{c^2}{(2\pi)^4} h_{cd}^{N-k}(\omega) \int\cdots\int \tilde{g}(t_1)a_k(t_2)a_k(t_3)a_\ell^*(t_4)a_\ell(t_5)a_\ell^*(t_6) \\ \times e^{-j\omega_2(t_1+t_3-t_6)-j\omega_1(t_2-t_3)-j\omega t_3+j\omega_3(t_4-t_6)-j\omega_4(t_5-t_6)} \\ \times d\omega_1 d\omega_2 d\omega_3 d\omega_4 dt_1 dt_2 dt_3 dt_4 dt_5 dt_6 \end{aligned}$$

Then, as the case of $s_1^{(k,\ell)}$, we introduce the Dirac delta function. Thus, we get an expression of $s_2^{(k,\ell)}$ including only integrations with respect to the time as following:

$$S_2^{(k,\ell)}(\omega) = c^2 h_{cd}^{N-k}(\omega) \int\int \tilde{g}(t'-t)(a_k(t))^2 |a_\ell(t')|^2 a_\ell^*(t') e^{-j\omega t} dt dt'$$

The next step consists in finding an expression containing convolution products. So, by setting

$$\tilde{x}_1(t) = c(a_k(t))^2 \quad \text{and} \quad \tilde{x}_2(t) = c|a_\ell(t)|^2 a_\ell^*(t) \quad \text{and} \quad \tilde{x}_3(t) = g^*(t) \star \tilde{x}_2(t)$$

we have an expression of $s_2^{(k,\ell)}$ with one integral with respect to the time. It can be seen as a convolution product and it given by:

$$S_2^{(k,\ell)}(\omega) = h_{cd}^{N-k}(\omega) \int \tilde{x}_1(t)\tilde{x}_3(t) e^{-j\omega t} dt$$

As h_{cd} is an even function, it is also true for its inverse Fourier transform $g(t)$, so we have

$$\tilde{x}_3(t) = g^*(-t) \star \tilde{x}_2(t)$$

which corresponds to a multiplication by $h_{cd}^{*k-\ell}$ in the frequency domain. Finally, if $\tilde{x}_4(t) = \tilde{x}_1(t)\tilde{x}_3(t)$ and $\tilde{X}_4(\omega)$ is its Fourier Transform, we obtain that

$$S_2^{(k,\ell)}(\omega) = h_{cd}^{N-k}(\omega)\tilde{X}_4(\omega) \tag{3.37}$$

Now, we have a practical implementation scheme of $s_1^{(k,\ell)}$ and $s_2^{(k,\ell)}$. If we define $S^{(k,\ell)}$ as the sum of these two terms as follow:

$$S^{(k,\ell)} = S_1^{(k,\ell)} + S_2^{(k,\ell)} \tag{3.38}$$

an optimized practical implementable scheme of $S^{(k,\ell)}$ is depicted in fig.3.3. First of all, a CD compensation is done in frequency domain before passing to time domain using an IFFT. After that, the nonlinear compensation is performed. Then, the residual dispersion is compensated in frequency domain. Finally, the output of the inverse Volterra operator applied on the signal

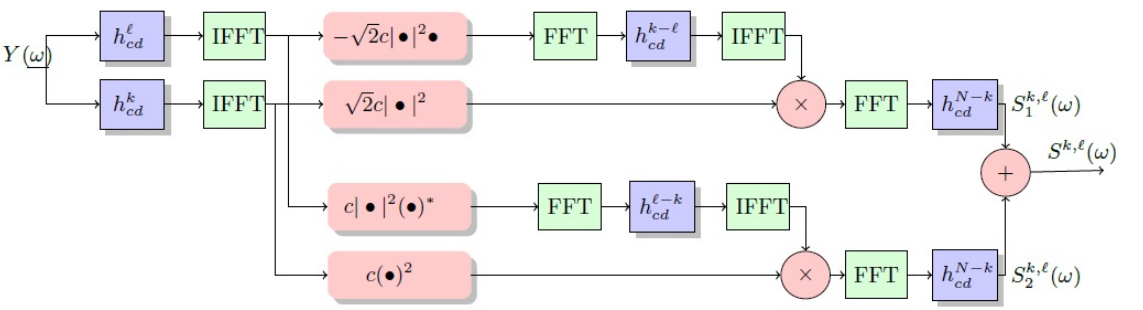

Figure 3.3: Fifth-order IVSTF scheme for single-polarization

Y is the double sum of $S^{(k,\ell)}$ and it is given by

$$Z_5(\omega) = \sum_{k,\ell=1}^{N} S^{(k,\ell)}(\omega) \tag{3.39}$$

3.2.2 Kernels derivation and implementation: dual-polarization configuration

The output Z_5 of the dual-polarization fifth-order inverse Volterra operator can be derived and implemented by proceeding in the same manner as the case of single-polarization. Then, it

will be combined to first-order and third-order terms and the decision is taken on the following signal:

$$Z = Z_1 + Z_3 + Z_5 \tag{3.40}$$

In dual-polarization transmission, the optical fiber model based on Volterra series, which corresponds to the solution of the Manakov equation, is detailed in section 2.3.2-b. We will first find a general form of Z_5. After that, explicit expressions of VSTFs h_1 and h_3 and IVSTF k_1 and k_3 will be integrated to get the real operations to be done at the receiver side. The details of the derivations are given in Appendix.A.

3.2.2-a Technical preliminaries

We remind that the expression of the inverse Volterra operator is given by:

$$K_5 \quad = \quad -K_1H_3L_1 + 3K_3 + 0.5K_1H_3L_2 + 0.5K_1H_3L_3 \tag{3.41}$$

in case of dual-polarization configuration, the terms L_i are expressed by the following

$$L_1 = \begin{pmatrix} L_{1,x} \\ L_{1,y} \end{pmatrix} = \begin{pmatrix} (K_1 - K_3)[Y_x, Y_y] \\ (K_1 - K_3)[Y_y, Y_x] \end{pmatrix}$$

$$L_2 = \begin{pmatrix} L_{2,x} \\ L_{2,y} \end{pmatrix} = \begin{pmatrix} -K_3[Y_x, Y_y] \\ -K_3[Y_y, Y_x] \end{pmatrix}$$

$$L_3 = \begin{pmatrix} L_{3,x} \\ L_{3,y} \end{pmatrix} = \begin{pmatrix} (2K_1 - K_3)[Y_x, Y_y] \\ (2K_1 - K_3)[Y_y, Y_x] \end{pmatrix}$$

According to eq.3.41, we can decompose Z_5 into several terms as :

$$Z_5 = K_5[y] = z_1 + z_2 + z_3 + z_4$$

with

$$z_1 = \begin{pmatrix} z_{1,x} \\ z_{1,y} \end{pmatrix} = \begin{pmatrix} -K_1H_3[\ell_{1,x}, \ell_{1,y}] \\ -K_1H_3[\ell_{1,y}, \ell_{1,x}] \end{pmatrix}$$

$$z_2 = \begin{pmatrix} z_{2,x} \\ z_{2,y} \end{pmatrix} = \begin{pmatrix} 3K_3[Y_x, Y_y] \\ 3K_3[Y_y, Y_x] \end{pmatrix}$$

$$z_3 = \begin{pmatrix} z_{3,x} \\ z_{3,y} \end{pmatrix} = \begin{pmatrix} 0.5K_1H_3[\ell_{2,x}, \ell_{2,y}] \\ 0.5K_1H_3[\ell_{2,y}, \ell_{2,x}] \end{pmatrix}$$

$$z_4 = \begin{pmatrix} z_{4,x} \\ z_{4,y} \end{pmatrix} = \begin{pmatrix} 0.5K_1H_3[\ell_{3,x}, \ell_{3,y}] \\ 0.5K_1H_3[\ell_{3,y}, \ell_{3,x}] \end{pmatrix}$$

Let us now work to find the kernels associated with each signal z_i. In fact, we compute the signal $z_{i,x}$ of polarization x and we can deduce the corresponding signal $z_{i,y}$ of polarization y by analogy. After tedious algebraic derivations, detailed in Appendix.A, we obtain a final

expression for the first component of Z_5, denoted by $Z_{5,x}$. It mainly contains three terms and is given as the following:

$$z_{5,x}(\omega) = -k_1(\omega) \iint h_3(\omega_1, \omega_2, \omega - \omega_1 + \omega_2) \times [q_{1,x}(\omega) + q_{2,x}(\omega) + q_{3,x}(\omega)] d\omega_1 d\omega_2 \tag{3.42}$$

with

$$\begin{aligned} q_{1,x}(\omega) = {} & k_1(\omega_1) k_1^*(\omega_2) \iint k_3(\omega_3, \omega_4, \omega - \omega_1 + \omega_2 - \omega_3 + \omega_4) \\ & \times Y_x(\omega_1) Y_x^*(\omega_2) Y_x(\omega_3) Y_x^*(\omega_4) Y_x(\omega - \omega_1 + \omega_2 - \omega_3 + \omega_4) d\omega_3 d\omega_4 \\ & + k_1(\omega_1) k_1(\omega - \omega_1 + \omega_2) \iint k_3^*(\omega_3, \omega_4, \omega_2 - \omega_3 + \omega_4) \\ & \times Y_x(\omega_1) Y_x(\omega - \omega_1 + \omega_2) Y_x^*(\omega_3) Y_x(\omega_4) Y_x^*(\omega_2 - \omega_3 + \omega_4) d\omega_3 d\omega_3 \\ & + k_1^*(\omega_2) k_1(\omega - \omega_1 + \omega_2) \iint k_3(\omega_3, \omega_4, \omega_1 - \omega_3 + \omega_4) \\ & Y_x^*(\omega_2) Y_x(\omega - \omega_1 + \omega_2) Y_x(\omega_3) Y_x^*(\omega_4) Y_x(\omega_1 - \omega_3 + \omega_4) d\omega_3 d\omega_4, \end{aligned} \tag{3.43}$$

$$\begin{aligned} q_{2,x}(\omega) = {} & k_1(\omega_1) k_1^*(\omega_2) \iint k_3(\omega_3, \omega_4, \omega - \omega_1 + \omega_2 - \omega_3 + \omega_4) \\ & \times [Y_x(\omega_1) Y_x^*(\omega_2) Y_y(\omega_3) Y_y^*(\omega_4) + Y_y(\omega_1) Y_y^*(\omega_2) Y_x(\omega_3) Y_x^*(\omega_4)] \\ & \times Y_1(\omega - \omega_1 + \omega_2 - \omega_3 + \omega_4) d\omega_3 d\omega_4 + k_1(\omega_1) k_1(\omega - \omega_1 + \omega_2) \\ & \times \iint k_3^*(\omega_3, \omega_4, \omega_2 - \omega_3 + \omega_4) [Y_x(\omega_1) Y_x^*(\omega_2 - \omega_3 + \omega_4) Y_y^*(\omega_3) Y_y(\omega_4) \\ & + Y_y(\omega_1) Y_y^*(\omega_2 - \omega_3 + \omega_4) Y_x^*(\omega_3) Y_x(\omega_4)] Y_x(\omega - \omega_1 + \omega_2) d\omega_3 d\omega_3 \\ & + k_1^*(\omega_2) k_1(\omega - \omega_1 + \omega_2) \iint k_3(\omega_3, \omega_4, \omega_1 - \omega_3 + \omega_4) \\ & \times [Y_x^*(\omega_2) Y_x(\omega_1 - \omega_3 + \omega_4) Y_y(\omega_3) Y_y^*(\omega_4) + Y_y^*(\omega_2) Y_y(\omega_1 - \omega_3 + \omega_4) \\ & \times Y_x(\omega_3) Y_x^*(\omega_4)] Y_x(\omega - \omega_1 + \omega_2) d\omega_3 d\omega_4, \end{aligned} \tag{3.44}$$

and

$$\begin{aligned} q_{3,x}(\omega) = {} & k_1(\omega_1) k_1^*(\omega_2) \iint k_3(\omega_3, \omega_4, \omega - \omega_1 + \omega_2 - \omega_3 + \omega_4) \\ & \times Y_y(\omega_1) Y_y^*(\omega_2) Y_y(\omega_3) Y_y^*(\omega_4) Y_x(\omega - \omega_1 + \omega_2 - \omega_3 + \omega_4) d\omega_3 d\omega_4 \\ & + k_1(\omega_1) k_1(\omega - \omega_1 + \omega_2) \iint k_3^*(\omega_3, \omega_4, \omega_2 - \omega_3 + \omega_4) \\ & \times Y_y(\omega_1) Y_y^*(\omega_2 - \omega_3 + \omega_4) Y_y^*(\omega_3) Y_y(\omega_4) Y_x(\omega - \omega_1 + \omega_2) d\omega_3 d\omega_3 \end{aligned} \tag{3.45}$$

We can obtain $Z_{5,y}(\omega)$ by permuting the role of y_x and y_y. The next step is finding a practical implementation scheme of Z_5. Thus, we include the explicit expressions of k_i and h_i for nonlinear effects compensation in optical link.

3.2.2-b Practical implementation scheme

We use the expressions of VSTFs h_1 and h_3 given by Eqs. (2.22)-(2.23). Similarly, we introduce the expression of IVSTFs k_1 and k_3 given by Eqs. (2.26)-(2.27). So, we can find the real operations to be done at the receiver side. First of all, we express $Z_{5,x}$ differently to get three terms $Q_{i,x}$ including k_1 and h_3. Consequently, we have

$$Z_{5,x}(\omega) = Q_{1,x}(\omega) + Q_{2,x}(\omega) + Q_{3,x}(\omega) \tag{3.46}$$

with

$$Q_{i,x} = -k_1(\omega) \iint h_3(\omega_1, \omega_2, \omega - \omega_1 + \omega_2) q_{i,x}(\omega) d\omega_1 d\omega_2$$

Then, we proceed in the same way as the case of single-polarization and we got a closed-form expression of each term $Q_{i,x}$. The details of the derivations are given in Appendix A.

$$Q_{1,x}(\omega) = \sum_{k,\ell=1}^{N} Q_{1,x}^{(k,\ell)}(\omega)$$

with

$$\begin{aligned} Q_{1,x}^{(k,\ell)}(\omega) = -2\frac{c'^2}{(2\pi)^4} h_{cd}^N(\omega) \iiiint & e^{j\beta_2 L(k\Delta\Omega + \ell\Delta\Omega_1)} \\ & \times Y_x^*(\omega_2) Y_x(\omega_1 - \omega_3 + \omega_4) Y_x(\omega_3) Y_x^*(\omega_4) Y_x(\omega - \omega_1 + \omega_2) d\boldsymbol{\omega} \\ & + \frac{c'^2}{(2\pi)^4} h_{cd}^N(\omega) \iiiint e^{j\beta_2 L(k\Delta\Omega - \ell\Delta\Omega_2)} \\ & \times Y_x(\omega_1) Y_x^*(\omega_2 - \omega_3 + \omega_4) Y_x^*(\omega_3) Y_x(\omega_4) Y_x(\omega - \omega_1 + \omega_2) d\boldsymbol{\omega} \end{aligned} \tag{3.47}$$

where $d\boldsymbol{\omega} = d\omega_1 d\omega_2 d\omega_3 d\omega_4$ and c'' defined in Appendix A. By using the same trick as in the single polarization case, it is possible to transform all the above fourth-order integrals based terms in a simpler structure by working in the time domain. So, instead of doing four integrals, we just have to multiply signals in time domain and apply some Fourier Transforms. Then, the practical implementation scheme of $Q_{1,x}^{(k,\ell)}$ is depicted in fig. B.12. Blue blocs correspond to the compensation of dispersion in frequency domain. While red blocs present time domain nonlinear effects compensation. FFT and IFFT are used to switch between time and frequency domain. Finally, by summing k and ℓ from 1 to N, we get the expression of $Q_{1,x}$.

The first term $Q_{1,x}$ does not include any multiplication by the signal Y_y of polarization y. However, the two other terms $Q_{2,x}$ and $Q_{3,x}$ include multiplications by the signal Y_y and

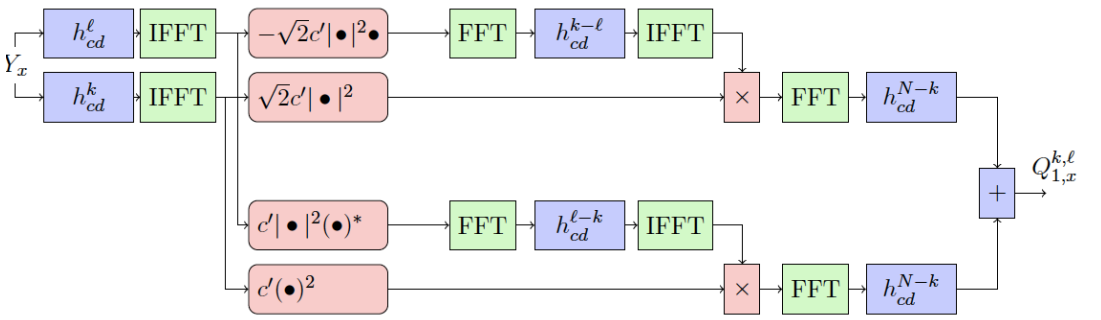

Figure 3.4: Scheme for $Q_{1,x}^{(k,\ell)}(\omega)$

correspond to the interactions between polarizations x and y. The second term $Q_{2,x}$ can be written as the following:

$$Q_{2,x}(\omega) = \sum_{k,\ell=1}^{N} Q_{2,x}^{(k,\ell)}(\omega)$$

with

$$Q_{2,x}^{(k,\ell)}(\omega) = -\frac{c'^2}{(2\pi)^4} h_{cd}^{N}(\omega) \iiint e^{j\beta_2 L(k\Delta\Omega+\ell\Delta\Omega_1)} [Y_x^*(\omega_2)Y_x(\omega_1-\omega_3+\omega_4)Y_y(\omega_3)Y_y^*(\omega_4) \tag{3.48}$$

$$\begin{aligned}
&+ Y_y^*(\omega_2)Y_y(\omega_1-\omega_3+\omega_4)Y_x(\omega_3)Y_x^*(\omega_4)]Y_x(\omega-\omega_1+\omega_2)d\boldsymbol{\omega} \\
&+ \frac{c'^2}{(2\pi)^4} h_{cd}^{N}(\omega) \iiint e^{j\beta_2 L(k\Delta\Omega-\ell\Delta\Omega_2)} [Y_x(\omega_1)Y_x^*(\omega_2-\omega_3+\omega_4)Y_y^*(\omega_3)Y_y(\omega_4) \\
&+ Y_y(\omega_1)Y_y^*(\omega_2-\omega_3+\omega_4)Y_x^*(\omega_3)Y_1(\omega_4)]Y_x(\omega-\omega_1+\omega_2)d\boldsymbol{\omega} \\
&- \frac{c'^2}{(2\pi)^4} h_{cd}^{N}(\omega) \iiint e^{j\beta_2 L(k\Delta\Omega+\ell\Delta\Omega_3)} [Y_x(\omega_1)Y_x^*(\omega_2)Y_y(\omega_3)Y_y^*(\omega_4) \\
&+ Y_y(\omega_1)Y_y^*(\omega_2)Y_1(\omega_3)Y_x^*(\omega_4)]Y_x(\omega-\omega_1+\omega_2-\omega_3+\omega_4)d\boldsymbol{\omega}
\end{aligned}$$

and $\Delta\Omega_3 = (\omega_3-\omega+\omega_1-\omega_2)(\omega_3-\omega_4)$. The corresponding implementation scheme of $Q_{2,x}^{(k,\ell)}$ is shown in fig. B.13. Similarly, dispersion compensation is performed in frequency domain and nonlinear mitigation is done in time domain.

The third term $Q_{3,x}$ can be written as the following:

$$Q_{3,x}(\omega) = \sum_{k,\ell=1}^{N} Q_{3,x}^{(k,\ell)}(\omega)$$

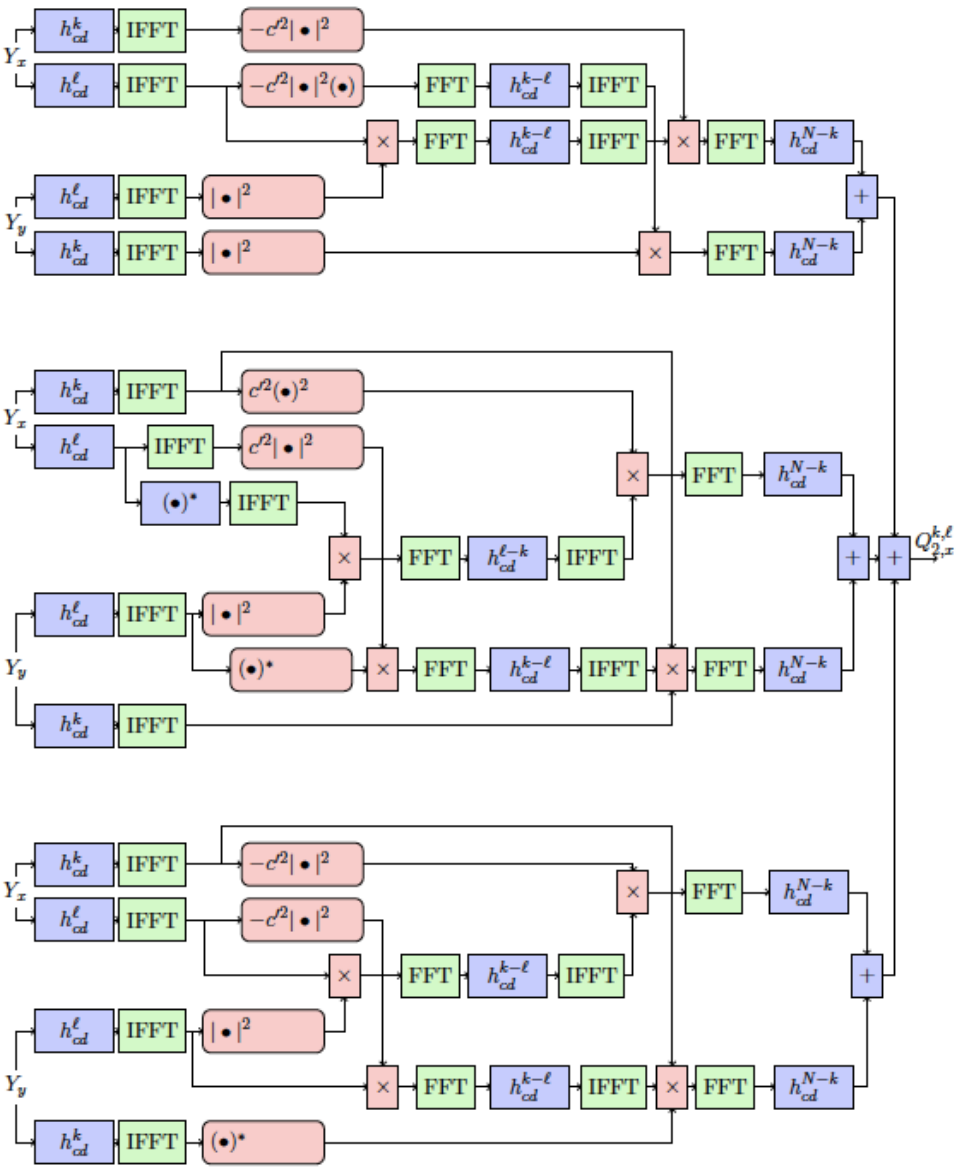

Figure 3.5: Scheme for $Q_{2,x}^{(k,\ell)}(\omega)$

with

$$
\begin{aligned}
Q_{3,x}^{(k,\ell)}(\omega) = &-\frac{c'^2}{(2\pi)^4} h_{cd}^N(\omega) \iiint e^{j\beta_2 L(k\Delta\Omega+\ell\Delta\Omega_1)} \\
&\times Y_y^*(\omega_2) Y_y(\omega_1-\omega_3+\omega_4) Y_y(\omega_3) Y_y^*(\omega_4) Y_x(\omega-\omega_1+\omega_2) d\boldsymbol{\omega} \\
&+ \frac{c'^2}{(2\pi)^4} h_{cd}^N(\omega) \iiint e^{j\beta_2 L(k\Delta\Omega-\ell\Delta\Omega_2)} \\
&\times Y_y(\omega_1) Y_y^*(\omega_2-\omega_3+\omega_4) Y_y^*(\omega_3) Y_y(\omega_4) Y_x(\omega-\omega_1+\omega_2) d\boldsymbol{\omega} \\
&- \frac{c'^2}{(2\pi)^4} h_{cd}^N(\omega) \iiint e^{j\beta_2 L(k\Delta\Omega+\ell\Delta\Omega_3)} \\
&\times Y_y(\omega_1) Y_y^*(\omega_2) Y_y(\omega_3) Y_y^*(\omega_4) Y_x(\omega-\omega_1+\omega_2-\omega_3+\omega_4) d\boldsymbol{\omega}.
\end{aligned}
\tag{3.49}
$$

A practical implementation scheme of $Q_{3,x}^{(k,\ell)}$ is depicted in fig. B.14.

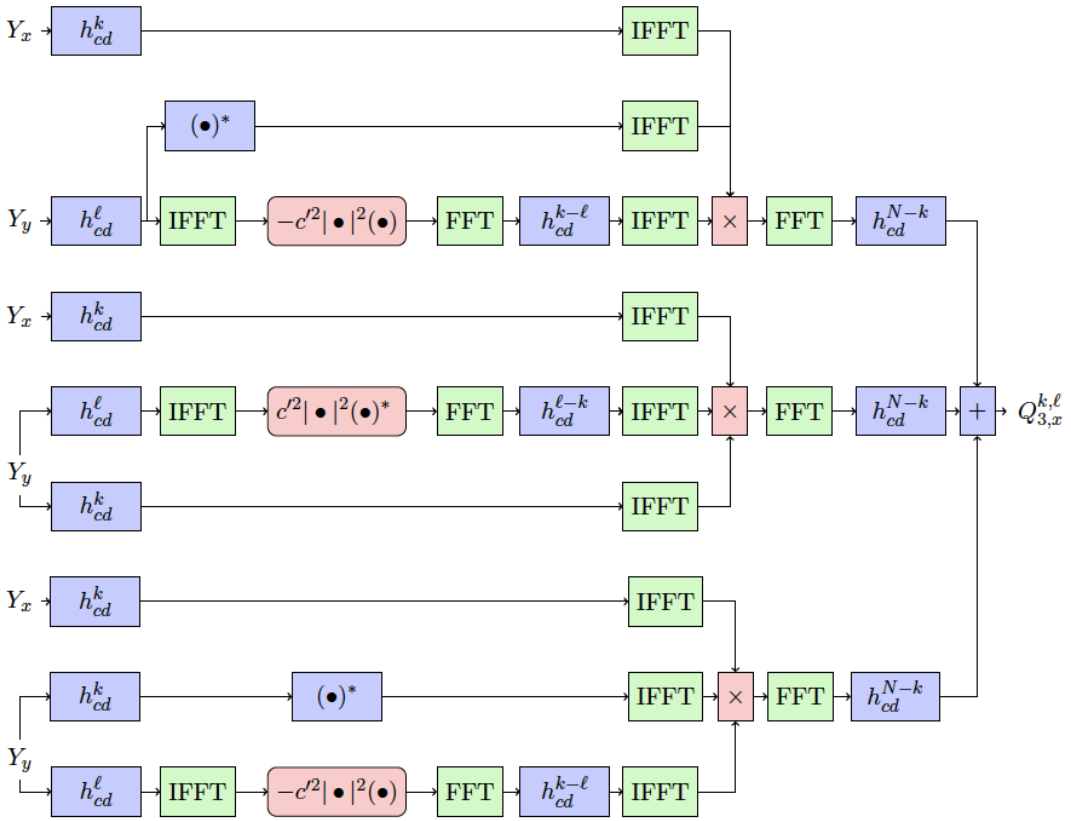

Figure 3.6: Scheme for $Q_{3,x}^{(k,\ell)}(\omega)$

Finally, the practical implementation scheme of $Z_{5,x}$ is the sum of the three terms $Q_{i,x}$. By analogy, a practical scheme for $Z_{5,y}$ can be easily determined by permitting the indexes of polarizations x and y.

3.3 Fifth-order VNLE simulations results

The simulation setup is inspired from the SASER European project. The goal is to design a $400Gbps$ transmission system for long-haul communications. Multi-band and dual-polarization coherent optical OFDM transmission is considered. When we consider one polarization, the data rate boils down only $200Gbps$. We have four bands of bandwidth $20GHz$ each and spaced by a $2GHz$ interval guard. On each band, we consider a 16-QAM OFDM with 512 subcarriers. The communication is done over 20 spans of $100km$ each. Each span is a standard SMF with $\lambda = 0.2dB.km^1$, $D = 17ps.nm^{-1}.km^{-1}$, and $\gamma = 0.0014m^{-1}.W^{-1}$. We use Erbium-Doped Fiber Amplifier (EDFA) with a $5.5dB$ noise figure and a $22dB$ gain at each span.

In Fig.B.16, we plot Q factor vs. input power for single polarization configuration and

when only one band is active. The fifth-order VNLE outperforms the third-order VNLE and the gain is about $2.2dB$. In addition, using fifth-order VNLE, an increase of injected optical power by $3dBm$ can be achieved at similar performance of third-order VNLE. Compared to linear equalizer which consists of chromatic dispersion compensation, the Q factor is improved by about $1.4dB$ and $3.6dB$ for third-order VNLE and fifth-order VNLE respectively.

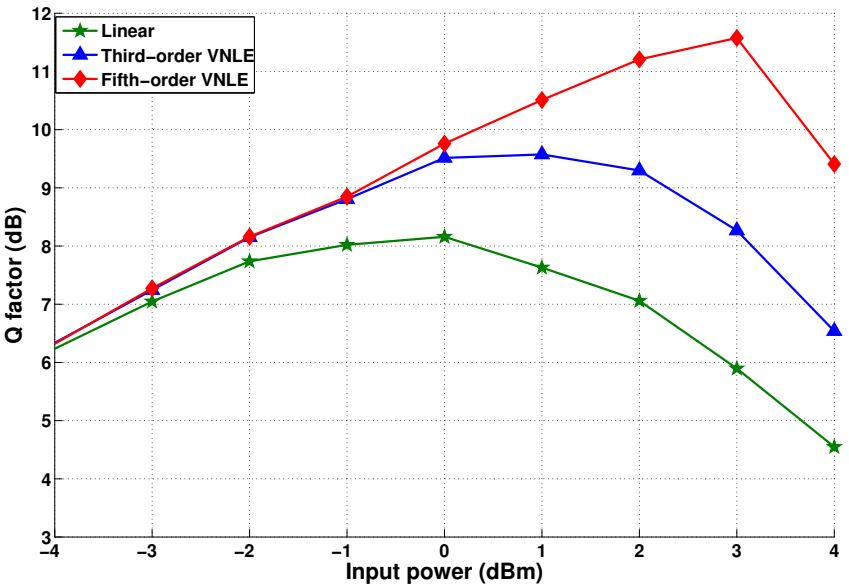

Figure 3.7: Q facor vs. input power for single-band single-pol 16-QAM OFDM (2000km)

In Fig.B.17, we plot the reached transmission distance for a target Q factor $Q = 7.7dB$ which corresponds to $BER = 10^{-2}$. Single polarization but with four bands (instead of one) spaced by $10GHz$ interval guard are considered. An increase of transmission reach by around 100km can be realized using fifth-order VNLE instead of third-order one. Compared to linear equalization, the gain is around $600km$ and $500km$ for fifth-order and third-order VNLE respectively.

When decreasing the interval guard to $2GHz$, we have limited improvement of Q factor as shown in fig.B.18. All multi-band results concern central bands because they are the most disturbed by nonlinear effects. The fifth-order VNLE is rather efficient for combating the intra-band nonlinear effect (see single-band case) than the inter-band effect (see multi-band case). The performance of third-order VNLE is also reduced in comparison with single-band transmission.

In Fig.B.19, we plot Q factor vs. injected input power when both polarizations are active and only one band is active.We unfortunately remark that the gain in performance is reduced. We can observe also a reduction of performance of third-order VNLE in case of dual-polarization configuration. We conclude that nonlinear equalization based on IVSTF can be useful to compensate intra-channel/band nonlinearities. However, when multi-band transmission is considered, inter-band nonlinear interference reduce significantly the nonlinear equalization performance.

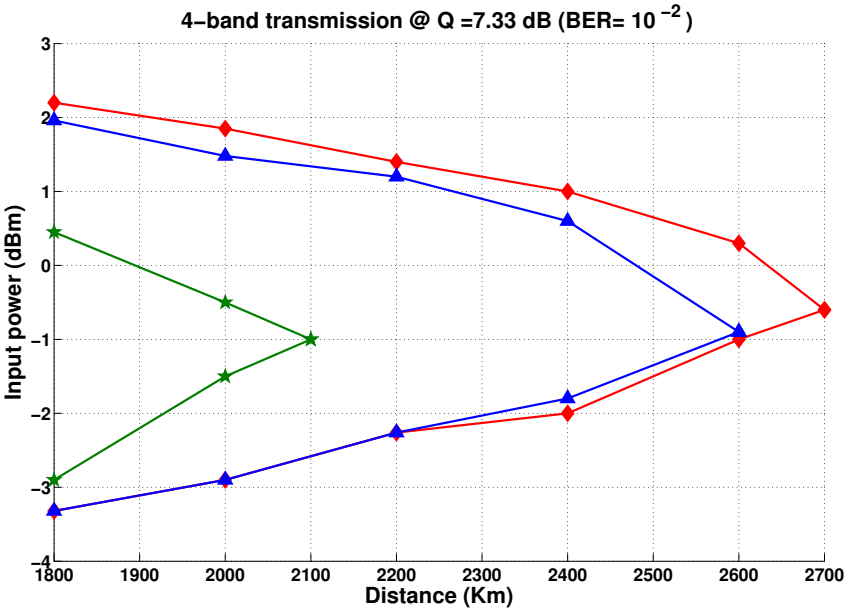

Figure 3.8: Input power vs. transmission reach for 4-band single-pol 16-QAM OFDM

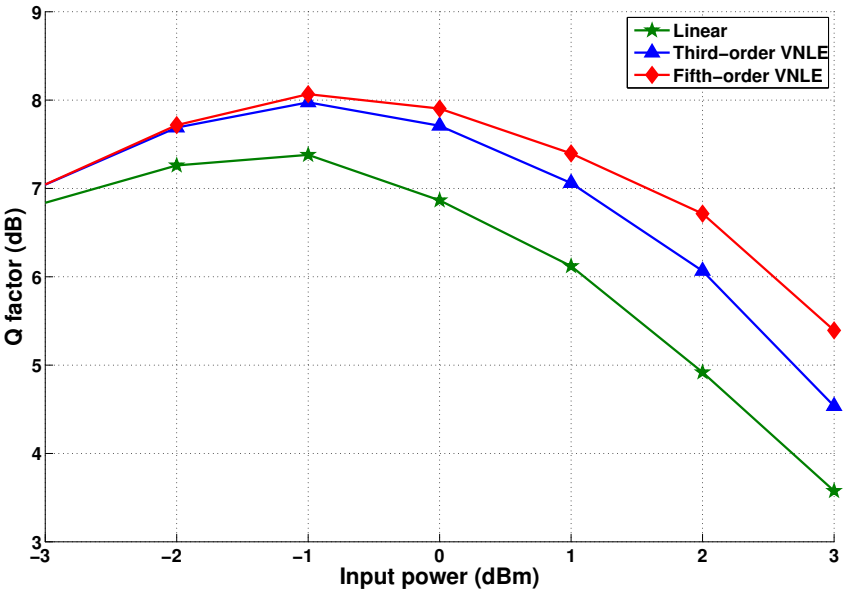

Figure 3.9: Q factor vs. input power for 4-band single-pol 16-QAM OFDM (2000km)

3.4 Conclusion

In this chapter, we derived the fifth-order VNLE based receiver for single-polarization and dual-polarization transmissions. We showed that the gain is very significant under single-band and single-polarization transmission system. Fifth-order VNLE is a powerful tool to combat intra-channel/band nonlinear effect (SPM). However, it presents a limited performance in dual-polarization and multi-band transmission. That can be explained by the fact that nonlinear ef-

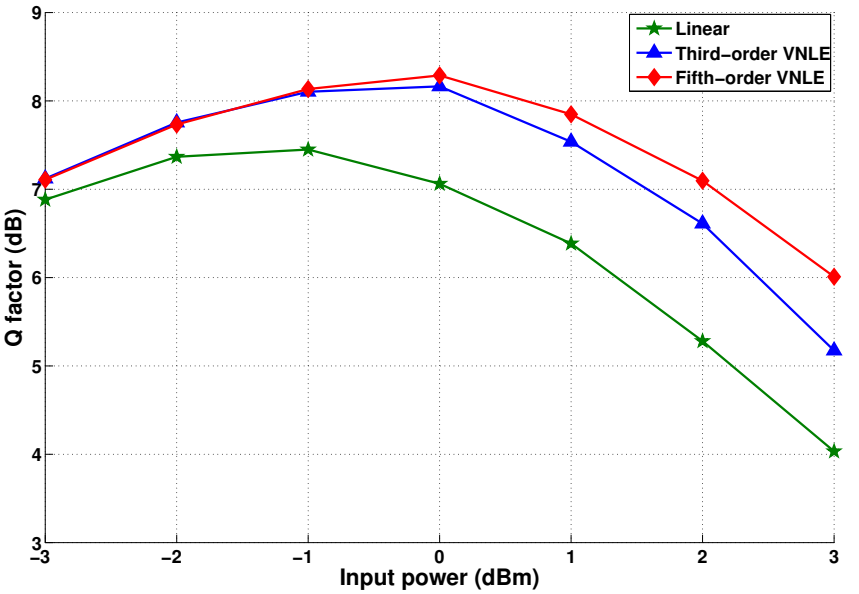

Figure 3.10: Q factor vs. input power for single-band dual-pol 16-QAM OFDM (2000km)

fects depending on the adjacent bands such as XPM, XpolM and FWM reduce the performance of fifth-order VNLE. Such kinds of nonlinear effects lead to nonlinear interference between the copropagating band/subcarrier in superchannel systems.

To combat inter-band/subcarrier nonlinear interference in superchannel systems, we implement an Inter-band/subcarrier Nonlinear Interference Canceler (INIC) which will be the object of the next chapter.

CHAPTER 4

NONLINEAR INTERFERENCE CANCELLATION

In the context of long-haul superchannel transmission system, Kerr-induced nonlinear effects present the major constraint to get the desired performance in terms of transmission reach. In addition to SPM, which is an intra-band/subcarrier nonlinearity, nonlinear interference caused by XPM, XpolM and FWM significantly reduces the transmission performance.

In this chapter, we propose an inter-band/subcarrier nonlinear interference canceler (INIC) based on Volterra series to deal with nonlinear interference in MB-ODFM and Nyquist WDM superchannels. The principle of INIC is based on decision-feedback equalizer (DFE) which is widely used in wireless communication system.

We begin by giving the principle of DFE based receiver. Then, the system model is given before detailing the INIC approach. Finally, simulations are done to evaluate INIC performance in MB-OFDM and Nyquist WDM superchannels.

4.1 Decision feedback equalizer principle

The principle of DFE consists in the use of the previous decisions to estimate the current symbol. DFE is based on symbol-by-symbol detection and the input of the feedback filter is the decision of the previous symbols. Fig.4.1 shows the DFE diagram. Y_k is the received signal and the decision is made on signal Z_k.

DFE is a powerful tool to deal with ISI. In fact, after reconstructing the signal of previous symbols, their contribution is subtracted from the signal associated with the current symbol and thus ISI can be often removed. Decision feedback equalization was already used to combat nonlinearities in wireless communication systems [64].

Our work idea is to use a DFE receiver structure to compensate nonlinear interference caused by adjacent bands/subcarriers in superchannel transmission systems. The main ideas of our proposed INIC are to use the prior knowledge of the detected adjacent bands/subcarriers

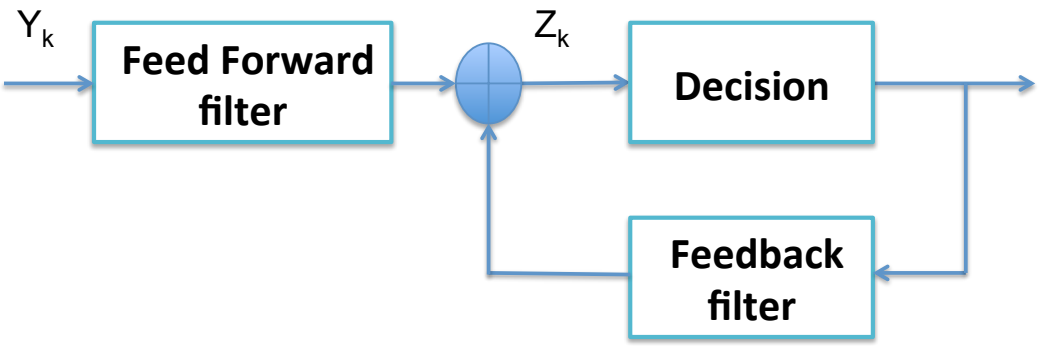

Figure 4.1: DFE block diagram

and then to remove INI by rebuilding the interference signals and subtracting them from the signal of interest.

4.2 System model

We consider a standard SMF with N spans, each of length L. The attenuation coefficient, the second-order dispersion parameter, and the nonlinear coefficient are denoted by α, β_2, and γ respectively. Let X and Y be the input/transmit signal of the first span of the fiber and the output/received signal of the N-th span of the fiber respectively. As we consider dual-polarization transmission, we denote the components of the signal X on polarization x and y by X_x and X_y respectively. Moreover, as we consider superchannel system which based on multi-band/subcarrier transmission, the transmitted signal on polarization x or y can be written in the frequency domain by

$$X_{x/y}(\omega) = \sum_{m=1}^{M} X_{x/y,m}(\omega) \tag{4.1}$$

where $X_{x/y,m}$ is the transmitted signal on the band/subcarrier m and M is the number of bands/subcarriers. Notice that the transmitted signal $X_{x/y,m}$ carries a sequence of information symbols $S_{x/y,m}$ thanks to a superchannel (MB-OFDM / Nyquist WDM) scheme.

As given in section 2.3.2-b, based on Volterra series expansion model of the optical fiber [59][60], we remind the received signal $Y_{x/y}$ on polarization x or y takes the following form

$$\begin{aligned} Y_{x/y}(\omega) &= h_1(\omega)X_{x/y}(\omega) \\ &+ \iint h_3(\omega_1,\omega_2,\omega-\omega_1+\omega_2)X_{x/y}(\omega-\omega_1+\omega_2) \\ &\times [X_x(\omega_1)X_x^*(\omega_2)+X_y(\omega_1)X_y^*(\omega_2)]d\omega_1 d\omega_2 \end{aligned} \tag{4.2}$$

where h_1 and h_3 denote the first-order and third-order VSTF kernels respectively. We recall

these kernels are given by

$$\begin{aligned} h_1(\omega) &= e^{-j\omega^2\beta_2 NL/2} \\ h_3(\omega_1,\omega_2,\omega-\omega_1+\omega_2) &= \frac{-jc'}{(2\pi)^2}h_1(\omega)\sum_{k=0}^{N-1}e^{-jk\beta_2\Delta\Omega L} \end{aligned} \tag{4.3}$$

with $\Delta\Omega=(\omega_1-\omega)(\omega_1-\omega_2)$, $L_{\text{eff}}=(1-e^{-\alpha L})/\alpha$, and $c'=8\gamma L_{\text{eff}}/9$.

4.3 Proposed INIC approach

The main idea of the proposed INIC approach relies on the Decision Feedback Equalizer (DFE) principle [64]. When focusing on one band/subcarrier of interest (let say m_0); the DFE principle consists in detecting the adjacent bands/subcarriers ($m=m_0+1, m_0-1$), regenerating them, and finally removing them from the band/subcarrier of interest.

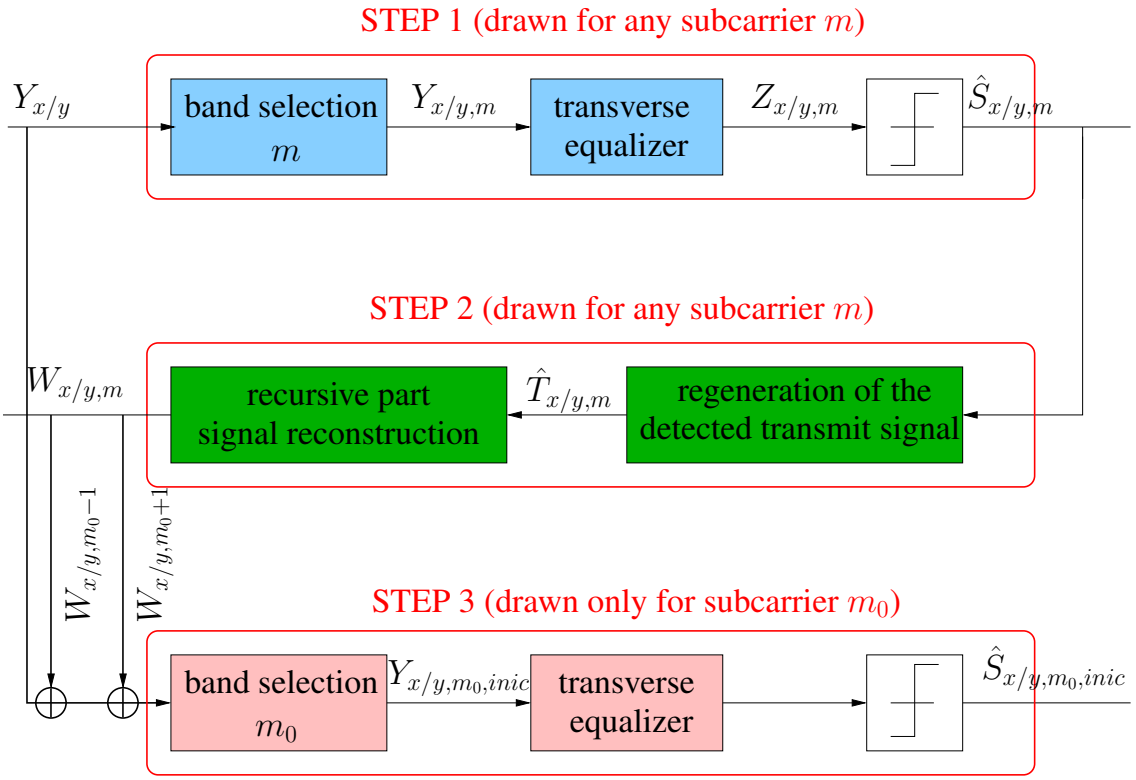

Figure 4.2: INIC receiver structure

As shown in Fig. B.20, the INIC structure has two main degrees of freedom: the transverse part and the recursive/feedback part. The transverse part basically consists of a third-order VNLE. It compensates for intra-band/subcarrier nonlinear effects. While the recursive part corresponds to the way the fiber signal is regenerated and it consists of a third-order Volterra fiber model. It compensates for inter-band/subcarrier interference. Interference can be purely

nonlinear. However, it can include also linear interference if the bands/subcarriers are overlapped such as in super-Nyquist systems (tableB.1).

To evaluate the performance of our proposed nonlinear interference cancellation technique. We implement three INIC receivers : the proposed INIC(3,3) which compensate for both linear and nonlinear interference in addition to intra-band/subcarrier nonlinearities, the already-existing one INIC(1,1) which compensate for only linear impairments and linear interference, and an intermediate one INIC(3,1) which compensate for intra-band/subcarrier nonlinear effects and only linear interference. The notation INIC(p,q) stands for a transverse part of order p and a recursive part of order q.

Notice that the transverse and recursive parts could be a Digital Back Propagation and a Digital Propagation respectively. This solution has not been studied in this thesis.

4.3.1 Nonlinear equalizer with nonlinear feedback: INIC(3,3)

In INIC(3,3), we use the third-order VNLE for the transverse part and the third-order Volterra fiber model for the recursive one. We hereafter assume that the band/subcarrier of interest is m_0. The other bands/subcarriers can be treated in a similar way. The implementation of the INIC(3,3) for the band/subcarrier m_0 can be split into three steps:

In the first step, each band/subcarrier is selected through a band-pass filter, leading to $Y_{x/y,m}$, and then demodulated according to the third-order VNLE. The frequency-domain output of the third-order VNLE is denoted by $Z_{x/y,m}$ and it can be written as

$$\begin{aligned} Z_{x/y,m}(\omega) &= k_1(\omega) Y_{x/y,m}(\omega) \\ &+ \iint k_3(\omega_1, \omega_2, \omega - \omega_1 + \omega_2) Y_{x/y,m}(\omega - \omega_1 + \omega_2) \\ &\times [Y_{x,m}(\omega_1) Y^*_{x,m}(\omega_2) + Y_{y,m}(\omega_1) Y^*_{y,m}(\omega_2)] d\omega_1 d\omega_2 \end{aligned} \tag{4.4}$$

where k_1 and k_3 are the first-order and third-order IVSTF kernels respectively given bye eq.2.26 and eq.2.27 . Then, a threshold detector is applied on $Z_{x/y,m}$ for each band/subcarrier m in order to find out the detected symbols $\widehat{S}_{x/y,m}$ corresponding to the transmitted symbols $S_{x/y,m}$.

In the second step, the detected symbols of each interference band/subcarrier m are re-modulated and regenerated based on third-order Volterra model of the optical fiber. Thus, the output $W_{x/y,m}$ can be written as:

$$\begin{aligned} W_{x/y,m}(\omega) &= h_1(\omega) \widehat{X}_{x/y,m}(\omega) \\ &+ \iint h_3(\omega_1, \omega_2, \omega - \omega_1 + \omega_2) \widehat{X}_{x/y,m}(\omega - \omega_1 + \omega_2) \\ &\times [\widehat{X}_{x,m}(\omega_1) \widehat{X}^*_{x,m}(\omega_2) + \widehat{X}_{y,m}(\omega_1) \widehat{X}^*_{y,m}(\omega_2)] d\omega_1 d\omega_2 \end{aligned} \tag{4.5}$$

where $\widehat{X} = [\widehat{X}_{x,m}, \widehat{X}_{y,m}]$ is the re-modulated signal corresponding to the detected symbols $\widehat{S} = [\widehat{S}_{x,m}, \widehat{S}_{y,m}]$. Because of the nonlinear effects, the signal $Y_{x,m}$ is not only on band/subcarrier m but is also spread over adjacent bands/subcarriers. As the INI caused by the two closest

adjacent bands/subcarriers is more important than other INI terms caused by further bands/subcarriers, the INI is well approximated by the contribution of the two closest adjacent bands/subcarriers when central ones are considered. In addition, in the context of super-Nyquist WDM, linear interference caused by the closest adjacent subcarriers also disturb the signal of subcarrier m.

In the third step, the two closest adjacent bands/subcarriers signals W_{m_0-1} and W_{m_0+1} are subtracted from the original received signal Y in order to obtain

$$Y_{m_0,inic}(\omega) = Y(\omega) - W_{m_0-1}(\omega) - W_{m_0+1}(\omega). \tag{4.6}$$

The final decision $\widehat{S}_{m_0,inic}$ is made on the signal $Y_{m_0,inic}$ after it has been passed through the subcarrier selection m_0 as well as through the third-order VNLE to compensate for the intra-band/subcarrier nonlinear effects.

4.3.2 Nonlinear equalizer with linear feedback: INIC(3,1)

In INIC(3,1), the third-order VNLE is used for the intra-band/subcarrier nonlinearities compensation but only linear interference due to bandwidth overlapping with adjacent bands/-subcarriers is considered. Therefore the recursive part relies on the first-order Volterra optical fiber model. Thus, Eq. (4.5) becomes

$$W_{x/y,m}(\omega) = h_1(\omega)\widehat{X}_{x/y,m}(\omega). \tag{4.7}$$

As in Eq. (B.14), before taking the final decision, $Y_{m_0,inic}$ is passed through the third-order VNLE to mitigate the intra-band/subcarrier nonlinear effects.

4.3.3 Linear equalizer with linear feedback: INIC(1,1)

In INIC(1,1), already proposed by [65], the nonlinear effects are not taken into account and the receiver only mitigates the intra-band/subcarrier and inter-band/subcarrier linear effects. More precisely, the received signal $Y_{x/y,m}$ is linearly equalized and the output signal $Z_{x/y,m}$ is given by

$$Z_{x/y,m}(\omega) = k_1(\omega)Y_{x/y,m}(\omega). \tag{4.8}$$

After detection on $Z_{x/y,m}$ to get $\widehat{S}_{x/y,m}$, the re-modulated signal $\widehat{X}_{x/y,m}$ is passed by the first-order Volterra model and the output $W_{x/y,m}$ is given by Eq. (4.7). Once again, we can apply Eq. (B.14), and the obtained signal $Y_{m_0,inic}$ is passed through the linear equalizer.

4.4 Simulation results

4.5 MB-OFDM simulation results

As MB-OFDM simulations in the previous chapters, the simulation setup is inspired from the SASER European project whose the goal is to design a 400 Gbps system for long-haul com-

munications. We generate four OFDM modulated bands of bandwidth 20 GHz and spaced by 2 GHz interval guard. We consider a Dual-Pol-16QAM OFDM with 512 subcarriers and a 11% loss in efficiency due to the cyclic prefix on each band. The transmission line consists of 8 spans of 100 km. Each span is a standard SMF with $\alpha = 0.2\text{dB.km}^{-1}$, $D = 17\text{ps.nm}^{-1}\text{.km}^{-1}$, and $\gamma = 1.4\text{W}^{-1}km^{-1}$. An Erbium-Doped Fiber Amplifier (EDFA) with a 5.5 dB noise figure and a 20 dB gain is also used at each span. All results in this work concern the central bands because they are the most degraded by nonlinear effects. Table.4.1 shows the OFDM parameters used for simulation.

Table 4.1: OFDM parameters

OFDM parameters	
FFT size	512
Cyclic prefix	11%
Subcarriers number	500
Modulation	16 QAM
Clipping ratio	13 dB
Quantization bits	5

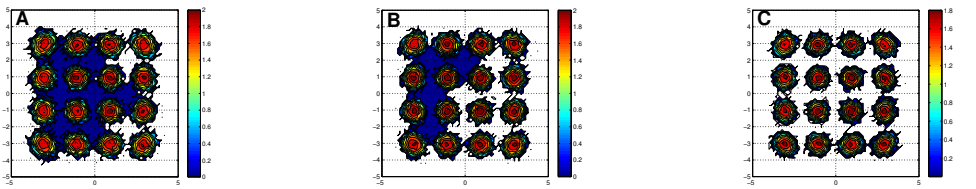

Figure 4.3: Constellations: (A) linear equalization; (B) VNLE; (C) Proposed INIC(3,3)

In Fig. 4.3, we show the constellations at optimum input power after linear equalization, third-order VNLE and INIC(3,3) respectively in a dual polarizartion context. The constellation after INIC(3,3) is clearer and the points are more visible which should lead to better performance in terms of Q factor.

In Fig. B.21, we plot Q factor vs. input power when only one single-polarization is active. The performance of the VNLE is closed to those of the linear equalization because of the inter-band interference. In contrast, the proposed INIC(3,3) strongly outperforms the VNLE.

In Fig. B.22, we plot Q factor vs. input power when both polarizations are active. The gain of the proposed INIC(3,3) compared to the VNLE is about $0.3dB$. The gain of both INIC(3,3) and VNLE are reduced in comparison with linear equalization. This can be explained by the appearence of XpolM nonlinear effects.

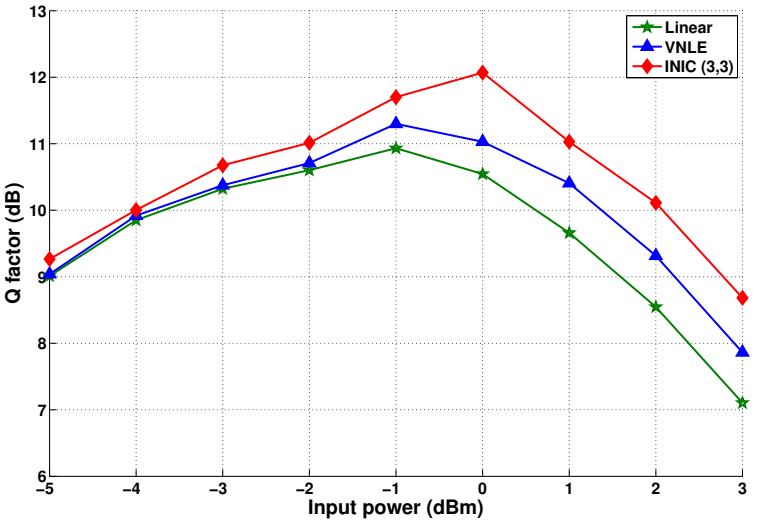

Figure 4.4: BER vs. input power for 4-band Single-Pol-16QAM OFDM

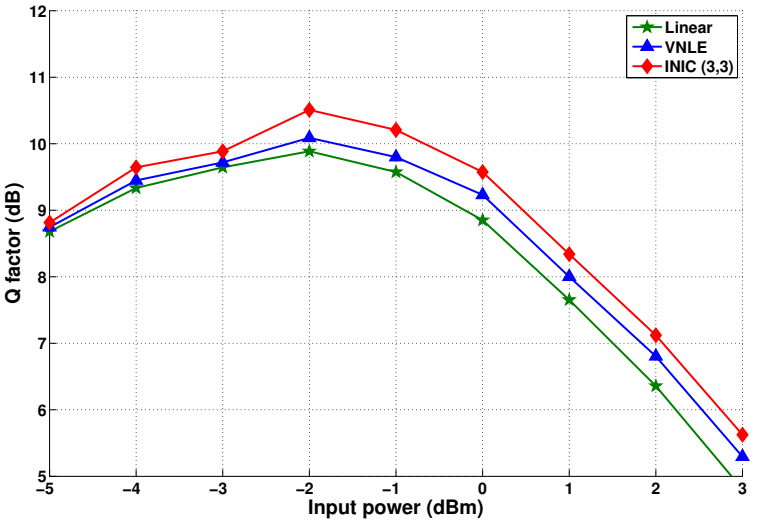

Figure 4.5: BER vs. input power for 4-band Dual-Pol-16QAM OFDM

4.6 Nyquist WDM simulation results

We generate a dual-polarization 16QAM modulated Nyquist-WDM superchannel with 4 subcarriers. The bit rate is 448Gbps and the symbol rate per subcarrier and per polarization is $R = 14$GBd. The transmission line consists of multi-span standard SMF with $\alpha = 0.2$dB.km^{-1}, $D = 17$ps.nm^{-1}.km^{-1}, and $\gamma = 1.4$W^{-1}.km^{-1}. The polarization mode dispersion (PMD) is 0.1ps.km$^{-1/2}$. The shaping filter is a Root-Raised Cosine (RRC) with roll off ρ. An Erbium-Doped Fiber Amplifier (EDFA) with a 5.5dB noise figure and a 20dB gain is used at each span of 100km. Notice that the analog to digital converter (ADC) works at twice the symbol rate. Table 4.2 summarizes the simulation parameters. All results will concern the central subcarriers

because they are the most disturbed ones by interference.

Table 4.2: Simulation parameters

Subcarrier number M	4
Bit rate	448Gbps
Symbol rate R	14GBd
Modulation	16QAM
RRC roll off ρ	0.1 or 0.01
ADC samples per symbol	2
EDFA noise figure	5.5dB
Span length L	100km

We also define the subcarrier spacing factor δ as the ratio between the subcarrier spacing Δf and the symbol rate R. Therefore, we have $\delta = \Delta f / R$.

In any figure, we plot the performance of each INIC receiver, and for comparison the (8-step per span) DBP, the classic third-order VNLE, and the linear equalizer. Unless otherwise stated, the transmission distance is $d = 1000$km.

In the first set of simulation, we fix the roll off ρ to be 0.1. In Fig. B.23, we plot the Q factor versus the input power for a subcarrier spacing factor $\delta = 1$. We observe that DBP, VNLE and linear equalizer offers similar performance far away from those proposed by the INIC. So the inter-subcarrier interference disturbs strongly the performance and has to be mitigate. The INIC(3,3) is the best ones and offers a gain about 0.3dB, 0.6dB and 1.5dB with respect to the INIC(3,1), the INIC(1,1) and the DBP.

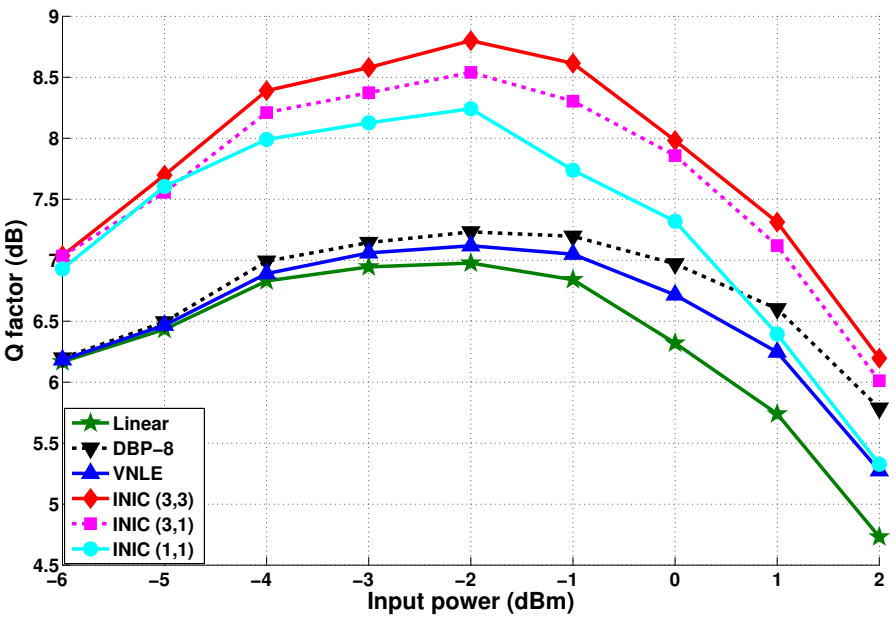

Figure 4.6: Q factor vs. input power ($\rho = 0.1$, $\delta = 1$)

In Fig. B.24, we plot the Q factor versus the subcarrier spacing factor δ at the optimum input power. When super-Nyquist WDM is considered, which means $\delta < 1$, the performance of DBP and VNLE are strongly reduced because of the high inter-subcarrier interference. At $\delta = 0.95$, the INIC(3,3) offers a gain of 2dB in comparison with DBP and VNLE and 0.5dB in comparison with INIC(3,1). At $\delta = 1.1$, any INIC leads to the same performance as DBP and VNLE due to the absence of interference.

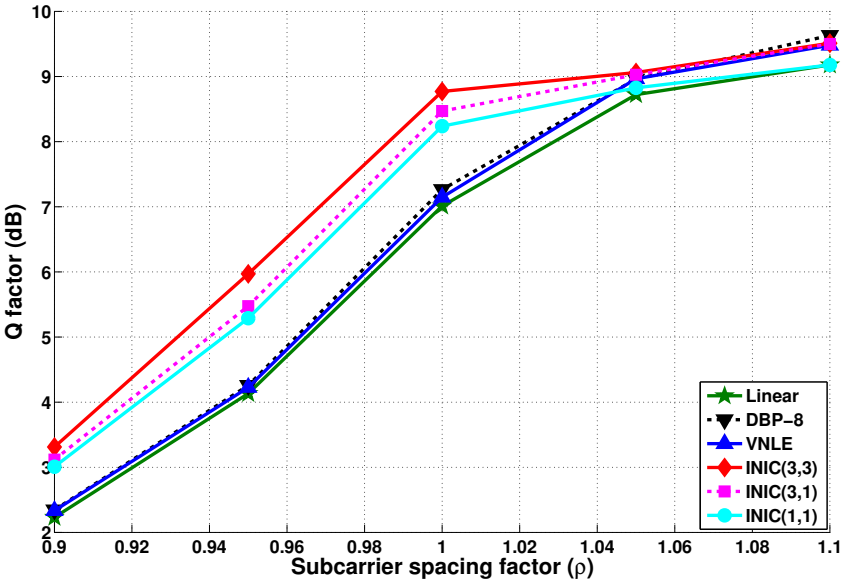

Figure 4.7: Q factor vs. subcarrier spacing factor δ ($\rho = 0.1$)

In Fig. B.25, we plot the transmission reach versus the input power for the Soft Decision Forward Error Correction (SD-FEC) limit $Q = 5.9$dB. INIC(3,3) improves the transmission reach by 500km compared to DBP, VNLE and linear INIC(1,1). Similar performance are obtained for INIC(3,3) and INIC(3,1) and the gain is less than the span length.

In the second set of simulation, we fix the roll off ρ to be strongly smaller and equal to 0.01. In Fig. B.27, we plot the Q factor versus the input power for a subcarrier spacing factor $\delta = 0.95$. Once again, INIC (3,3) outperforms INIC(3,1), INIC(1,1) and DBP with a gain respectively equal to 0.5dB, 0.7dB and 1.8dB. This substantial gain is obtained since there is a large inter-subcarrier nonlinear interference in this configuration.

In Fig. B.26, we plot the Q factor versus the subcarrier spacing factor δ at optimum input power. The INIC receiver gain reduces drammatically as soon as $\delta \geq 1$ (since the subcarrier interference becomes very weak) and $\delta \leq 0.9$ (since the interference is too high and difficult to compensate for due to the numerous errors in the first step of the INIC).

4.7 Complexity analysis

The complexity will be roughly analyzed through the required number of real multiplications. Notice that PMD is handled through an adaptive CMA and its complexity is neglected

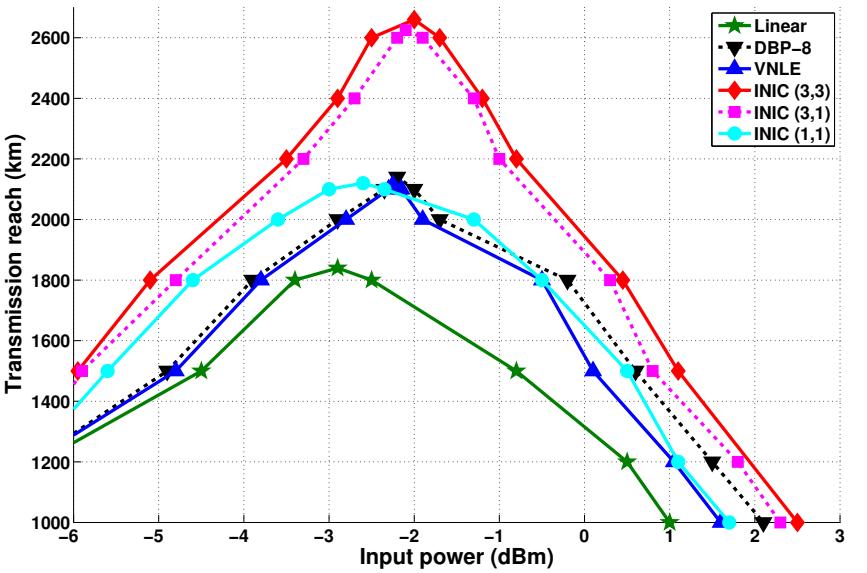

Figure 4.8: Transmission reach vs. input power ($\rho = 0.1$)

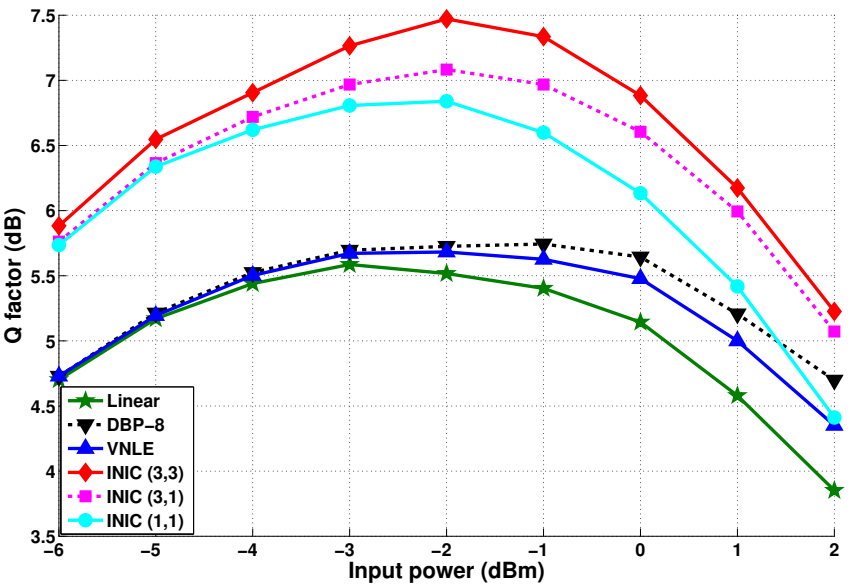

Figure 4.9: Q factor vs. input power ($\rho = 0.01$, $\delta = 0.95$)

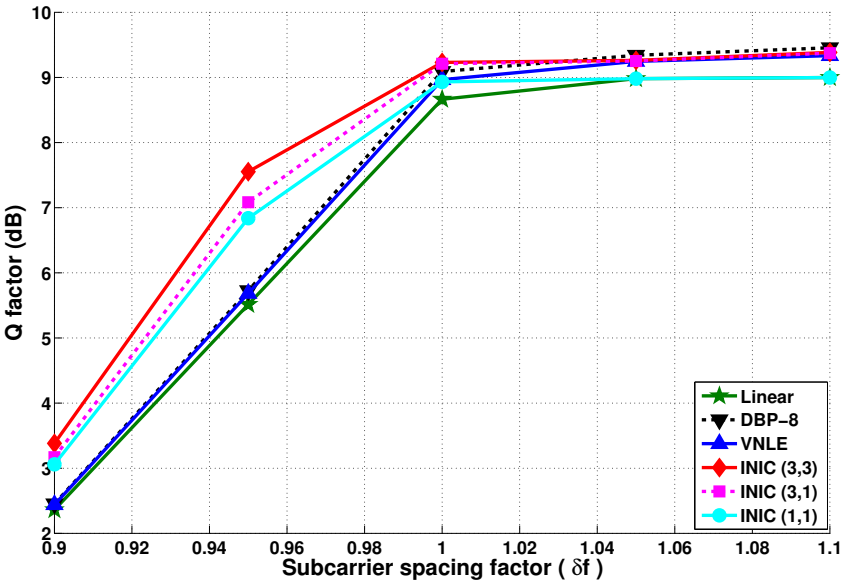

Figure 4.10: Q factor vs. subcarrier spacing factor δ ($\rho = 0.01$)

since it corresponds only to a few multiplications and additions per symbol. According to [59], the complexity of the single-step DBP and the third-order VLNE per band/subcarrier are $C_{\text{single–step DBP}} = 4NL\log_2(L) + 10.5NL$ and $C_{\text{VLNE}} = 2NL\log_2(L) + 4.25NL$ respectively, where L is the number of Fourier transforms. So we have $C_{\text{single–step DBP}} \approx 2C_{\text{VLNE}}$. Assuming the multiplications needed for applying the Volterra kernels H_1 and H_3 are almost equal to those of the inverse Volterra kernels K_1 and K_3, the complexity of INIC(3,3) is $C_{\text{INIC(3,3)}} = 3C_{\text{VLNE}} = (3/2)C_{\text{single–step DBP}}$ because we need to regenerate the two adjacent bands/subcarriers and to pass them through the third-order VNLE. As for INIC(3,1), the recursive part is linear and needs $4L\log_2(L) + 4L$ real multiplications. If N is large enough, this term can be neglected and we so have $C_{\text{INIC(3,1)}} = 2C_{\text{VLNE}} = C_{\text{single–step DBP}}$. Consequently, INIC(3,3) and INIC(3,1) are much less complex than the multi-step DBP such as the eight-step per span DBP used in simulation.

4.8 Conclusion

In this chapter, we described a new approach to combat nonlinear interference in the context of superchannel transmission systems. INIC showed a significant improvement of performance in terms of transmission reach and Q factor in Nyquist WDM and syper-Nyquist WDM systems. A significant gain in performance is also observed in MB-OFDM systems. Moreover, the proposed INIC have also reduced complexity compared to the classic multi-step DBP. Then, depending in system configuration, INIC(3,3) and INIC(3,1) when INI are negligible can be potential candidates to replace more complex multi-step DBP due to their high performance.

CONCLUSIONS AND PERSPECTIVES

Conclusions

The work carried out in this thesis deals with the compensation of nonlinear effects in the context of long-haul superchannel transmission systems. We have proposed two new approaches to combat nonlinear effects in optical fiber and we evaluated their performance in MB-OFDM and Nyquist WDM superchannels. Superchannels systems suffer from two kinds of nonlinearities: intra-band/subcarrier nonlinear effects which mainly caused by SPM ,and inter-band/subcarrier nonlinear interference caused by other Kerr-induced nonlinear effects such as XPM, XPolM and FWM.

To combat intra-band/subcarrier nonlinear effects, we proposed fifth-order Volterra based nonlinear equalizer. The main work was first the derivation of fifth order Volterra kernel and the determination of an implementation scheme in single-polarization and dual-polarization configurations. Then, the performance of the fifth-order VNLE was evaluated in MB-OFDM superchannel system. We observed that fifth-order VNLE strongly outperformed third-order VNLE in single-band and single-polarization OFDM configuration. In the case of multi-band and dual-polarization configuration, we observed a reduction of performance because of the inter-band nonlinear effects and the interaction between polarizations. Thus, the fifth-order VNLE is rather efficient for combating the intra-band nonlinear effects than the inter-band effects.

To deal with inter-band/subcarrier nonlinear interference in MB-OFDM and Nyquist WDM superchannel systems. We proposed inter-band/subcarrier nonlinear interference canceler based on third-order Volterra series. INIC has significantly improved the performance in MB-OFDM systems. We also implemented INIC approach in Nyquist WDM and super-Nyquist WDM systems. This approach outperformed the classic nonlinear effects mitigation DBP and third-order VNLE in terms of transmission reach. An improvement in terms of Q factor and subcarrier spacing was also observed.

Perspectives

As a future work, one can remark that the INIC implementation can rely on other nonlinear effects compensation technique such as DBP instead of Volterra series. A combination of Volterra series fiber model and DBP based equalizer can be also implemented.

The proposed INIC based on decision-feedback approach can be also used for combating the intra-band/subcarrier nonlinear effects. The major constraint when considering intra-band/subcarrier nonlinear effects is the causality issue. This issue consists of the the presence of nonlinear interference dependent on the current symbol in addition to precursor nonlinear interference. Thus, to implement intra-band/subcarrier nonlinear compensation based on DFE, causality issue should be resolved. Some approaches to deal with nonlinear interference caused by current symbol and precursor interference have been already proposed in wireless communication systems such as the Root Method and Precursor Enhanced RAM-DFE Canceler.

To improve the performance fifth-order VNLE, we suggest in a further work to take also into account the fifth-order VSTF for the fiber model in order to really work on the fifth-order and so to push the non-linear effects on seventh-order. Actually, we can see that this will lead to only add an extra box to our proposed receiver.

Appendix A

Derivations of fifth-order inverse Volterra kernel

A.1 Technical preliminaries

Before introducing new derivations, we just remind some useful expressions for the Volterra operator [63]. When the even-order of a Volterra operator is null, the Volterra operator for its inverse is given up to fifth-order as follows

$$\begin{aligned} K_1 &= H_1^{-1} && \text{(A.1)} \\ K_3 &= -K_1 H_3 K_1 && \text{(A.2)} \\ K_5 &= K_1[-H_3[K_1 + K_1 H_3 K_1] - 3H_3 K_1] && \text{(A.3)} \\ &+ K_1[0.5 H_3 K_1 H_3 K_1 + 0.5 H_3[2K_1 + K_1 H_3 K_1]] \end{aligned}$$

By using Eq.(A.2), we easily obtain that

$$K_5 = -K_1 H_3 L_1 + 3K_3 + 0.5 K_1 H_3 L_2 + 0.5 K_1 H_3 L_3 \quad \text{(A.4)}$$

with

$$L_1 = \begin{pmatrix} L_{1,x}(Y_x, Y_y) \\ L_{1,y}(Y_x, Y_y) \end{pmatrix}$$

$$L_2 = \begin{pmatrix} L_{2,x}(Y_x, Y_y) \\ L_{2,y}(Y_x, Y_y) \end{pmatrix}$$

$$L_3 = \begin{pmatrix} L_{3,x}(Y_x, Y_y) \\ L_{3,y}(Y_x, Y_y) \end{pmatrix}$$

According to Eq.(A.4), we get

$$Z_5 = K_5[Y] = z_1 + z_2 + z_3 + z_4$$

with

$$z_1 = \begin{pmatrix} z_{1,x} \\ z_{1,y} \end{pmatrix} = \begin{pmatrix} -K_1 H_3[L_{1,x}, L_{1,y}] \\ -K_1 H_3[L_{1,y}, L_{1,x}] \end{pmatrix}$$
$$z_2 = \begin{pmatrix} z_{2,x} \\ z_{2,y} \end{pmatrix} = \begin{pmatrix} 3K_3[Y_x, Y_y] \\ 3K_3[Y_y, Y_x] \end{pmatrix}$$
$$z_3 = \begin{pmatrix} z_{3,x} \\ z_{3,y} \end{pmatrix} = \begin{pmatrix} 0.5K_1 H_3[L_{2,x}, L_{2,y}] \\ 0.5K_1 H_3[L_{2,y}, L_{2,x}] \end{pmatrix}$$
$$z_4 = \begin{pmatrix} z_{4,x} \\ z_{4,y} \end{pmatrix} = \begin{pmatrix} 0.5K_1 H_3[L_{3,x}, L_{3,y}] \\ 0.5K_1 H_3[L_{3,y}, L_{3,x}] \end{pmatrix}$$

Let us now work to find the kernels associated with each signal z_i. In fact we compute the signal $z_{i,x}$ and we can deduce $z_{i,y}$ by analogy.

Derivations of z_1

$$z_{1,x}(\omega) = -k_1(\omega) \int_{\omega_1} \int_{\omega_2} h_3(\omega_1, \omega_2, \omega - \omega_1 + \omega_2) \tag{A.5}$$
$$\times [\ell_{1,x}(\omega_1)\ell^*_{1,x}(\omega_2) + \ell_{1,y}(\omega_1)\ell^*_{1,y}(\omega_2)]\ell_{1,x}(\omega - \omega_1 + \omega_2) d\omega_1 d\omega_2$$

After that replacing the $\ell_{1,i}$ by its value

$$z_{1,x}(\omega) = -k_1(\omega) \int_{\omega_1} \int_{\omega_2} h_3(\omega_1, \omega_2, \omega - \omega_1 + \omega_2) \tag{A.6}$$
$$\times [[k_1(\omega_1)Y_x(\omega_1) - \int_{\omega_3} \int_{\omega_4} k_3(\omega_3, \omega_4, \omega_1 - \omega_3 + \omega_4)[Y_x(\omega_3)Y^*_x(\omega_4$$
$$+ Y_y(\omega_3)Y^*_y(\omega_4)]Y_x(\omega_1 - \omega_3 + \omega_4) d\omega_3 d\omega_4][k^*_1(\omega_2)Y^*_x(\omega_2)$$
$$- \int_{\omega_5} \int_{\omega_6} k^*_3(\omega_5, \omega_6, \omega_2 - \omega_5 + \omega_6)[Y^*_x(\omega_5)Y_x(\omega_6) + Y^*_y(\omega_5)Y_y(\omega_6)]Y^*_x(\omega_2 - \omega_5 + \omega_6) d\omega_5 d\omega_6]$$
$$\times [k_1(\omega - \omega_1 + \omega_2)Y_x(\omega - \omega_1 + \omega_2) - \int_{\omega_7} \int_{\omega_8} k_3(\omega_7, \omega_8, \omega - \omega_1 + \omega_2 - \omega_7 + \omega_8)$$
$$\times [Y_x(\omega_7)Y^*_x(\omega_8) + Y_y(\omega_7)Y^*_y(\omega_8)]Y_x(\omega - \omega_1 + \omega_2 - \omega_7 + \omega_8) d\omega_7 d\omega_8] + [k_1(\omega_1)Y_x(\omega_1)$$
$$- \int_{\omega_3} \int_{\omega_4} k_3(\omega_3, \omega_4, \omega_1 - \omega_3 + \omega_4)[Y_x(\omega_3)Y^*_x(\omega_4) + Y_y(\omega_3)Y^*_y(\omega_4)]$$
$$\times Y_y(\omega_1 - \omega_3 + \omega_4) d\omega_3 d\omega_4][k^*_1(\omega_2)Y^*_y(\omega_2)$$
$$- \int_{\omega_5} \int_{\omega_6} k^*_3(\omega_5, \omega_6, \omega_2 - \omega_5 + \omega_6)[Y^*_x(\omega_5)Y_x(\omega_6) + Y^*_y(\omega_5)Y_y(\omega_6)]Y^*_y(\omega_2 - \omega_5 + \omega_6) d\omega_5 d\omega_6]$$
$$\times [k_1(\omega - \omega_1 + \omega_2)Y_x(\omega - \omega_1 + \omega_2) - \int_{\omega_7} \int_{\omega_8} k_3(\omega_7, \omega_8, \omega - \omega_1 + \omega_2 - \omega_7 + \omega_8)[Y_x(\omega_7)Y^*_x(\omega_8)$$
$$+ Y_y(\omega_7)Y^*_y(\omega_8)]Y_x(\omega - \omega_1 + \omega_2 - \omega_7 + \omega_8) d\omega_7 d\omega_8] d\omega_1 d\omega_2]$$

By developing, we obviously obtain the following terms

$$z_{1,x}(\omega) = -\sum_{i=1}^{16} k_1(\omega) \int_{\omega_1} \int_{\omega_2} h_3(\omega_1, \omega_2, \omega - \omega_1 + \omega_2) t_{i,1}(\omega_1, \omega_2) d\omega_1 d\omega_2$$

with

$$t_{1,x}(\omega_1, \omega_2) = k_1(\omega_1) k_1^*(\omega_2) k_1(\omega - \omega_1 + \omega_2) Y_x(\omega_1) Y_x^*(\omega_2) Y_x(\omega - \omega_1 + \omega_2) \tag{A.7}$$

$$t_{2,x}(\omega_1, \omega_2) = -k_1(\omega_1) k_1^*(\omega_2) Y_x(\omega_1) Y_x^*(\omega_2) \int_{\omega_7} \int_{\omega_8} k_3(\omega_7, \omega_8, \omega - \omega_1 + \omega_2 - \omega_7 + \omega_8) \tag{A.8}$$

$$\times [Y_x(\omega_7) Y_x^*(\omega_8) + Y_y(\omega_7) Y_y^*(\omega_8)] Y_x(\omega - \omega_1 + \omega_2 - \omega_7 + \omega_8) d\omega_7 d\omega_8$$

$$t_{3,x}(\omega_1, \omega_2) = -k_1(\omega_1) k_1(\omega - \omega_1 + \omega_2) Y_x(\omega_1) Y_x(\omega - \omega_1 + \omega_2) \int_{\omega_5} \int_{\omega_6} k_3^*(\omega_5, \omega_6, \omega_2 - \omega_5 + \omega_6) \tag{A.9}$$

$$\times [Y_x^*(\omega_5) Y_x(\omega_6) + Y_y^*(\omega_5) Y_y(\omega_6)] Y_x^*(\omega_2 - \omega_5 + \omega_6) d\omega_5 d\omega_6$$

$$t_{4,x}(\omega_1, \omega_2) = k_1(\omega_1) Y_x(\omega_1) \int_{\omega_5} \int_{\omega_6} k_3^*(\omega_5, \omega_6, \omega_2 - \omega_5 + \omega_6) [Y_x^*(\omega_5) Y_x(\omega_6) + \tag{A.10}$$

$$Y_y^*(\omega_5) Y_y(\omega_6)] Y_x^*(\omega_2 - \omega_5 + \omega_6) d\omega_5 d\omega_6 \int_{\omega_7} \int_{\omega_8} k_3(\omega_7, \omega_8, \omega - \omega_1 + \omega_2 - \omega_7 + \omega_8)$$

$$\times [Y_x(\omega_7) Y_x^*(\omega_8) + Y_y(\omega_7) Y_y^*(\omega_8)] Y_x(\omega - \omega_1 + \omega_2 - \omega_7 + \omega_8) d\omega_7 d\omega_8$$

$$t_{5,x}(\omega_1, \omega_2) = -k_1^*(\omega_2) k_1(\omega - \omega_1 + \omega_2) Y_x^*(\omega_2) Y_x(\omega - \omega_1 + \omega_2) \int_{\omega_3} \int_{\omega_4} k_3(\omega_3, \omega_4, \omega_1 - \omega_3 + \omega_4) \tag{A.11}$$

$$\times [Y_x(\omega_3) Y_x^*(\omega_4) + Y_y(\omega_3) Y_y^*(\omega_4)] Y_y(\omega_1 - \omega_3 + \omega_4) d\omega_3 d\omega_4$$

$$t_{6,x}(\omega_1, \omega_2) = k_1^*(\omega_2) Y_x^*(\omega_2) \int_{\omega_3} \int_{\omega_4} k_3(\omega_3, \omega_4, \omega_1 - \omega_3 + \omega_4) \tag{A.12}$$

$$\times [Y_x(\omega_3) Y_x^*(\omega_4) + Y_y(\omega_3) Y_y^*(\omega_4)] Y_x(\omega_1 - \omega_3 + \omega_4) d\omega_3 d\omega_4$$

$$\times \int_{\omega_7} \int_{\omega_8} k_3(\omega_7, \omega_8, \omega - \omega_1 + \omega_2 - \omega_7 + \omega_8) [Y_x(\omega_7) Y_x^*(\omega_8) + Y_y(\omega_7) Y_y^*(\omega_8)]$$

$$\times Y_x(\omega - \omega_1 + \omega_2 - \omega_7 + \omega_8) d\omega_7 d\omega_8$$

$$t_{7,x}(\omega_1,\omega_2) = k_1(\omega-\omega_1+\omega_2)Y_x(\omega-\omega_1+\omega_2)\int_{\omega_3}\int_{\omega_4} k_3(\omega_3,\omega_4,\omega_1-\omega_3+\omega_4) \quad \text{(A.13)}$$
$$\times [Y_x(\omega_3)Y_x^*(\omega_4)+Y_y(\omega_3)Y_y^*(\omega_4)]Y_x(\omega_1-\omega_3+\omega_4)d\omega_3 d\omega_4$$
$$\times \int_{\omega_5}\int_{\omega_6} k_3^*(\omega_5,\omega_6,\omega_2-\omega_5+\omega_6)[Y_x^*(\omega_5)Y_x(\omega_6)+Y_y^*(\omega_5)Y_y(\omega_6)]$$
$$\times Y_x^*(\omega_2-\omega_5+\omega_6)d\omega_5 d\omega_6$$

$$t_{8,x}(\omega_1,\omega_2) = -\int_{\omega_3}\int_{\omega_4} k_3(\omega_3,\omega_4,\omega_1-\omega_3+\omega_4)[Y_x(\omega_3)Y_x^*(\omega_4) \quad \text{(A.14)}$$
$$+Y_y(\omega_3)Y_y^*(\omega_4)]Y_x(\omega_1-\omega_3+\omega_4)d\omega_3 d\omega_4 \int_{\omega_5}\int_{\omega_6} k_3^*(\omega_5,\omega_6,\omega_2-\omega_5+\omega_6)$$
$$\times [Y_x^*(\omega_5)Y_x(\omega_6)+Y_y^*(\omega_5)Y_y(\omega_6)]Y_x^*(\omega_2-\omega_5+\omega_6)d\omega_5 d\omega_6$$
$$\times \int_{\omega_7}\int_{\omega_8} k_3(\omega_7,\omega_8,\omega-\omega_1+\omega_2-\omega_7+\omega_8)$$
$$\times [Y_x(\omega_7)Y_x^*(\omega_8)+Y_y(\omega_7)Y_y^*(\omega_8)]Y_x(\omega-\omega_1+\omega_2-\omega_7+\omega_8)d\omega_7 d\omega_8$$

$$t_{9,x}(\omega_1,\omega_2) = k_1(\omega_1)k_1^*(\omega_2)k_1(\omega-\omega_1+\omega_2)Y_y(\omega_1)Y_y^*(\omega_2)Y_x(\omega-\omega_1+\omega_2) \quad \text{(A.15)}$$

$$t_{10,x}(\omega_1,\omega_2) = -k_1(\omega_1)k_1^*(\omega_2)Y_y(\omega_1)Y_y^*(\omega_2)\int_{\omega_7}\int_{\omega_8} k_3(\omega_7,\omega_8,\omega-\omega_1+\omega_2-\omega_7+\omega_8) \quad \text{(A.16)}$$
$$\times [Y_x(\omega_7)Y_x^*(\omega_8)+Y_y(\omega_7)Y_y^*(\omega_8)]Y_x(\omega-\omega_1+\omega_2-\omega_7+\omega_8)d\omega_7 d\omega_8$$

$$t_{11,x}(\omega_1,\omega_2) = k_1(\omega_1)Y_y(\omega_1)\int_{\omega_5}\int_{\omega_6} k_3^*(\omega_5,\omega_6,\omega_2-\omega_5+\omega_6) \quad \text{(A.17)}$$
$$\times [Y_x^*(\omega_5)Y_x(\omega_6)+Y_y^*(\omega_5)Y_y(\omega_6)]Y_y^*(\omega_2-\omega_5+\omega_6)d\omega_5 d\omega_6 \int_{\omega_7}\int_{\omega_8} k_3(\omega_7,\omega_8,\omega-\omega_1+\omega_2$$
$$\times -\omega_7+\omega_8)[Y_x(\omega_7)Y_x^*(\omega_8)+Y_y(\omega_7)Y_y^*(\omega_8)]Y_x(\omega-\omega_1+\omega_2-\omega_7+\omega_8)d\omega_7 d\omega_8$$

$$t_{12,x}(\omega_1,\omega_2) = -k_1^*(\omega_2)k_1(\omega-\omega_1+\omega_2)Y_y^*(\omega_2)Y_x(\omega-\omega_1+\omega_2)\int_{\omega_3}\int_{\omega_4} k_3(\omega_3,\omega_4,\omega_1-\omega_3+\omega_4) \quad \text{(A.18)}$$
$$\times [Y_x(\omega_3)Y_x^*(\omega_4)+Y_y(\omega_3)Y_y^*(\omega_4)]Y_y(\omega_1-\omega_3+\omega_4)d\omega_3 d\omega_4$$

$$t_{13,x}(\omega_1,\omega_2)=k_1^*(\omega_2)Y_y^*(\omega_2)\int_{\omega_3}\int_{\omega_4}k_3(\omega_3,\omega_4,\omega_1-\omega_3+\omega_4) \tag{A.19}$$
$$\times[Y_x(\omega_3)Y_x^*(\omega_4)+Y_y(\omega_3)Y_y^*(\omega_4)]Y_y(\omega_1-\omega_3+\omega_4)d\omega_3 d\omega_4$$
$$\times\int_{\omega_7}\int_{\omega_8}k_3(\omega_7,\omega_8,\omega-\omega_1+\omega_2-\omega_7+\omega_8)[Y_x(\omega_7)Y_x^*(\omega_8)+Y_y(\omega_7)Y_y^*(\omega_8)]$$
$$\times Y_x(\omega-\omega_1+\omega_2-\omega_7+\omega_8)d\omega_7 d\omega_8$$

$$t_{14,x}(\omega_1,\omega_2)=k_1(\omega-\omega_1+\omega_2)Y_x(\omega-\omega_1+\omega_2)\int_{\omega_3}\int_{\omega_4}k_3(\omega_3,\omega_4,\omega_1-\omega_3+\omega_4) \tag{A.20}$$
$$\times[Y_x(\omega_3)Y_x^*(\omega_4)+Y_y(\omega_3)Y_y^*(\omega_4)]Y_y(\omega_1-\omega_3+\omega_4)d\omega_3 d\omega_4\int_{\omega_5}\int_{\omega_6}k_3^*(\omega_5,\omega_6,\omega_2-\omega_5+\omega_6)$$
$$\times[Y_x^*(\omega_5)Y_x(\omega_6)+Y_y^*(\omega_5)Y_y(\omega_6)]Y_y^*(\omega_2-\omega_5+\omega_6)d\omega_5 d\omega_6$$

$$t_{15,x}(\omega_1,\omega_2)=-k_1(\omega_1)k_1(\omega-\omega_1+\omega_2)Y_y(\omega_1)Y_x(\omega-\omega_1+\omega_2) \tag{A.21}$$
$$\times\int_{\omega_5}\int_{\omega_6}k_3^*(\omega_5,\omega_6,\omega_2-\omega_5+\omega_6)[Y_x^*(\omega_5)Y_x(\omega_6)+Y_y^*(\omega_5)Y_y(\omega_6)]$$
$$\times Y_x^*(\omega_2-\omega_5+\omega_6)d\omega_5 d\omega_6$$

$$t_{16,x}(\omega_1,\omega_2)=-\int_{\omega_3}\int_{\omega_4}k_3(\omega_3,\omega_4,\omega_1-\omega_3+\omega_4)[Y_x(\omega_3)Y_x^*(\omega_4)+Y_y(\omega_3)Y_y^*(\omega_4)] \tag{A.22}$$
$$\times Y_y(\omega_1-\omega_3+\omega_4)d\omega_3 d\omega_4\int_{\omega_5}\int_{\omega_6}k_3^*(\omega_5,\omega_6,\omega_2-\omega_5+\omega_6)[Y_x^*(\omega_5)Y_x(\omega_6)+Y_y^*(\omega_5)Y_y(\omega_6)]$$
$$\times Y_y^*(\omega_2-\omega_5+\omega_6)d\omega_5 d\omega_6\int_{\omega_7}\int_{\omega_8}k_3(\omega_7,\omega_8,\omega-\omega_1+\omega_2-\omega_7+\omega_8)$$
$$\times[Y_x(\omega_7)Y_x^*(\omega_8)+Y_y(\omega_7)Y_y^*(\omega_8)]Y_x(\omega-\omega_1+\omega_2-\omega_7+\omega_8)d\omega_7 d\omega_8$$

Derivations of z_2

$$z_{2,x}(\omega)=3\int_{\omega_1}\int_{\omega_2}k_3(\omega_1,\omega_2,\omega-\omega_1+\omega_2)[Y_x(\omega_1)Y_x^*(\omega_2)+Y_y(\omega_1)Y_y^*(\omega_2)] \tag{A.23}$$
$$\times Y_x(\omega-\omega_1+\omega_2)d\omega_1 d\omega_2$$

Derivations of z_3

$$z_{3,x}(\omega)=0.5k_1(\omega)\int_{\omega_1}\int_{\omega_2}h_3(\omega_1,\omega_2,\omega-\omega_1+\omega_2) \tag{A.24}$$
$$\times[\ell_{2,x}(\omega_1)\ell_{2,x}^*(\omega_2)+\ell_{2,x}(\omega_1)\ell_{2,x}^*(\omega_2)]\ell_2(\omega-\omega_1+\omega_2)d\omega_1 d\omega_2$$

with

$$\ell_{2,x}(\omega) = -\int_{\omega_3}\int_{\omega_4} k_3(\omega_3,\omega_4,\omega-\omega_3+\omega_4)[Y_x(\omega_3)Y_x^*(\omega_4)+Y_y(\omega_3)Y_y^*(\omega_4)]Y_x(\omega-\omega_3+\omega_4)d\omega_3 d\omega_4.$$

$$\ell_{2,x}(\omega) = -\int_{\omega_3}\int_{\omega_4} k_3(\omega_3,\omega_4,\omega-\omega_3+\omega_4)[Y_x(\omega_3)Y_x^*(\omega_4)+Y_y(\omega_3)Y_y^*(\omega_4)]Y_y(\omega-\omega_3+\omega_4)d\omega_3 d\omega_4.$$

So we get:

$$\begin{aligned}
z_{3,x}(\omega) &= 0.5k_1(\omega)\int_{\omega_1}\int_{\omega_2} h_3(\omega_1,\omega_2,\omega-\omega_1+\omega_2) \\
&\times[-\int_{\omega_3}\int_{\omega_4} k_3(\omega_3,\omega_4,\omega_1-\omega_3+\omega_4)[Y_x(\omega_3)Y_x^*(\omega_4)+Y_y(\omega_3)Y_y^*(\omega_4)] \\
&\times Y_x(\omega_1-\omega_3+\omega_4)d\omega_3 d\omega_4 \\
&\times\int_{\omega_5}\int_{\omega_6} k_3^*(\omega_5,\omega_6,\omega_2-\omega_5+\omega_6)[Y_x^*(\omega_5)Y_x(\omega_6)+Y_y^*(\omega_5)Y_y(\omega_6)] \\
&\times Y_x^*(\omega_2-\omega_5+\omega_6)d\omega_5 d\omega_6\int_{\omega_7}\int_{\omega_8} k_3(\omega_7,\omega_8,\omega-\omega_1+\omega_2-\omega_7+\omega_8) \\
&\times[Y_x(\omega_7)Y_x^*(\omega_8)+Y_y(\omega_7)Y_y^*(\omega_8)]Y_x(\omega-\omega_1+\omega_2-\omega_7+\omega_8)d\omega_7 d\omega_8 \\
&\times-\int_{\omega_3}\int_{\omega_4} k_3(\omega_3,\omega_4,\omega_1-\omega_3+\omega_4)[Y_x(\omega_3)Y_x^*(\omega_4)+Y_y(\omega_3)Y_y^*(\omega_4)] \\
&\times Y_y(\omega_1-\omega_3+\omega_4)d\omega_3 d\omega_4\int_{\omega_5}\int_{\omega_6} k_3^*(\omega_5,\omega_6,\omega_2-\omega_5+\omega_6) \\
&\times[Y_x^*(\omega_5)Y_x(\omega_6)+Y_y^*(\omega_5)Y_y(\omega_6)]Y_y^*(\omega_2-\omega_5+\omega_6)d\omega_5 d\omega_6 \\
&\times\int_{\omega_7}\int_{\omega_8} k_3(\omega_7,\omega_8,\omega-\omega_1+\omega_2-\omega_7+\omega_8) \\
&\times[Y_x(\omega_7)Y_x^*(\omega_8)+Y_y(\omega_7)Y_y^*(\omega_8)]Y_x(\omega-\omega_1+\omega_2-\omega_7+\omega_8)d\omega_7 d\omega_8]d\omega_1 d\omega_2
\end{aligned} \tag{A.25}$$

Derivations of z_4

$$\begin{aligned}
z_{4,x}(\omega) &= 0.5k_1(\omega)\int_{\omega_1}\int_{\omega_2} h_3(\omega_1,\omega_2,\omega-\omega_1+\omega_2) \\
&\times[\ell_{3,x}(\omega_1)\ell_{3,x}^*(\omega_2)+\ell_{3,y}(\omega_1)\ell_{3,y}^*(\omega_2)]\ell_{3,x}(\omega-\omega_1+\omega_2)d\omega_1 d\omega_2
\end{aligned} \tag{A.26}$$

with

$$\begin{aligned}
\ell_{3,x}(\omega) &= 2k_1(\omega)y_x(\omega)-\int_{\omega_3}\int_{\omega_4} k_3(\omega_3,\omega_4,\omega-\omega_3+\omega_4) \\
&\times[Y_x(\omega_3)Y_x^*(\omega_4)+Y_y(\omega_3)Y_y^*(\omega_4)]Y_x(\omega-\omega_3+\omega_4)d\omega_3 d\omega_4
\end{aligned} \tag{A.27}$$

$$\begin{aligned}
\ell_{3,y}(\omega) &= 2k_1(\omega)y_y(\omega)-\int_{\omega_3}\int_{\omega_4} k_3(\omega_3,\omega_4,\omega-\omega_3+\omega_4) \\
&\times[Y_x(\omega_3)Y_x^*(\omega_4)+Y_y(\omega_3)Y_y^*(\omega_4)]Y_y(\omega-\omega_3+\omega_4)d\omega_3 d\omega_4
\end{aligned} \tag{A.28}$$

As done for z_1 we obtain almost the same expression, only some coefficients before t_i are different. We so have

$$z_{4,x}(\omega) = 0.5k_1(\omega)\int_{\omega_1}\int_{\omega_2} h_3(\omega_1,\omega_2,\omega-\omega_1+\omega_2)$$
$$\times[8t_{1,x}(\omega_1,\omega_2)+t_{9,x}(\omega_1,\omega_2)+4[t_{2,x}(\omega_1,\omega_2)+t_{3,x}(\omega_1,\omega_2)+t_{5,x}(\omega_1,\omega_2)+t_{10,x}(\omega_1,\omega_2)$$
$$+t_{12,x}(\omega_1,\omega_2)+t_{15,x}(\omega_1,\omega_2)]+2[t_{4,x}(\omega_1,\omega_2)+t_{6,x}(\omega_1,\omega_2)+t_{7,x}(\omega_1,\omega_2)+t_{11,x}(\omega_1,\omega_2)$$
$$+t_{13,x}(\omega_1,\omega_2)+t_{14,x}(\omega_1,\omega_2)]+t_{8,x}(\omega_1,\omega_2)+t_{16,x}(\omega_1,\omega_2)]d\omega_1 d\omega_2$$

We can also express $z_{3,x}$ in function of $t_{i,x}$ as:

$$z_{3,x}(\omega) = 0.5k_1(\omega)\int_{\omega_1}\int_{\omega_2} h_3(\omega_1,\omega_2,\omega-\omega_1+\omega_2)[t_{2,x}(\omega_1,\omega_2)+t_{16,x}(\omega_1,\omega_2)]d\omega_1 d\omega_2$$

As the case of single polarization, we replace K_3 by its expression : $K_3 = -K_1H_3[K_1]$ and we have:

$$z_{3,x}(\omega) = -3k_1(\omega)\int_{\omega_1}\int_{\omega_2} h_3(\omega_1,\omega_2,\omega-\omega_1+\omega_2)[t_{1,x}(\omega_1,\omega_2)+t_{9,x}(\omega_1,\omega_2)]d\omega_1 d\omega_2$$

So the final expression of the first component of $Z_{5,x}$ in function of $t_{i,x}$:

$$Z_5(\omega) = \begin{pmatrix} Z_{5,x} \\ Z_{5,x} \end{pmatrix}$$

$$Z_{5,x}(\omega) = k_1(\omega)\int_{\omega_1}\int_{\omega_2} h_3(\omega_1,\omega_2,\omega-\omega_1+\omega_2)[t_{2,1}(\omega_1,\omega_2)+t_{3,1}(\omega_1,\omega_2)+$$
$$t_{5,1}(\omega_1,\omega_2)+t_{10,1}(\omega_1,\omega_2)+t_{12,1}(\omega_1,\omega_2)+t_{15,1}(\omega_1,\omega_2)]d\omega_1 d\omega_2 \quad (A.29)$$

After replacing each $t_{i,x}$ by its expression and regrouping the terms in function of Y_i products,we can express $Z_{5,x}$ as:

$$Z_{5,x}(\omega) = -k_1(\omega)\int_{\omega_1}\int_{\omega_2} h_3(\omega_1,\omega_2,\omega-\omega_1+\omega_2)[q_{1,x}(\omega)+q_{2,x}(\omega)+q_{3,x}(\omega)]d\omega_1 d\omega_2$$

With :

$$q_{1,x}(\omega) = f(Y_x^5); q_{2,x}(\omega) = f(Y_x^3, Y_y^2); q_{3,x}(\omega) = f(Y_x, Y_y^4);$$

The expression of each $q_{i,x}$ is

$$\begin{aligned}
q_{1,x}(\omega) &= k_1(\omega_1)k_1^*(\omega_2)\int_{\omega_3}\int_{\omega_4} k_3(\omega_3,\omega_4,\omega-\omega_1+\omega_2-\omega_3+\omega_4)\\
&\times Y_x(\omega_1)Y_x^*(\omega_2)Y_x(\omega_3)Y_x^*(\omega_4)Y_x(\omega-\omega_1+\omega_2-\omega_3+\omega_4)d\omega_3 d\omega_4\\
&+ k_1(\omega_1)k_1(\omega-\omega_1+\omega_2)\int_{\omega_3}\int_{\omega_4} k_3^*(\omega_3,\omega_4,\omega_2-\omega_3+\omega_4)Y_x(\omega_1)Y_x(\omega-\omega_1+\omega_2)\\
&\times Y_x^*(\omega_3)Y_x(\omega_4)Y_x^*(\omega_2-\omega_3+\omega_4)d\omega_3 d\omega_3\\
&+ k_1^*(\omega_2)k_1(\omega-\omega_1+\omega_2)\int_{\omega_3}\int_{\omega_4} k_3(\omega_3,\omega_4,\omega_1-\omega_3+\omega_4)\\
&\times Y_x^*(\omega_2)Y_x(\omega-\omega_1+\omega_2)Y_x(\omega_3)Y_x^*(\omega_4)Y_x(\omega_1-\omega_3+\omega_4)d\omega_3 d\omega_4
\end{aligned}$$

$$\begin{aligned}
q_{2,x}(\omega) &= k_1(\omega_1)k_1^*(\omega_2)\int_{\omega_3}\int_{\omega_4} k_3(\omega_3,\omega_4,\omega-\omega_1+\omega_2-\omega_3+\omega_4)\\
&\times [Y_x(\omega_1)Y_x^*(\omega_2)Y_y(\omega_3)Y_y^*(\omega_4)+Y_y(\omega_1)Y_y^*(\omega_2)Y_x(\omega_3)Y_x^*(\omega_4)]\\
&\times Y_x(\omega-\omega_1+\omega_2-\omega_3+\omega_4)d\omega_3 d\omega_4\\
&+ k_1(\omega_1)k_1(\omega-\omega_1+\omega_2)\int_{\omega_3}\int_{\omega_4} k_3^*(\omega_3,\omega_4,\omega_2-\omega_3+\omega_4)\\
&\times [Y_x(\omega_1)Y_x^*(\omega_2-\omega_3+\omega_4)Y_y^*(\omega_3)Y_y(\omega_4)+Y_y(\omega_1)Y_y^*(\omega_2-\omega_3+\omega_4)Y_x^*(\omega_3)Y_x(\omega_4)]\\
&\times Y_x(\omega-\omega_1+\omega_2)d\omega_3 d\omega_3 + k_1^*(\omega_2)k_1(\omega-\omega_1+\omega_2)\int_{\omega_3}\int_{\omega_4} k_3(\omega_3,\omega_4,\omega_1-\omega_3+\omega_4)\\
&\times [Y_x^*(\omega_2)Y_x(\omega_1-\omega_3+\omega_4)Y_y(\omega_3)Y_y^*(\omega_4)+Y_y^*(\omega_2)Y_y(\omega_1-\omega_3+\omega_4)Y_x(\omega_3)Y_x^*(\omega_4)]\\
&\times Y_x(\omega-\omega_1+\omega_2)d\omega_3 d\omega_4
\end{aligned}$$

$$\begin{aligned}
q_{3,x}(\omega) &= k_1(\omega_1)k_1^*(\omega_2)\int_{\omega_3}\int_{\omega_4} k_3(\omega_3,\omega_4,\omega-\omega_1+\omega_2-\omega_3+\omega_4)Y_y(\omega_1)Y_y^*(\omega_2)Y_y(\omega_3)\\
&\times Y_y^*(\omega_4)Y_x(\omega-\omega_1+\omega_2-\omega_3+\omega_4)d\omega_3 d\omega_4 + k_1(\omega_1)k_1(\omega-\omega_1+\omega_2)\\
&\times \int_{\omega_3}\int_{\omega_4} k_3^*(\omega_3,\omega_4,\omega_2-\omega_3+\omega_4)Y_y(\omega_1)Y_y^*(\omega_2-\omega_3+\omega_4)Y_y^*(\omega_3)Y_y(\omega_4)\\
&\times Y_x(\omega-\omega_1+\omega_2)d\omega_3 d\omega_3 + k_1^*(\omega_2)k_1(\omega-\omega_1+\omega_2)\int_{\omega_3}\int_{\omega_4} k_3(\omega_3,\omega_4,\omega_1-\omega_3+\omega_4)\\
&\times Y_y^*(\omega_2)Y_y(\omega_1-\omega_3+\omega_4)Y_y(\omega_3)Y_y^*(\omega_4)Y_x(\omega-\omega_1+\omega_2)d\omega_3 d\omega_4
\end{aligned}$$

So far, no properties of optical fiber have been used for deriving the inverse Volterra series. In next Section, we will use closed-form expression for h_1 and h_3 in order to find the real operations to be done at the receiver side.

A.2 Closed-form expressions for nonlinear compensation in optical fiber

After N spans, the Volterra kernels are as follows

$$h_1(\omega) = e^{-j\omega^2\beta_2 NL/2}$$

$$h_3(\omega_1,\omega_2,\omega-\omega_1+\omega_2) = -\frac{j\gamma'}{4\pi^2}h_1(\omega)\frac{1-e^{-(\alpha+j\beta_2\Delta\Omega)L}}{\alpha+j\beta_2\Delta\Omega}\sum_{k=0}^{N-1}e^{-j\beta_2\Delta\Omega L}$$

With $\gamma' = \frac{8}{9}\gamma$ and $\Delta\Omega = (\omega_1-\omega)(\omega_1-\omega_2)$
We can express $Z_{5,x}$ as

$$\boxed{Z_{5,x}(\omega) = Q_{1,x}(\omega) + Q_{2,x}(\omega) + Q_{3,x}(\omega)} \tag{A.30}$$

With

$$Q_{i,x} = -k_1(\omega)\int_{\omega_1}\int_{\omega_2} h_3(\omega_1,\omega_2,\omega-\omega_1+\omega_2)q_{i,x}(\omega)d\omega_1 d\omega_2$$

Derivations for $Q_{1,1}$ According to Eq.(2.27), we know that the kernel k_3 takes the following form

$$k_3(\omega_1,\omega_2,\omega-\omega_1+\omega_2) = -k_1(\omega)h_3(\omega_1,\omega_2,\omega-\omega_1+\omega_2)k_1(\omega_1)k_1^*(\omega_2)k_1(\omega-\omega_1+\omega_2)$$

so

$$h_3(\omega_1,\omega_2,\omega-\omega_1+\omega_2) = -k_3(\omega_1,\omega_2,\omega-\omega_1+\omega_2)k_1^*(\omega)k_1^*(\omega_1)k_1(\omega_2)k_1^*(\omega-\omega_1+\omega_2)$$

By replacing h_3 with its previous expression, we obtain

$$\begin{aligned}
Q_{1,x}(\omega) &= \int_{\omega_1}\int_{\omega_2}\int_{\omega_3}\int_{\omega_4} k_3(\omega_1,\omega_2,\omega-\omega_1+\omega_2)k_3(\omega_3,\omega_4,\omega-\omega_1+\omega_2-\omega_3+\omega_4)\\
&\times\ k_1^*(\omega-\omega_1+\omega_2)Y_x(\omega_1)Y_x^*(\omega_2)Y_x(\omega_3)Y_x^*(\omega_4)Y_x(\omega-\omega_1+\omega_2-\omega_3+\omega_4)\\
&\times\ d\omega_3 d\omega_4 d\omega_1 d\omega_2\\
&+\ \int_{\omega_1}\int_{\omega_2}\int_{\omega_3}\int_{\omega_4} k_3(\omega_1,\omega_2,\omega-\omega_1+\omega_2)k_3^*(\omega_3,\omega_4,\omega_2-\omega_3+\omega_4)k_1(\omega_2)\\
&\times\ Y_x(\omega_1)Y_x^*(\omega_2-\omega_3+\omega_4)Y_x^*(\omega_3)Y_x(\omega_4)Y_x(\omega-\omega_1+\omega_2)d\omega_3 d\omega_4 d\omega_1 d\omega_2\\
&+\ \int_{\omega_1}\int_{\omega_2}\int_{\omega_3}\int_{\omega_4} k_3(\omega_1,\omega_2,\omega-\omega_1+\omega_2)k_3(\omega_3,\omega_4,\omega_1-\omega_3+\omega_4)k_1^*(\omega_1)\\
&\times\ Y_x^*(\omega_2)Y_x(\omega_1-\omega_3+\omega_4)Y_x(\omega_3)Y_x^*(\omega_4)Y_x(\omega-\omega_1+\omega_2)d\omega_3 d\omega_4 d\omega_1 d\omega_2
\end{aligned}$$

By looking at the expression for k_3, we can express it as

$$k_3(\omega_1,\omega_2,\omega-\omega_1+\omega_2) = k_1(\omega)\tilde{k}_3(\omega_1,\omega_2,\omega-\omega_1+\omega_2)$$

with

$$\tilde{k}_3(\omega_1,\omega_2,\omega-\omega_1+\omega_2) = \frac{j\gamma}{4\pi^2}\frac{1-e^{-(\alpha+j\beta_2\Delta\Omega)L}}{\alpha+j\beta_2\Delta\Omega}\sum_{k=1}^{N} e^{j\beta_2\Delta\Omega L}.$$

Notice that compared to h_3, the summation over k goes from 1 to N instead of 0 to $N-1$.

We thus obtain that

$$\begin{aligned}
Q_{1,x}(\omega) &= k_1(\omega)\int_{\omega_1}\int_{\omega_2}\int_{\omega_3}\int_{\omega_4} \tilde{k}_3(\omega_1,\omega_2,\omega-\omega_1+\omega_2)\tilde{k}_3(\omega_3,\omega_4,\omega-\omega_1+\omega_2-\omega_3+\omega_4)\\
&\times\ Y_x(\omega_1)Y_x^*(\omega_2)Y_x(\omega_3)Y_x^*(\omega_4)Y_x(\omega-\omega_1+\omega_2-\omega_3+\omega_4)d\omega_3 d\omega_4 d\omega_1 d\omega_2\\
&+\ k_1(\omega)\int_{\omega_1}\int_{\omega_2}\int_{\omega_3}\int_{\omega_4} \tilde{k}_3(\omega_1,\omega_2,\omega-\omega_1+\omega_2)\tilde{k}_3^*(\omega_3,\omega_4,\omega_2-\omega_3+\omega_4)\\
&\times\ Y_x(\omega_1)Y_x^*(\omega_2-\omega_3+\omega_4)Y_x^*(\omega_3)Y_x(\omega_4)Y_x(\omega-\omega_1+\omega_2)d\omega_3 d\omega_4 d\omega_1 d\omega_2\\
&+\ k_1(\omega)\int_{\omega_1}\int_{\omega_2}\int_{\omega_3}\int_{\omega_4} \tilde{k}_3(\omega_1,\omega_2,\omega-\omega_1+\omega_2)\tilde{k}_3(\omega_3,\omega_4,\omega_1-\omega_3+\omega_4)\\
&\times\ Y_x^*(\omega_2)Y_x(\omega_1-\omega_3+\omega_4)Y_x(\omega_3)Y_x^*(\omega_4)Y_x(\omega-\omega_1+\omega_2)d\omega_3 d\omega_4 d\omega_1 d\omega_2
\end{aligned}$$

By simplifying $\tilde{k}_3$ as done in the case of single polarization, one can assume that

$$\tilde{k}_3(\omega_1,\omega_2,\omega-\omega_1+\omega_2) \approx j\frac{c'}{(2\pi)^2}\sum_{k=1}^{N} e^{jk\beta_2\Delta\Omega L}.$$

with

$$c' = \gamma'\frac{1-e^{-\alpha L}}{\alpha}.$$

For other term in $\tilde{k}_3$, we have

$$\tilde{k}_3(\omega_3,\omega_4,\omega-\omega_1+\omega_2-\omega_3+\omega_4) = j\frac{c'}{(2\pi)^2}\sum_{k=1}^{N} e^{jk\beta_2 L\Delta\Omega_1}$$

with $\Delta\Omega_1 = (\omega_3 - \omega + \omega_1 - \omega_2)(\omega_3 - \omega_4)$.

$$\tilde{k}_3(\omega_3, \omega_4, \omega_2 - \omega_3 + \omega_4) = j\frac{c'}{(2\pi)^2}\sum_{k=1}^{N} e^{-jk\beta_2 L\Delta\Omega_2}$$

with $\Delta\Omega_2 = (\omega_3 - \omega_2)(\omega_3 - \omega_4)$.

$$\tilde{k}_3(\omega_3, \omega_4, \omega_1 - \omega_3 + \omega_4) = j\frac{c'}{(2\pi)^2}\sum_{k=1}^{N} e^{jk\beta_2 L\Delta\Omega_3}$$

with $\Delta\Omega_3 = (\omega_3 - \omega_1)(\omega_3 - \omega_4)$. By introducing

$$h_{cd}(\omega) = e^{j\beta_2\omega^2\frac{L}{2}},$$

we get that , as for the case of single polarization, after doing the change of variable $\omega_1' = \omega - \omega_1 + \omega_2$ and $\omega_1 = \omega_1'$ in the first term of $Q_{1,x}$

$$\begin{aligned}
Q_{1,x}(\omega) &= -2\frac{c'^2}{(2\pi)^4}h_{cd}^N(\omega)\int_{\omega_1}\int_{\omega_2}\int_{\omega_3}\int_{\omega_4}\sum_{k,\ell=1}^{N} e^{j\beta_2 L(k\Delta\Omega+\ell\Delta\Omega_3)} \\
&\times\ Y_x^*(\omega_2)Y_x(\omega_1-\omega_3+\omega_4)Y_x(\omega_3)Y_x^*(\omega_4)Y_x(\omega-\omega_1+\omega_2)d\omega_3 d\omega_4 d\omega_1 d\omega_2 \\
&+\ \frac{c'^2}{(2\pi)^4}h_{cd}^N(\omega)\int_{\omega_1}\int_{\omega_2}\int_{\omega_3}\int_{\omega_4}\sum_{k,\ell=1}^{N} e^{j\beta_2 L(k\Delta\Omega-\ell\Delta\Omega_2)} \\
&\times\ Y_x(\omega_1)Y_x^*(\omega_2-\omega_3+\omega_4)Y_x^*(\omega_3)Y_x(\omega_4)Y_x(\omega-\omega_1+\omega_2)d\omega_3 d\omega_4 d\omega_1 d\omega_2
\end{aligned}$$

Derivations for $Q_{2,x}$

$$Q_{2,x} = -k_1(\omega)\int_{\omega_1}\int_{\omega_2} h_3(\omega_1, \omega_2, \omega-\omega_1+\omega_2)q_{2,x}(\omega)d\omega_1 d\omega_2$$

Once again, by replacing h_3 with respect to k_3, we obtain

$$\begin{aligned}
Q_{2,x}(\omega) = \int_{\omega_1}\int_{\omega_2}\int_{\omega_3}\int_{\omega_4} & k_3(\omega_1,\omega_2,\omega-\omega_1+\omega_2)k_3(\omega_3,\omega_4,\omega-\omega_1+\omega_2-\omega_3+\omega_4)k_1^*(\omega-\omega_1+\omega_2) \\
& [Y_x(\omega_1)Y_x^*(\omega_2)Y_y(\omega_3)Y_y^*(\omega_4) + Y_y(\omega_1)Y_y^*(\omega_2)Y_x(\omega_3)Y_x^*(\omega_4)] \\
& Y_x(\omega-\omega_1+\omega_2-\omega_3+\omega_4)d\omega_1 d\omega_2 d\omega_3 d\omega_4 \\
+\int_{\omega_1}\int_{\omega_2}\int_{\omega_3}\int_{\omega_4} & k_3(\omega_1,\omega_2,\omega-\omega_1+\omega_2)k_3^*(\omega_3,\omega_4,\omega_2-\omega_3+\omega_4)k_1(\omega_2) \\
& [Y_x(\omega_1)Y_x^*(\omega_2-\omega_3+\omega_4)Y_y^*(\omega_3)Y_y(\omega_4) + Y_y(\omega_1)Y_y^*(\omega_2-\omega_3+\omega_4)Y_x^*(\omega_3)Y_x(\omega_4)]
\end{aligned}$$

$$Y_x(\omega-\omega_1+\omega_2)d\omega_1 d\omega_2 d\omega_3 d\omega_4$$

$$+\int_{\omega_1}\int_{\omega_2}\int_{\omega_3}\int_{\omega_4} k_3(\omega_1,\omega_2,\omega-\omega_1+\omega_2)k_3(\omega_3,\omega_4,\omega_1-\omega_3+\omega_4)k_1^*(\omega_1)$$

$$[Y_x^*(\omega_2)Y_x(\omega_1-\omega_3+\omega_4)Y_y(\omega_3)Y_y^*(\omega_4)+Y_y^*(\omega_2)Y_y(\omega_1-\omega_3+\omega_4)Y_x(\omega_3)Y_x^*(\omega_4)]$$

$$Y_x(\omega-\omega_1+\omega_2)d\omega_1 d\omega_2 d\omega_3 d\omega_4$$

By replacing k_3 with respect to $\tilde{k}_3$ and after that replacing k_i by its expression, we have finally

$$\begin{aligned}
Q_{2,x}(\omega) &= -\frac{c'^2}{(2\pi)^4}h_{cd}^N(\omega)\int_{\omega_1}\int_{\omega_2}\int_{\omega_3}\int_{\omega_4}\sum_{k,\ell=1}^{N} e^{j\beta_2 L(k\Delta\Omega+\ell\Delta\Omega_1)}[Y_x(\omega_1)Y_x^*(\omega_2)Y_y(\omega_3)Y_y^*(\omega_4)\\
&+ Y_y(\omega_1)Y_y^*(\omega_2)Y_x(\omega_3)Y_x^*(\omega_4)]Y_y(\omega-\omega_1+\omega_2-\omega_3+\omega_4)d\omega_3 d\omega_4 d\omega_1 d\omega_2\\
&+ \frac{c'^2}{(2\pi)^4}h_{cd}^N(\omega)\int_{\omega_1}\int_{\omega_2}\int_{\omega_3}\int_{\omega_4}\sum_{k,\ell=1}^{N} e^{j\beta_2 L(k\Delta\Omega-\ell\Delta\Omega_2)}[Y_x(\omega_1)Y_x^*(\omega_2-\omega_3+\omega_4)Y_y^*(\omega_3)Y_y(\omega_4)\\
&+ Y_y(\omega_1)Y_y^*(\omega_2-\omega_3+\omega_4)Y_x^*(\omega_3)Y_x(\omega_4)]Y_x(\omega-\omega_1+\omega_2)d\omega_3 d\omega_4 d\omega_1 d\omega_2\\
&- \frac{c'^2}{(2\pi)^4}h_{cd}^N(\omega)\int_{\omega_1}\int_{\omega_2}\int_{\omega_3}\int_{\omega_4}\sum_{k,\ell=1}^{N} e^{j\beta_2 L(k\Delta\Omega+\ell\Delta\Omega_3)}[Y_x^*(\omega_2)Y_x(\omega_1-\omega_3+\omega_4)Y_y(\omega_3)Y_y^*(\omega_4)\\
&+ Y_y^*(\omega_2)Y_y(\omega_1-\omega_3+\omega_4)Y_x(\omega_3)Y_x^*(\omega_4)]Y_x(\omega-\omega_1+\omega_2)d\omega_1 d\omega_2 d\omega_3 d\omega_4
\end{aligned}$$

Derivations for $Q_{3,x}$

$$Q_{3,x}=-k_1(\omega)\int_{\omega_1}\int_{\omega_2} h_3(\omega_1,\omega_2,\omega-\omega_1+\omega_2)q_{3,x}(\omega)d\omega_1 d\omega_2$$

Replacing h_3 with respect to k_3

$$\begin{aligned}
Q_{3,x}(\omega) &= \int_{\omega_1}\int_{\omega_2}\int_{\omega_3}\int_{\omega_4} k_3(\omega_1,\omega_2,\omega-\omega_1+\omega_2)k_3(\omega_3,\omega_4,\omega-\omega_1+\omega_2-\omega_3+\omega_4)\\
&\times k_1^*(\omega-\omega_1+\omega_2)Y_y(\omega_1)Y_y^*(\omega_2)Y_y(\omega_3)Y_y^*(\omega_4)Y_x(\omega-\omega_1+\omega_2-\omega_3+\omega_4)\\
&\times d\omega_3 d\omega_4 d\omega_1 d\omega_2\\
&+ \int_{\omega_1}\int_{\omega_2}\int_{\omega_3}\int_{\omega_4} k_3(\omega_1,\omega_2,\omega-\omega_1+\omega_2)k_3^*(\omega_3,\omega_4,\omega_2-\omega_3+\omega_4)k_1(\omega_2)\\
&\times Y_y(\omega_1)Y_y^*(\omega_2-\omega_3+\omega_4)Y_y^*(\omega_3)Y_y(\omega_4)Y_x(\omega-\omega_1+\omega_2)d\omega_3 d\omega_4 d\omega_1 d\omega_2\\
&+ \int_{\omega_1}\int_{\omega_2}\int_{\omega_3}\int_{\omega_4} k_3(\omega_1,\omega_2,\omega-\omega_1+\omega_2)k_3(\omega_3,\omega_4,\omega_1-\omega_3+\omega_4)k_1^*(\omega_1)\\
&\times Y_y^*(\omega_2)Y_y(\omega_1-\omega_3+\omega_4)Y_y(\omega_3)Y_y^*(\omega_4)Y_x(\omega-\omega_1+\omega_2)d\omega_3 d\omega_4 d\omega_1 d\omega_2
\end{aligned}$$

We obtain finally

$$
\begin{aligned}
Q_{3,x}(\omega) &= -\frac{c'^2}{(2\pi)^4} h_{cd}^N(\omega) \int_{\omega_1}\int_{\omega_2}\int_{\omega_3}\int_{\omega_4} \sum_{k,\ell=1}^{N} e^{j\beta_2 L(k\Delta\Omega+\ell\Delta\Omega_1)} \\
&\times Y_y(\omega_1) Y_y^*(\omega_2) Y_y(\omega_3) Y_y^*(\omega_4) Y_x(\omega-\omega_1+\omega_2-\omega_3+\omega_4) d\omega_3 d\omega_4 d\omega_1 d\omega_2 \\
&+ \frac{c'^2}{(2\pi)^4} h_{cd}^N(\omega) \int_{\omega_1}\int_{\omega_2}\int_{\omega_3}\int_{\omega_4} \sum_{k,\ell=1}^{N} e^{j\beta_2 L(k\Delta\Omega-\ell\Delta\Omega_2)} \\
&\times Y_y(\omega_1) Y_y^*(\omega_2-\omega_3+\omega_4) Y_y^*(\omega_3) Y_y(\omega_4) Y_x(\omega-\omega_1+\omega_2) d\omega_3 d\omega_4 d\omega_1 d\omega_2 \\
&- \frac{c'^2}{(2\pi)^4} h_{cd}^N(\omega) \int_{\omega_1}\int_{\omega_2}\int_{\omega_3}\int_{\omega_4} \sum_{k,\ell=1}^{N} e^{j\beta_2 L(k\Delta\Omega+\ell\Delta\Omega_3)} \\
&\times Y_y^*(\omega_2) Y_y(\omega_1-\omega_3+\omega_4) Y_y(\omega_3) Y_y^*(\omega_4) Y_x(\omega-\omega_1+\omega_2) d\omega_3 d\omega_4 d\omega_1 d\omega_2
\end{aligned}
$$

APPENDIX B

CONDENSED FRENCH VERSION

Compensation des effets nonlinéaires pour les transmissions WDM longue distance à 400Gbps et au-delà

B.1 Introduction

Les systèmes de communications optiques ont révolutionné l'industrie de télécommunications et ont joué un rôle important dans le développement des réseaux de communications actuels. Ces systèmes présentent une très large bande passante avec une faible latence et un coût raisonnable. Ces avantages ont permet aux systèmes de communications optiques de dominer les transmissions terrestres longue distance et les transmissions de données à travers les océans. Aujourd'hui, les systèmes à fibre optique dominent aussi les réseaux métropolitains et les réseaux d'accès. Depuis leur déploiement dans les années 70, les systèmes de communications optiques ont évolué pour satisfaire la demande incessante de l'augmentation de débits. Plusieurs technologies sont utilisées afin de combattre les distorsions et augmenter les débits de transmission. L'invention des amplificateurs optiques EDFAs ont stimulé l'utilisation de la communication optique et ont permet le déploiement de systèmes de transmission WDM. Cette technologie a conduit à une énorme augmentation de la capacité des fibres. La ré-introduction de la détection cohérente au début des années 2000s a été la deuxième découverte importante qui a permet aux systèmes optiques de continuer à satisfaire la demande croissante de trafics de données. Cette technologie a permet de coder l'information en phase et en polarisation en plus de l'amplitude. D'autre part, la détection cohérente peut être aussi combiner avec les algorithmes de traitement de signal numérique, et par conséquent les distorsions de la fibre peuvent être compensées dans le domaine numérique.

La demande croissante et incessante des trafics de données, stimulée par l'émergence des applications comme les services cloud et l'Internet des objets, nécessite une augmentation continue de débit de transmission des réseaux cœurs optiques. La prochaine génération de systèmes de transmission WDM longue distance devrait opérer à des débits de 400Gbps ou

1Tbps. Pour générer ces débits élevés, une nouvelle approche, nommée super-canal, est utilisée. Des types de super-canal, basés sur les systèmes OFDM multi-bande et Nyquist WDM, font actuellement l'objet d'un certain nombre de travaux de recherche pour évaluer leurs performances. Ces systèmes consistent à diviser le canal WDM en plusieurs sous-canaux, nommés bandes (OFDM multi-bande) ou sous-porteuses (Nyquist WDM), espacés par des intervalles de garde réduits. Chaque sous-bande/sous-porteuse est modulée en modulation multi-états à efficacité spectrale élevée pour générer les débits désirés.

Ce type de systèmes est extrêmement vulnérable aux effets nonlinéaires de la fibre optique. En effet, les effets nonlinéaires dépendent de la puissance de transmission et sont inversement proportionnels à l'intervalle de garde. L'augmentation de la puissance pour utiliser des modulations multi-états engendre l'augmentation des effets nonlinéaires comme le SPM (Self-Phase Modulation), le XPM (Cross-Phase Modulation) et le XPolM (Cross-Polarization Modulation). D'autre part, l'utilisation des intervalles de garde réduits cause l'augmentation des effets nonlinéaires inter-bande/sous-porteuse comme le XPM, le XpolM et le FWM (Four-Wave mixing). Par conséquent, la compensation des effets nonliéaires est indispensable pour maintenir des bonnes performances de systèmes en terme de distance de transmission. Grâce à l'emploi de récepteurs à détection cohérente, des techniques de traitement du signal numérique sont utilisées pour combattre ces effets.

Contributions de la thèse Ce travail de thèse a été financé par le projet européen SASER. Dans cette thèse, nous proposons deux nouvelles techniques numériques pour compenser les effets nonlinéaires dans le contexte de système de transmission super-canal.

La première technique, nommée égaliseur nonlinéaire basé sur les séries de Volterra (VNLE) d'ordre 5, consiste à compenser les effets nonlinéaires intra-bande. L'idée de cette approche est d'augmenter l'ordre de technique basée sur l'égalisation nonlinéaire de troisième ordre déjà proposée. Dans un premier temps, on a calculé le noyau de Volterra du cinquième ordre. Puis, on a trouvé un schéma d'implémentation qui consiste à compenser la dispersion chromatique en domaine fréquentiel et les effets nonlinéaires dans le domaine temporel. Finalement, on a évalué les performances de cette technique dans le contexte de super-canal OFDM multi-bande. En comparaison avec le VNLE d'ordre 3, les résultats ont montré que l'égaliseur nonlinéaire basé sur les séries de Volterra d'ordre 5 augmente significativement les performances dans le cas de transmission OFDM mono-bande. Cependant, les interférences nonlinéaires inter-bande réduisent les performances du VNLE de cinquième ordre ainsi que le VNLE de troisième ordre dans le cas de transmission OFDM multi-bande.

Par conséquent, on a proposé l'annulateur des interférences nonlinéaires (INIC) pour combattre les interférences nonlinéaires dans le contexte de transmission OFDM multi-bande et Nyquist WDM. Le principe de cette approche est basée sur l'égaliseur à retour de décision. Les symboles décidés de bandes/sous-porteuses adjacentes sont d'abord régénérés, et puis reconstruits en utilisant un modèle de fibre basé sur les séries de Volterra. Finalement, les signaux reconstruits de bandes/sous-porteuses adjacentes sont soustraits du signal de la sous-

bande/sous-porteuse considérée. L'INIC augmente significativement les performances dans le contexte de transmission Nyquist WDM et OFDM multi-bande en comparaison avec les approches classique comme le VNLE et la rétro-propagation numérique (DBP).

B.2 Évolution des systèmes de transmissions optiques

Les systèmes de communications optiques ont été introduit dans les années 70. Grâce à ses avantages, essentiellement la large bande passante, la faible latence et le coût raisonnable, les systèmes de communications optiques représentent aujourd'hui la "colonne vertébrale" de réseaux de communication modernes. Deux technologies importantes ont stimulé l'utilisation de systèmes optiques et ont permis à ce type de système à évoluer pour satisfaire la demande croissante et incessante de trafic de données. Ces deux découvertes importantes sont l'invention de amplificateurs optiques EDFA et l'introduction de systèmes de transmission à détection cohérente.

B.2.1 L'invention de l'EDFA et le déploiement de système de transmission WDM

Les amplificateurs EDFAs permettent l'amplification des signaux lumineux et par suite résoudre le problème de l'atténuation de signaux durant la propagation. L'avantage de l'EFDA est d'amplifier le signal transmis optiquement. Cela évite le passage par des amplificateurs électriques et la reconversion du signal optique en signal électrique pour être amplifié. En plus, l'EDFA possède une très large bande passante. Cette caractéristique de l'EDFA a permis l'utilisation de systèmes de transmission WDM qui ont engendré une évolution importante en terme d'augmentation de la capacité de la fibre optique.

La technologie WDM, présentée par la figure.B.1, a été déployée dans les années 1990 et a augmenté le débit jusqu'au 1Tbps par canal optique dans l'année 2000 [6]. Cette technologie consiste à mélanger plusieurs signaux optiques portés par des longueurs d'ondes différentes sur une fibre optique. Un multiplexeur assure le combinaison des signaux à l'émission alors que un démultiplexeur est utilisé pour le processus inverse au niveau du récepteur.

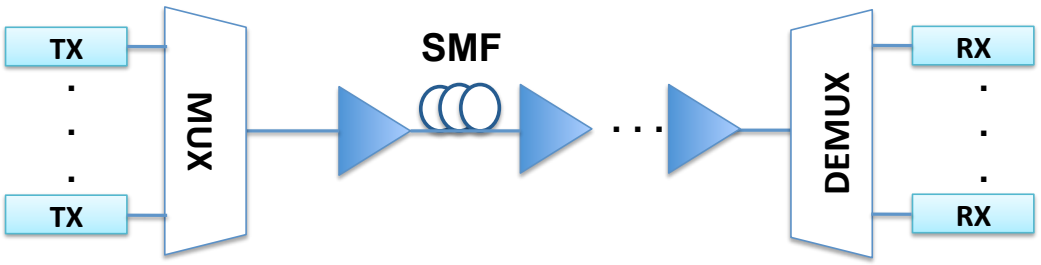

Figure B.1: système de transmission WDM

L'augmentation de débit dans les systèmes WDM utilisant la modulation OOK et la détection directe, de 2.5Gbps à 10Gbps et puis de 10Gbps à 40Gbps par longueur d'onde, a été ralentie par les distorsions de la fibre comme la dispersion chromatique et la dispersion

modale de polarisation. Par conséquent, plusieurs technologies de fibre sont utilisées afin de combattre ces distorsions et augmenter les débits de transmission comme les fibres DSF (Dispersion Shifted Fiber) et DCF (Dispersion Compensating Fiber). Augmenter le débit de 40Gbps à 100Gbps par longueur d'onde n'a pas été possible en utilisant la modulation OOK à cause de l'impact élevé de la dispersion et les effets nonlinéaires. En plus, augmenter le débit total par fibre en augmentant le nombre de canaux WDM n'a pas été possible aussi à cause de la bande passante de l'EFDA. Ces contraintes ont orienté la recherche à se concentrer sur l'augmentation de l'efficacité spectrale et par suite utiliser des modulations à efficacité spectrale élevée. Pour cette raison, la détection cohérente a remplacé la détection directe puisqu'elle permet d'utiliser les modulations multi-états. Les modulations multi-états encodent l'information sur la phase et la polarisation en plus de l'amplitude déjà utilisé dans la modulation OOK et les systèmes à détection directe. L'introduction de la détection cohérente a relancé l'augmentation de la capacité de systèmes optiques.

B.2.2 Système à détection cohérente

La détection cohérente a été introduite dans les systèmes de transmission par fibre optique dans les années 70 [12]. Sa complexité élevée, en plus de la performance de systèmes à détection directe permettant de générer les débits demandés, ont défavorisé son déploiement. Cependant, au début des années 2000, la nécessité d'augmenter le débit de transmission et l'existence des convertisseurs analogiques numériques à vitesse de conversion élevée ont relancé l'idée de l'utilisation de la détection cohérente pour profiter de ses avantages. En fait, la détection cohérente permet d'avoir accès à l'intensité, la phase et la polarisation du signal contrairement à la détection directe qui permet uniquement l'accès à l'intensité du signal. Par conséquent, les modulations multi-états peuvent être utilisées pour augmenter le débit de transmission grâce à leur efficacité spectrale élevée. La figure. B.2 montre le principe de la détection cohérente pour un système de transmission à multiplexage en polarisation.

Le principe de la détection cohérente est de mélanger le signal optique reçu au niveau du récepteur avec un signal issu d'un oscillateur local, dont la fréquence est égale à celle du signal reçu.

La détection cohérente permet aussi de combattre les distorsions linéaires et nonlinéaires du signal transmis en utilisant des algorithmes de traitement de signal numérique. Elle a été employée dans les systèmes WDM à 40Gbps par longueur d'onde et dans le standard actuel 100Gbps par longueur d'onde [14]. Les systèmes de transmission à détection cohérente sont aussi adoptés pour la prochaine génération de systèmes WDM à 400Gbps/1Tbps.

B.2.3 Prochaine génération de systèmes WDM longue distance

La prochaine génération de systèmes WDM longue distance devrait opérée à des débits de 400Gbps ou 1Tbps. Cette montée en débit s'appuiera sur des nouvelles formes d'ondes avancées de type mono-porteuse (Nyquist-WDM) ou multi-porteuse (OFDM multi-bande). Ces approches

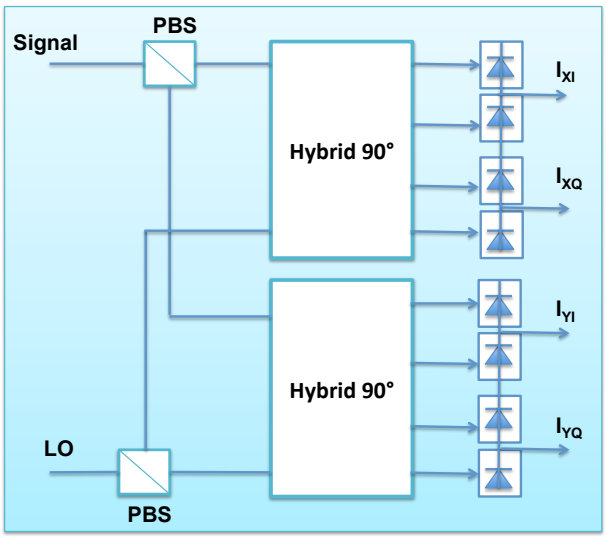

Figure B.2: Récepteur à diversité de phase et de polarisation

sont basées sur le multiplexage de plusieurs porteuses optiques indépendantes et espacées par des intervalles de garde réduits. Le schema. B.3 montre les spectres des systèmes Nyquist-WDM et OFDM multi-bande respectivement.

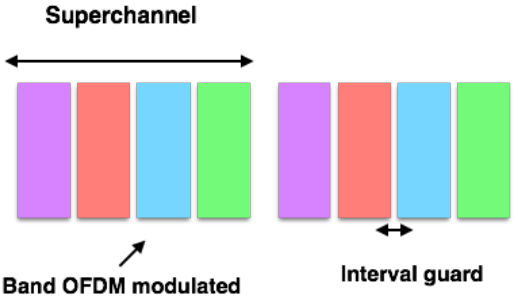

Figure B.3: Spectre de l'OFDM multi-bande

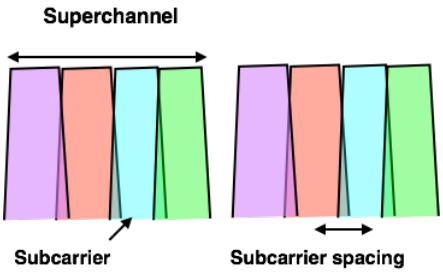

Figure B.4: Spectre de Nyquist WDM

D'autre part, comme dans le cas du standard 100Gbps actuel, des modulations multi-états vont être utilisées pour augmenter le débit par porteuse grâce à leur efficacité spectrale élevée.

B.2.3-a Système OFDM multi-bande

La modulation OFDM est une modulation multi-porteuses. Elle est introduite dans le domaine de communication sans fil pour les canaux sélectifs en fréquences. Grâce à l'utilisation de la détection cohérente, l'OFDM optique cohérent a été proposée comme alternative à la modulation QPSK pour les systèmes de transmission optiques à 100Gbps [33]. Cette technique consiste à répartir les données à transmettre sur des sous-porteuses orthogonales et modulées à bas débit. Elle présente plusieurs avantages comme la robustesse intrinsèque aux effets dispersifs.

Le principe de système OFDM multi-bande consiste à diviser le canal WDM en plusieurs bandes générées par plusieurs émetteurs. Cela permet d'utiliser des convertisseurs analogiques numériques à vitesse de conversion réduite, et par conséquent résoudre le problème de l'indisponibilité de convertisseurs à vitesse élevée actuellement dans le marché. Ensuite ces sous-bandes sont multiplexées et transmises à travers le canal optique. A la réception, chaque sous-bande est détectée séparément.

Le schéma. B.5 montre le diagramme de l'émetteur pour chaque bande de système de transmission OFDM multi-bande. La séquence binaire générée est d'abord modulée en M-QAM. Puis, le signal modulé est converti en parallèle et transmis vers une IFFT. L'IFFT convertie le signal du domaine fréquentiel au domaine temporel et assure la modulation OFDM. Ensuite, après l'insertion du préfixe cyclique, le signal OFDM est reconverti en série et par suite séparé en partie réelle (I) et partie imaginaire (Q). Les signaux I and Q sont transmis aux convertisseurs analogiques numériques (DAC). Finalement, après le passage par deux filtres passe-bas, ces signaux sont combinés en utilisant un modulateur IQ. Le même processus est réalisé pour le signal de la deuxième polarisations. Finalement, après la combinaison de deux polarisation de chaque bande, les signaux de bandes OFDM, dans le contexte d'un système de OFDM multi-bande, sont multiplexés et transmis à travers le canal optique.

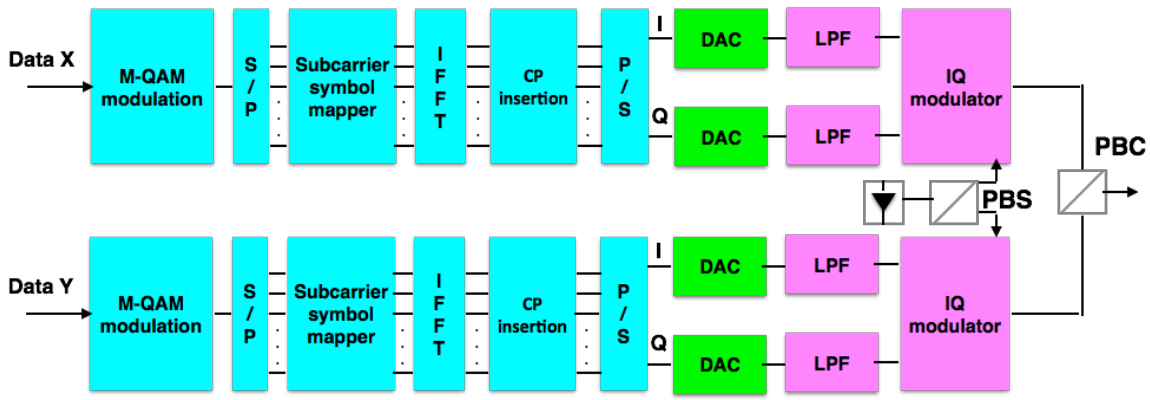

Figure B.5: Architecture de l'émetteur OFDM multi-bande

Au niveau du récepteur, comme le montre la Figure.B.6, le signal reçu est d'abord passé par un récepteur cohérent à diversité de phase et polarisation. Ce dernier assure la séparation du signal en deux polarisations orthogonales. Dans un système de transmission OFDM multi-bande, puisque le récepteur procède bande par bande, un filtre est utilisé pour la sélection de chaque sous-bande. Ensuite, les deux signaux de chaque bande sont passés par deux convertisseurs analogiques numériques (ADC). Puis, un égaliseur nonlinéaire est utilisé pour compenser les effets nonlinéaires et la dispersion chromatique avant la démodulation du signal OFDM.

La démodulation du signal OFDM est représentée dans la Figure.B.7. La première étape consiste en la synchronisation du temps et de la fréquence pour réduire les effets des inter-

férences inter-symboles et les interférences inter-sous-porteuses OFDM. Après le conversion du signal en parallèle, la suppression du préfixe cyclique est effectuée. Ensuite, une FFT est appliquée pour convertir le signal du domaine temporel au domaine fréquentiel avant la suppression de sous-porteuses nulles ajoutées comme un intervalle de garde entre les sous-bandes. À ce niveau, l'estimation du canal et du bruit de phase sont effectuées. Finalement, la décision sur les symboles est réalisée avant la démodulation M-QAM.

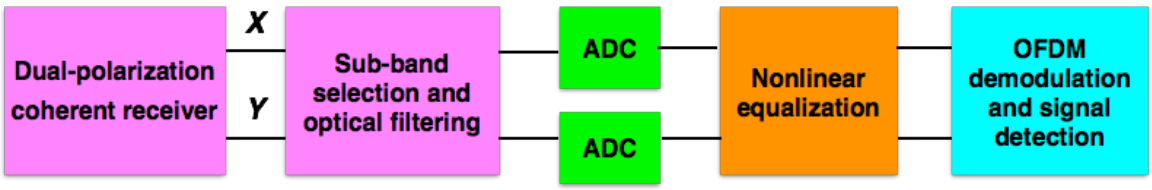

Figure B.6: Architecture de récepteur OFDM multi-bande

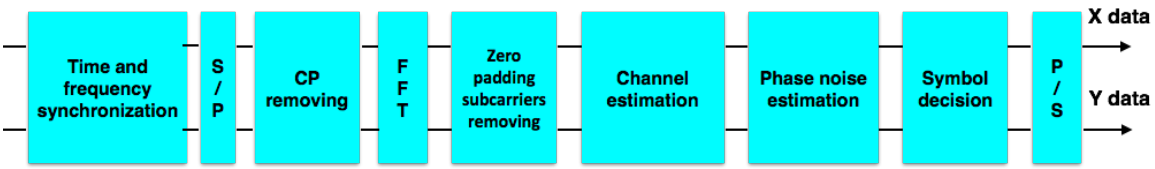

Figure B.7: OFDM démodulation

B.2.3-b Système Nyquist WDM

Depuis leur déploiement dans les années 1990s, les systèmes WDM sont évolués en terme de nombre de canaux dans la bande des amplificateurs EDFA pour augmenter la capacité de la fibre. Différents types de systèmes WDM sont commercialisés comme les systèmes coarse WDM (CWDM) et dense WDM (DWDM). Actuellement, on parle de systèmes quasi-Nyquist WDM, Nyquist WDM et aussi super-Nyquist WDM. Ces trois derniers systèmes de transmission sont proposés pour la prochaine génération des systèmes WDM dont le but est d'atteindre 400Gbps ou 1Tbps comme débit de transmission. On peut classifier les systèmes WDM selon le facteur d'espacement entre les canaux $\delta = \Delta f / R_s$, qui est le rapport entre le débit de symbole R_s et l'espacement entre les canaux Δf. Le tableau. B.1 montre les différents types de systèmes WDM.

Le principe de l'approche Nyquist WDM est d'agréger plusieurs canaux WDM, nommés sous-porteuse dans la littérature [18], avec un espacement égal à la limite de Nyquist pour une transmission sans interférence inter-symbole. Ces sous-porteuses sont routées à travers les OADMs et les WSSs comme une seule entité. Dans le cas de super-Nyquist WDM, les sous-porteuses se chevauchent pour mieux profiter de la bande de l'EDFA.

Table B.1: Classes des systèmes WDM

Définition	facteur d'espacement δ
Coarse WDM	$\delta > 50$
WDM	$\delta > 5$
Dense WDM	$1.2 < \delta \leq 5$
Quasi-Nyquist WDM	$1 < \delta \leq 1.2$
Nyquist WDM	$\delta = 1$
Super-Nyquist WDM	$\delta < 1$

L'architecture de l'émetteur pour chaque sous-porteuse et chaque polarisation dans une transmission Nyquist WDM est représentée par la Figure.B.8. Premièrement, la séquence bi-

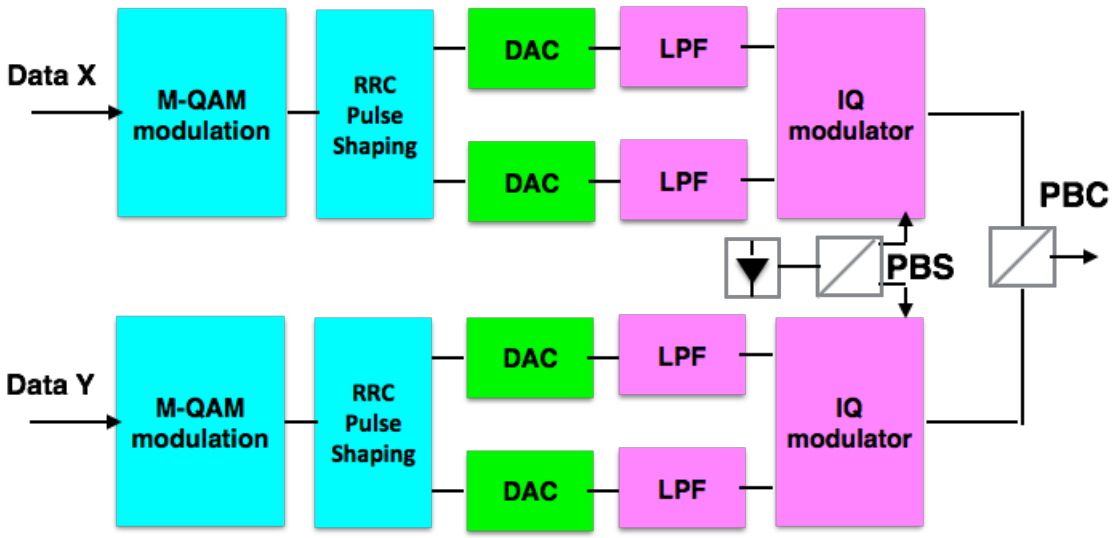

Figure B.8: Architecture de l'émetteur Nyquist WDM

naire à transmettre est modulée en M-QAM. Un filtre en racine de cosinus surélevé est utilisé pour avoir une forme spectrale quasi-rectangulaire. Ensuite, le signal est converti dans le domaine analogique à l'aide de convertisseurs analogiques numériques (DAC). Puis, les deux signaux en sortie de convertisseurs sont passés à travers deux filtres passe-bas avant la combinaison de ces signaux et la conversion en domaine optique en utilisant un modulateur IQ. Finalement, les signaux de deux polarisations sont combinés avant le multiplexage de sous-porteuses optiques et la transmission à travers la fibre.

A la réception, un récepteur cohérent à diversité de phase et polarisation assure l'extraction de la phase et l'amplitude de chaque polarisation avant la détection à l'aide de photo-détecteurs. Puis, le signal de chaque sous-porteuse est converti dans le domaine numérique et par conséquent les effets nonlinéaires et linéaires sont compensés numériquement. Finalement, la décision sur les symboles et la démodulation M-QAM sont effectuées. L'architecture du récep-

teur pour un système Nyquist WDM est représentée par la figure. B.9.

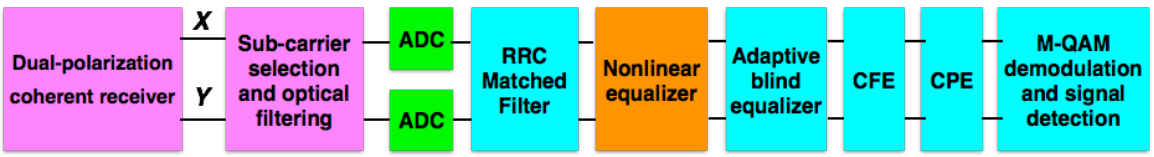

Figure B.9: Architecture du récepteur Nyquist WDM

B.2.3-c État-de-l'art sur les techniques de compensation des effets nonlinéaires

Les effets nonlinéaires représentent la limite majeure de la prochaine génération de systèmes de transmission WDM. En fait, la fibre optique est un milieu nonlinéaire à cause de l'effet Kerr. Cet effet correspond à la variation de l'indice du milieu optique en fonction de la puissance du signal se propageant dans ce milieu comme le montre l'équation suivante [16]:

$$n(P) = n_0 + n_2 \frac{P(t)}{A_{eff}} \tag{B.1}$$

avec n_0 et n_2 sont les indices linéaire et nonlinéaire respectivement. P est la puissance de signal transmis et A_{eff} est la surface effective. L'effet Kerr engendre plusieurs types de nonlinéarité dans la fibre:

- Auto-modulation de phase (SPM): auto-modification de la phase du signal à cause de son interaction nonlinéaire avec le canal optique.
- Modulation croisée de phase (XPM): modification de la phase du signal par un autre signal se propageant à une longueur d'onde proche.
- Mélange à quatre ondes (FWM): génération d'un nouveau signal à une nouvelle fréquence à cause de l'inter-modulation entre trois signaux à différentes fréquences.
- Modulation croisée de polarisation (XPolM): Modification du statut de polarisation (SOP) du signal par un signal se propageant à une longueur d'onde proche.

Plusieurs techniques ont été proposées pour compenser les effets nonlinéaires. Les techniques numériques sont implémentées au niveau de l'émetteur ou récepteur, alors que les approches optiques sont implémentées au niveau du lien optique [51]. En effet, grâce à l'introduction de la détection cohérente, des techniques de traitement de signal numériques ont été utilisé pour combattre les distorsions dans la fibre, et en particulier les effets nonlinéaires.

Deux principales techniques numériques ont été proposées pour compenser les effets nonlinéaires: la rétro-propagation numérique (DBP) [53] et l'égaliseur nonlinéaire basé sur les séries de Volterra de troisième ordre (VNLE) [59]. Ces deux approches représentent une solution numérique de l'équation de Manakov (équation de Schrödinger en cas de transmission mono-polarisation) qui gouverne la propagation de l'onde à travers la fibre optique, donnée

par:

$$\frac{\partial Y_{x/y}}{\partial z} + j\frac{\beta_2}{2}\frac{\partial^2 Y_{x/y}}{\partial t^2} + \frac{\alpha}{2}Y_{x/y} = j\gamma'(|Y_x|^2 + |Y_y|^2)Y_{x/y} \tag{B.2}$$

avec $Y_{x/y}$ est l'enveloppe complexe du champ électrique pour la polarisation x/y, α est coefficient d'atténuation, β_2 est le paramètre de dispersion de second d'ordre, γ est le coefficient de nonlinéarité dans la fibre, et $\gamma' = \frac{8}{9}\gamma$.

Les performances de DBP mono-découpage par span et VNLE de troisième ordre sont données par les figures suivantes. La figure. B.10, montre la variation du facteur Q en fonction

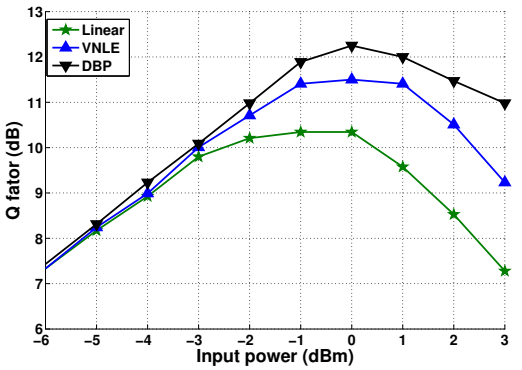

Figure B.10: Facteur Q vs. la puissance injectée par bande pour une transmission OFDM double-polarisation et mono-bande

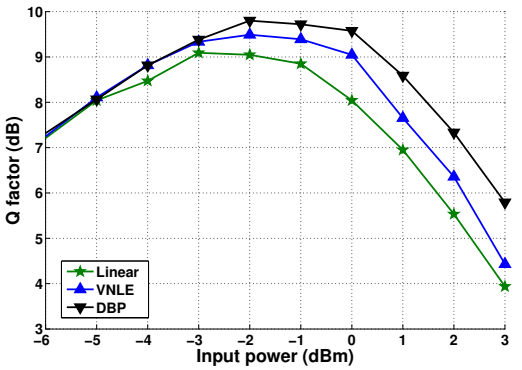

Figure B.11: Facteur Q vs. la puissance injectée par bande pour une transmission OFDM double-polarisation et multi-bande

de la puissance injectée par sous-bande pour une transmission OFDM double-polarisation et mono-bande. On observe que les deux techniques de compensation des effets nonlinéaires DBP et VNLE sont beaucoup plus performantes que l'égalisation linéaire. Le gain de DBP et VNLE est de $2dB$ et $1.2dB$ respectivement en comparaison avec le cas linéaire. En passant à un système de transmission super-canal OFDM 4-bandes, comme le montre la figure. B.10, on observe une réduction de performance de deux techniques DBP et VNLE. Le gain de DBP et VNLE par rapport au cas linéaire se réduit à 0.8 et 0.6 respectivement. Cela peut être expliqué par l'apparition des interférences nonlinéaires causées par les bandes adjacentes.

Par conséquent, nous proposons deux techniques de compensation des effets nonlinéaires intra-bande et inter-bande pour améliorer les performances de systèmes de transmission super-canal. La première approche, nommée l'égaliseur nonlinéaire basé sur les séries de Volterra d'ordre 5, compense les effets nonlinéaires intra-bande alors que l'annulateur des interférences nonlinéaires compense les effets inter-bande.

B.3 Égaliseur nonlinéaire basé sur les séries de Volterra d'ordre 5

La compensation des effets nonlinéaires basée sur les séries de Volterra de troisième ordre a fait l'objet d'un certain nombre de travaux de recherche [59],[60]. Dans cette partie, nous

proposons un passage à l'ordre 5 pour améliorer la compensation des effets nonlinéaires intra-canal/bande.

B.3.1 Principe de l'égaliseur nonlinéaire basé sur les séries de Volterra de cinquième ordre

L'objectif de cette partie est de calculer le noyau de Volterra inverse de cinquième ordre et de trouver un schéma pratique pour l'implémentation de l'égaliseur nonlinéaire basé sur les séries de Volterra de cinquième ordre.

Les noyaux de Volterra inverses k_i sont calculés en fonction de noyaux de Volterra h_i en se basant sur la théorie de p-ème ordre inverse (p-th order inverse) développée par Schetzen [58]. Pour se faire, on calcule d'abord les expressions des opérateurs inverses de Volterra K_i données par:

$$\begin{aligned} K_1 &= H_1^{-1} && \text{(B.3)} \\ K_3 &= -K_1 H_3 K_1 && \text{(B.4)} \\ K_5 &= K_1[-H_3[K_1 + K_1 H_3 K_1] - 3H_3 K_1] && \text{(B.5)} \\ &+ K_1[0.5 H_3 K_1 H_3 K_1 + 0.5 H_3[2K_1 + K_1 H_3 K_1]] \end{aligned}$$

H_i correspond à l'opérateur de Volterra d'ordre i.

Ensuite, la sortie de l'égaliseur nonlinéaire basé sur les séries de Volterra de cinquième ordre est donnée par:

$$Z = K_1[Y] + K_3[Y] + K_5[Y] = Z_1 + Z_3 + Z_5 \tag{B.6}$$

Pour trouver l'expression de Z, on doit d'abord calculer les expressions des sorties Z_1, Z_3 et Z_5, qui correspondent au premier ordre, troisième ordre et cinquième ordre respectivement. Les expression de Z_1 et Z_3 sont déjà calculées pour le VNLE de troisième ordre et sont données par:

$$\begin{aligned} &Z_{1,x/y}(\omega) = k_1(\omega) Y_{x/y}(\omega) \\ &Z_{3,x/y}(\omega) = \iint k_3(\omega_1, \omega_2, \omega - \omega_1 + \omega_2) \\ &\times [Y_x(\omega_1) Y_x^*(\omega_2) + Y_y(\omega_1) Y_y^*(\omega_2)] Y_{x/y}(\omega - \omega_1 + \omega_2) d\omega_1 d\omega_2 \end{aligned} \tag{B.7}$$

Avec k_1 et k_3 sont les noyaux de Volterra inverses de premier et troisième ordre respectivement [59].

En passant à la forme intégrale de l'eq.B.5 et après un long calcul donné en Annexe A, l'expression de Z_5 peut être écrite sous la forme suivante:

$$Z_{5,x}(\omega) = Q_{1,x}(\omega) + Q_{2,x}(\omega) + Q_{3,x}(\omega) \tag{B.8}$$

Le premier terme $Q_{1,x}$ est donné par l'expression suivante:

$$Q_{1,x}(\omega) = \sum_{k,\ell=1}^{N} Q_{1,x}^{(k,\ell)}(\omega)$$

avec

$$\begin{aligned} Q_{1,x}^{(k,\ell)}(\omega) = -2\frac{c'^2}{(2\pi)^4} h_{cd}^{N}(\omega) \iiint e^{j\beta_2 L(k\Delta\Omega+\ell\Delta\Omega_1)} \\ \times Y_x^*(\omega_2) Y_x(\omega_1-\omega_3+\omega_4) Y_x(\omega_3) Y_x^*(\omega_4) Y_x(\omega-\omega_1+\omega_2) d\boldsymbol{\omega} \\ + \frac{c'^2}{(2\pi)^4} h_{cd}^{N}(\omega) \iiint e^{j\beta_2 L(k\Delta\Omega-\ell\Delta\Omega_2)} \\ \times Y_x(\omega_1) Y_x^*(\omega_2-\omega_3+\omega_4) Y_x^*(\omega_3) Y_x(\omega_4) Y_x(\omega-\omega_1+\omega_2) d\boldsymbol{\omega} \end{aligned} \tag{B.9}$$

avec $d\boldsymbol{\omega} = d\omega_1 d\omega_2 d\omega_3 d\omega_4$ et c'' définie en Annexe A.

Pour implémenter le VNLE de cinquième ordre, on doit trouver d'abord un schéma pratique pour Z_5, et par suite un schéma pratique de chaque terme Q_i. L'idée est de transformer les quatre intégrales de chaque terme en une structure plus simple en passant au domaine temporel. Dans ce cas, au lieu de calculer les quatre intégrales, on fait simplement une multiplication dans le domaine temporel et on utilise des IFFTs/FFTs. Par conséquent, le schéma pratique d'implémentation du terme $Q_{1,x}^{(k,\ell)}$ est représentée par la figure. B.12.

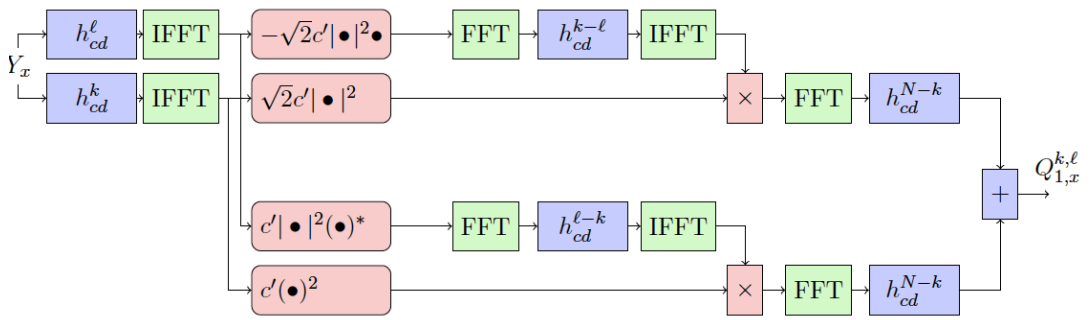

Figure B.12: Schéma d'implémentation du terme $Q_{1,x}^{(k,\ell)}(\omega)$

D'abord, la dispersion, représentée par les blocs en bleu, est compensée dans le domaine fréquentiel. Puis, les IFFTs assurent la conversion du domaine fréquentiel au domaine temporel pour compenser les effets nonlinéaires. Cette opération est représentée par les blocs en rouge. Ensuite, les FFTs sont utilisées pour repasser au domaine fréquentiel et par suite compenser la dispersion résiduelle. Enfin, en faisant la somme de différents termes en k et ℓ de 1 à N, on retrouve l'expression du terme $Q_{1,x}$. Le premier $Q_{1,x}$ est purement en polarisation x. Cependant, les deux termes $Q_{2,x}$ et $Q_{3,x}$ représentent l'interaction de la polarisation y avec la polarisation x.

Concernant le second terme $Q_{2,x}$, il est donné par l'expression suivante:

$$Q_{2,x}(\omega) = \sum_{k,\ell=1}^{N} Q_{2,x}^{(k,\ell)}(\omega)$$

avec

$$Q_{2,x}^{(k,\ell)}(\omega) = -\frac{c'^2}{(2\pi)^4} h_{cd}^N(\omega) \iiint e^{j\beta_2 L(k\Delta\Omega+\ell\Delta\Omega_1)} [Y_x^*(\omega_2) Y_x(\omega_1-\omega_3+\omega_4) Y_y(\omega_3) Y_y^*(\omega_4) \tag{B.10}$$

$$\begin{aligned}
&+ Y_y^*(\omega_2) Y_y(\omega_1-\omega_3+\omega_4) Y_x(\omega_3) Y_x^*(\omega_4)] Y_x(\omega-\omega_1+\omega_2) d\boldsymbol{\omega} \\
&+ \frac{c'^2}{(2\pi)^4} h_{cd}^N(\omega) \iiint e^{j\beta_2 L(k\Delta\Omega-\ell\Delta\Omega_2)} [Y_x(\omega_1) Y_x^*(\omega_2-\omega_3+\omega_4) Y_y^*(\omega_3) Y_y(\omega_4) \\
&+ Y_y(\omega_1) Y_y^*(\omega_2-\omega_3+\omega_4) Y_x^*(\omega_3) Y_1(\omega_4)] Y_x(\omega-\omega_1+\omega_2) d\boldsymbol{\omega} \\
&- \frac{c'^2}{(2\pi)^4} h_{cd}^N(\omega) \iiint e^{j\beta_2 L(k\Delta\Omega+\ell\Delta\Omega_3)} [Y_x(\omega_1) Y_x^*(\omega_2) Y_y(\omega_3) Y_y^*(\omega_4) \\
&+ Y_y(\omega_1) Y_y^*(\omega_2) Y_1(\omega_3) Y_x^*(\omega_4)] Y_x(\omega-\omega_1+\omega_2-\omega_3+\omega_4) d\boldsymbol{\omega}
\end{aligned}$$

Le schéma d'implémentation du terme $Q_{2,x}^{(k,\ell)}$ est représenté par la figure. B.13. Pareil, la dispersion est compensée dans le domaine fréquentiel, alors que les termes de nonlinéarité sont compensés dans le domaine temporel.

Le troisième terme $Q_{3,x}$ est donné par:

$$Q_{3,x}(\omega) = \sum_{k,\ell=1}^{N} Q_{3,x}^{(k,\ell)}(\omega)$$

avec

$$\begin{aligned}
Q_{3,x}^{(k,\ell)}(\omega) = &-\frac{c'^2}{(2\pi)^4} h_{cd}^N(\omega) \iiint e^{j\beta_2 L(k\Delta\Omega+\ell\Delta\Omega_1)} \\
&\times Y_y^*(\omega_2) Y_y(\omega_1-\omega_3+\omega_4) Y_y(\omega_3) Y_y^*(\omega_4) Y_x(\omega-\omega_1+\omega_2) d\boldsymbol{\omega} \\
&+ \frac{c'^2}{(2\pi)^4} h_{cd}^N(\omega) \iiint e^{j\beta_2 L(k\Delta\Omega-\ell\Delta\Omega_2)} \\
&\times Y_y(\omega_1) Y_y^*(\omega_2-\omega_3+\omega_4) Y_y^*(\omega_3) Y_y(\omega_4) Y_x(\omega-\omega_1+\omega_2) d\boldsymbol{\omega} \\
&- \frac{c'^2}{(2\pi)^4} h_{cd}^N(\omega) \iiint e^{j\beta_2 L(k\Delta\Omega+\ell\Delta\Omega_3)} \\
&\times Y_y(\omega_1) Y_y^*(\omega_2) Y_y(\omega_3) Y_y^*(\omega_4) Y_x(\omega-\omega_1+\omega_2-\omega_3+\omega_4) d\boldsymbol{\omega}.
\end{aligned} \tag{B.11}$$

Comme $Q_{2,x}$, $Q_{3,x}$ est un terme d'interaction entre la polarisation x et la polarisation y. En procédant de la même façon que précédemment, le schéma d'implémentation du terme $Q_{3,x}^{(k,\ell)}$ est présenté par la figure. B.14.

Finalement, le schéma d'implémentation de $Z_{5,x}$ correspond à la somme de trois termes $Q_{i,x}$. Pour la polarisation y, grâce à la symétrie, $Z_{5,y}$ peut être calculée par une simple permutation de x et y dans la formule de $Z_{5,x}$.

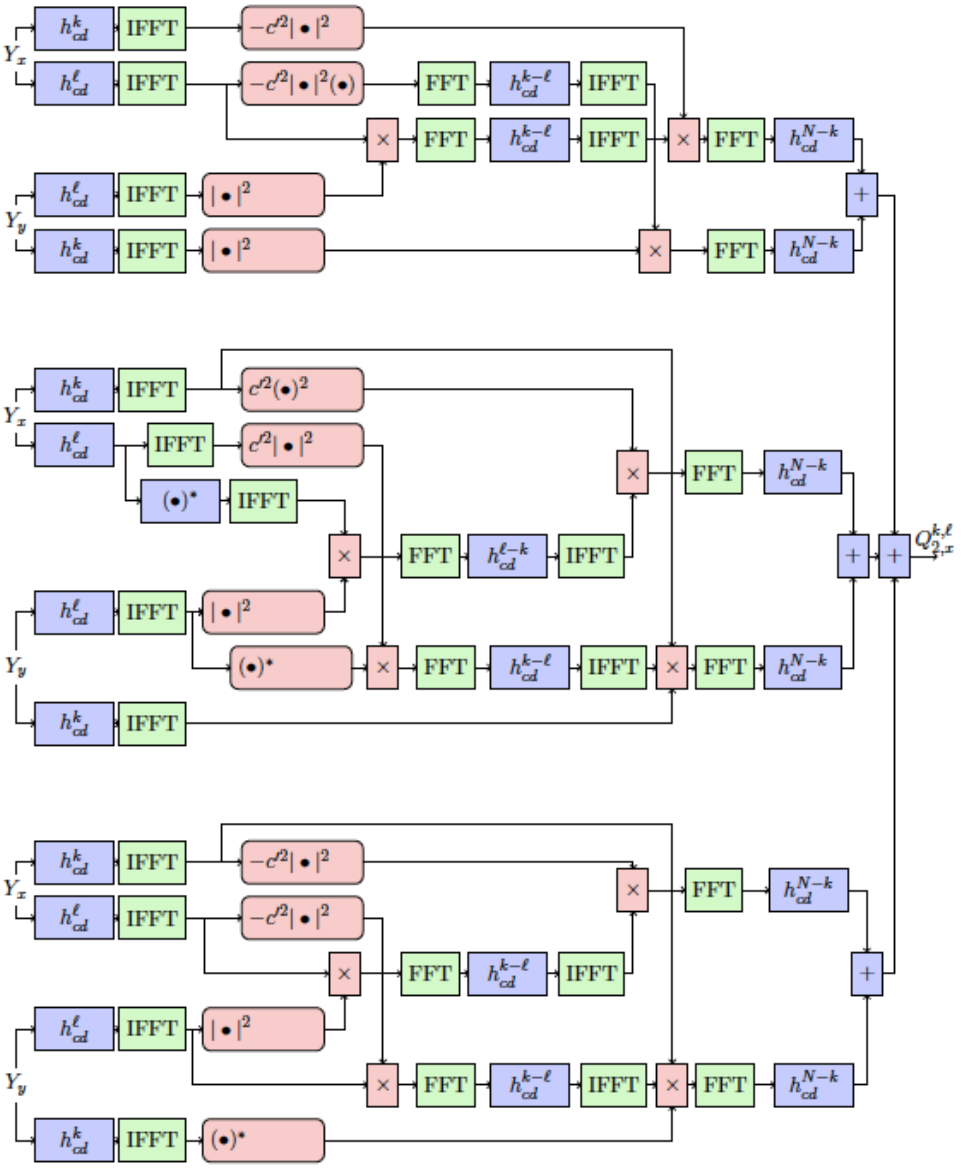

Figure B.13: Schéma d'implémentation du terme $Q_{2,x}^{(k,\ell)}(\omega)$

La sortie du VNLE de cinquième ordre Z est donc la somme de trois termes: le terme linéaire Z_1, le terme nonlinéaire de troisième ordre Z_3 et le terme calculé Z_5. Ces trois termes sont implémentés en parallèle comme le montre la figure.B.15.

Dans la suite, une évaluation de performance de l'égaliseur nonlinéaire basé sur les séries de Volterra de cinquième ordre est présentée.

B.3.2 Simulations et résultats

On évalue les performances de l'égaliseur nonlinéaire basé sur les séries de Volterra de cinquième ordre en comparaison avec celui basé sur les séries de Volterra de troisième ordre

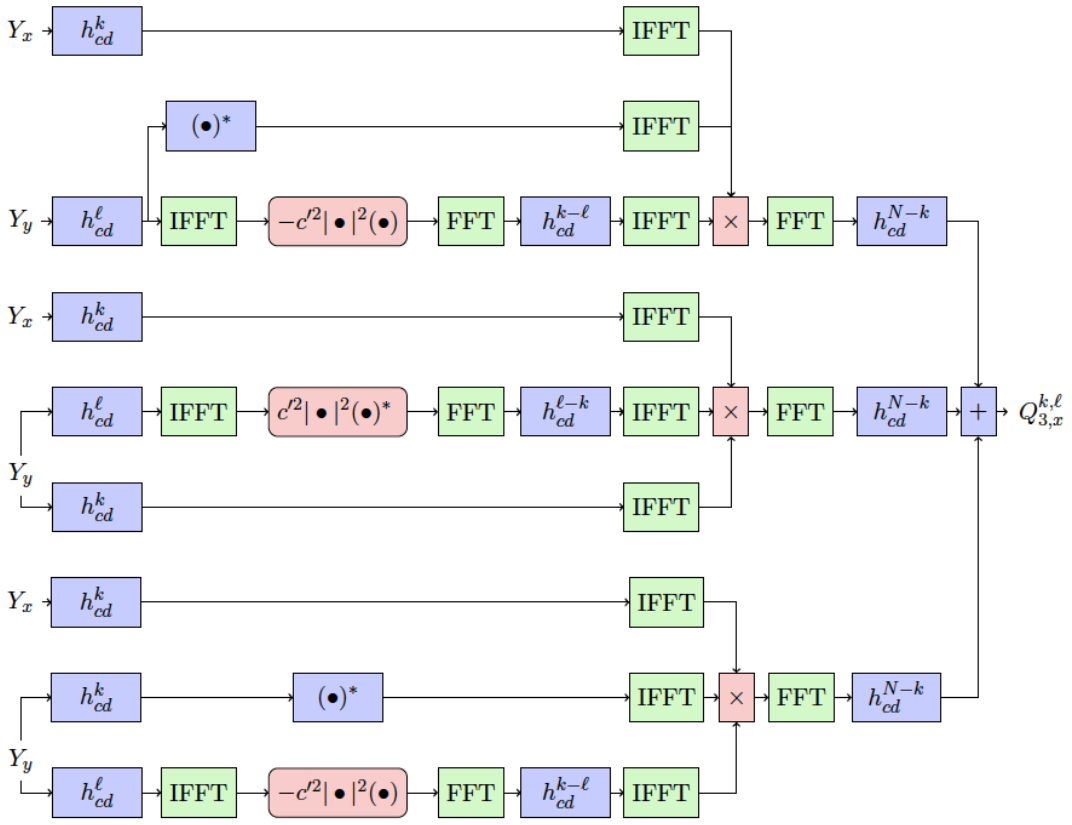

Figure B.14: Schéma d'implémentation du terme $Q_{3,x}^{(k,\ell)}(\omega)$

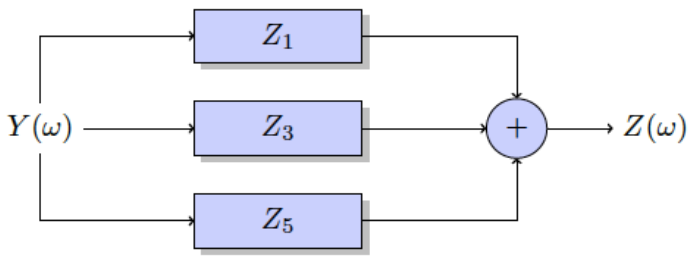

Figure B.15: Implémentation du VNLE de cinquième ordre

dans le contexte d'un système de transmission OFDM multi-bande. On utilise la configuration du projet européen SASER dont l'objectif est de transmettre un signal OFDM multi-bande à $400Gbps$ pour une transmission longue distance. Donc, on génère 4 sous-bandes OFDM ayant un largeur de bande $20GHz$ chacune et espacées par un intervalle de garde de $2GHz$. Chaque sous-bande est modulée en 16-QAM OFDM avec 512 sous-porteuses. Concernant les paramètres de la fibre optique mono-mode utilisée pour la transmission, le coefficient

d'atténuation est $\lambda = 0.2dB.km^1$, le paramètre de la dispersion est $D = 17ps.nm^{-1}.km^{-1}$ et le coefficient de la nonlinéarité est $\gamma = 0.0014m^{-1}.W^{-1}$. Un amplificateur EDFA, ayant un gain de $22dB$ et un facteur de bruit de $5.5dB$, est inséré après chaque $100km$ de distance.

La Fig.B.16 montre la variation du facteur Q en fonction de la puissance injectée par bande pour une transmission OFDM mono-polarisation et mono-bande. La distance de transmission est de 2000km. Le VNLE de cinquième ordre montre un gain de $2.2dB$ en comparaison avec le VNLE de troisième ordre. Cela montre que les effets nonlinéaires de cinquième ordre ont un effet non-negligéable et leur compensation se traduit en une augmentation très importante des performances de transmission. Un gain de $3dB$ en terme de la puissance injectée par sous-bande est aussi observée. Ce gain permet d'augmenter le nombre d'états de la modulation et par conséquent une augmentation du débit. D'autre part, le gain de VNLE de cinquième ordre et celui de troisième ordre sont de $1.4dB$ et $3.6dB$ respectivement par rapport à l'égalisation linéaire. Noter que l'égalisation linéaire correspond à la compensation de la dispersion chromatique.

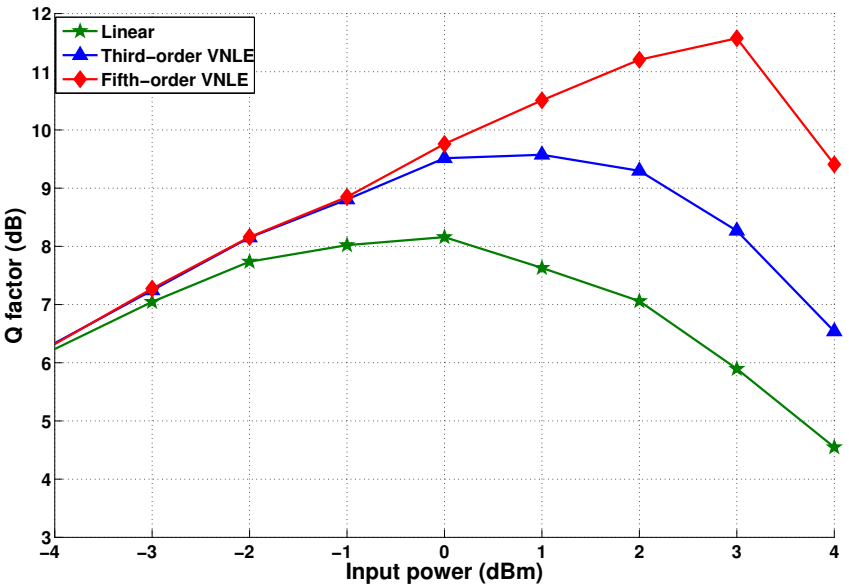

Figure B.16: Facteur Q vs. Puissance injectée pour une transmission mono-polarisation et mono-bande 16QAM OFDM (2000km)

La Fig.B.17 montre la variation de la puissance injectée par bande en fonction de la distance de transmission pour une transmission OFDM mono-polarisation et 4-bandes. A un taux d'erreur binaire BER $= 10^{-2}$ (Q $= 7.33$ dB) et un intervalle de garde de 10GHz , un gain de 100km en terme de la distance de transmission est observé en utilisant le VNLE de cinquième ordre au lieu de celui de troisième ordre.

La Fig.B.18 montre la variation du facteur Q en fonction de la puissance injectée par bande pour une transmission OFDM mono-polarisation et 4-bandes. La distance de transmission est de 2000km et l'intervalle de garde est de 2GHz. Dans ce cas, on observe une réduction du gain du VNLE de cinquième ordre en comparaison avec le VNLE de troisième ordre et aussi

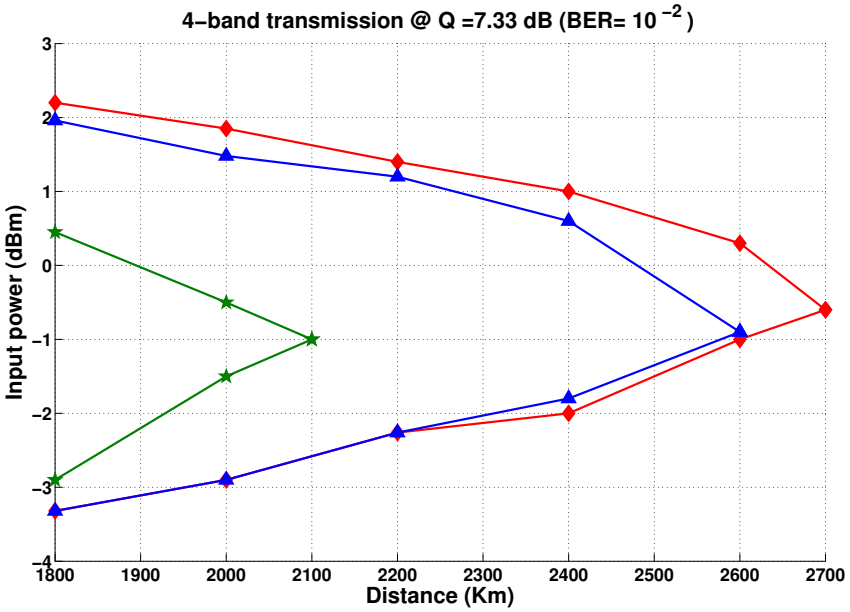

Figure B.17: Puissance injectée vs. distance de transmission pour une transmission mono-polarisation et 4-bandes 16QAM OFDM

une réduction de performance du VNLE de troisième ordre par rapport à l'égalisation linéaire. On constate aussi une réduction des performances des VNLE de troisième et cinquième ordre dans le cas d'une transmission OFDM double-polarisation et mono-bande comme le montre la Fig.B.19. Cela peut être expliqué par l'apparition des effets nonlinéaires inter-bandes comme l'XPolM, XPM and FWM. Ces effets deviennent plus importants dans le cas de transmission à débit élevé et à intervalle de garde réduit.

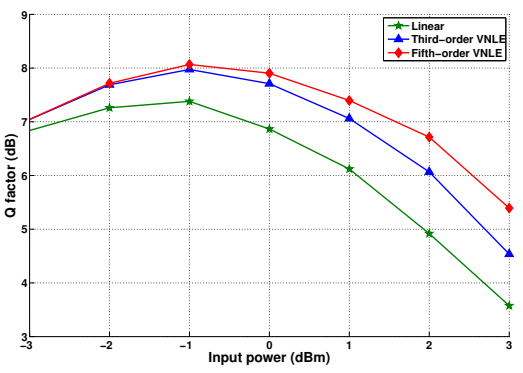

Figure B.18: Facteur Q vs. Puissance injectée pour une transmission mono-polarisation et 4-bandes 16QAM OFDM (2000km)

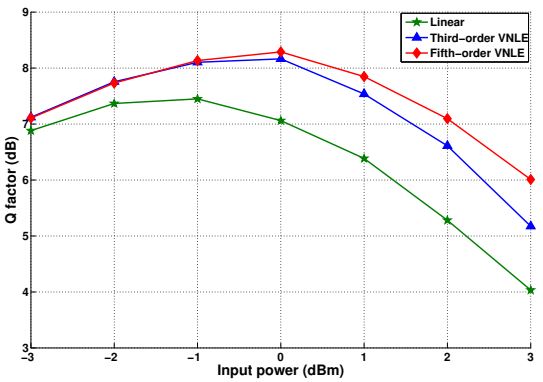

Figure B.19: Facteur Q vs. Puissance injectée pour une transmission double-polarisations et mono-bande 16QAM OFDM (2000km)

B.4 Annulation des interférences nonlinéaires

Dans cette partie, on commence d'abord par donner le principe de l'annulation des interférences nonlinéaires. Puis, on évalue les performances de cette approche dans le contexte des systèmes de transmission OFDM multi-bande et Nyquist WDM.

B.4.1 Principe de l'annulation des interférences nonlinéaires

L'annulateur des interférences nonlinéaires (INIC) utilise la structure de l'égaliseur à retour de décision [64] pour compenser les interférences nonlinéaires inter-bande/sous-porteuse. L'idée est d'exploiter les décisions précédentes des bandes/sous-porteuses adjacentes. Après la reconstruction des signaux de bandes/sous-porteuses adjacentes en utilisant un modèle de la fibre optique, ces signaux reconstruits sont soustraits du signal reçu de la bande/sous-porteuse considéré.

L'architecture du récepteur utilisant la technique d'annulation des interférences nonlinéaires est représentée dans la Figure. B.20. L'implémentation de l'annulateur des interférences nonlinéaires peut être divisée en trois étapes.

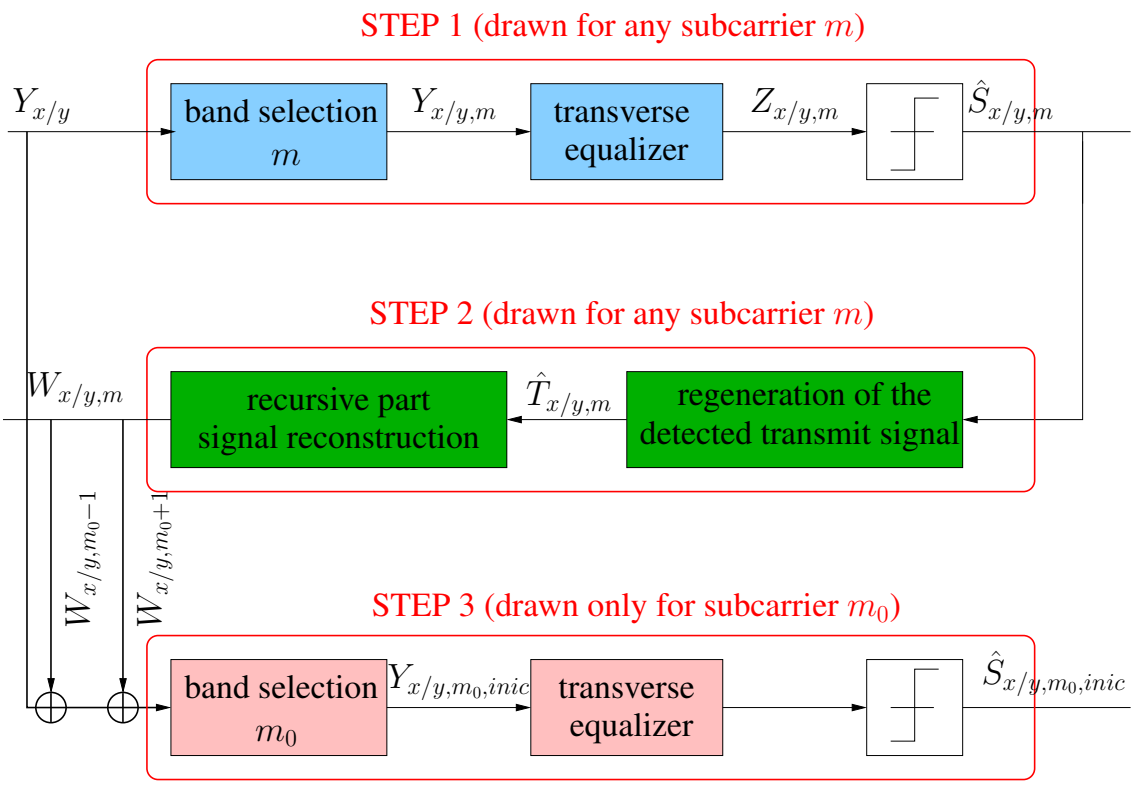

Figure B.20: INIC receiver structure

Pour la première étape, le signal reçu est passé à travers un filtre pour sélectionner la bande/sous-porteuse car le récepteur procède bande par bande. Un égaliseur nonlinéaire est

appliqué pour compenser les effets nonlinéaires intra-bande/sous-porteuse. L'INIC proposé est basé sur les séries de Volterra et donc l'égaliseur nonlinéaire consiste en un VNLE de troisième ordre. La sortie de cet égaliseur pour une bande/sous-porteuse m et une polarisation x ou y est donnée par:

$$\begin{aligned} Z_{x/y,m}(\omega) &= k_1(\omega)Y_{x/y,m}(\omega) \\ &+ \iint k_3(\omega_1,\omega_2,\omega-\omega_1+\omega_2)Y_{x/y,m}(\omega-\omega_1+\omega_2) \\ &\times [Y_{x,m}(\omega_1)Y^*_{x,m}(\omega_2)+Y_{y,m}(\omega_1)Y^*_{y,m}(\omega_2)]d\omega_1 d\omega_2 \end{aligned} \tag{B.12}$$

avec $Y_{x/y,m}$ est le signal reçu après le passage par le filtre de sélection de bande. k_1 et k_3 sont les noyaux inverses de Volterra de premier et troisième ordre respectivement. Puis, après la compensation des autres effets linéaires comme la PMD et le bruit de phase, la décision sur les symboles est effectuée.

Concernant la deuxième étape, les symboles détectés de chaque bande/sous-porteuse adjacente, sont d'abord re-modulés et par suite reconstruits en utilisant un modèle de la fibre optique. La sortie de ce modèle, qui est un modèle basé sur les séries de Volterra de troisième ordre, pour une bande/sous-porteuse m et une polarisation x ou y est donnée par:

$$\begin{aligned} W_{x/y,m}(\omega) &= h_1(\omega)\widehat{X}_{x/y,m}(\omega) \\ &+ \iint h_3(\omega_1,\omega_2,\omega-\omega_1+\omega_2)\widehat{X}_{x/y,m}(\omega-\omega_1+\omega_2) \\ &\times [\widehat{X}_{x,m}(\omega_1)\widehat{X}^*_{x,m}(\omega_2)+\widehat{X}_{y,m}(\omega_1)\widehat{X}^*_{y,m}(\omega_2)]d\omega_1 d\omega_2 \end{aligned} \tag{B.13}$$

avec $\widehat{X}_{x/y,m}$ est le signal re-modulé des symboles $\widehat{S}_{x/y,m}$ de la bande/sous-porteuse m. h_1 et h_3 sont les noyaux de Volterra de premier et troisième ordre respectivement.

Pour la troisième étape, on considère m_0 comme la bande/sous-porteuse pour laquelle on va compenser les interférences nonlinéaires. Dans ce cas, on soustrait les signaux reconstruits des bandes adjacentes m_0-1 et m_0+1 du signal reçu $Y_{x/y}$:

$$Y_{m_0,inic}(\omega) = Y(\omega) - W_{m_0-1}(\omega) - W_{m_0+1}(\omega). \tag{B.14}$$

Finalement, la décision finale sur les symboles est effectuée après le passage du signal $Y_{m_0,inic}$ par un filtre de sélection de bande et un VNLE de troisième ordre pour compenser les effets nonlinéaires intra-bande/sous-porteuse.

On note cette technique INIC(3,3) puisque elle utilise un VNLE de troisième ordre pour l'égalisation et un modèle basé sur les séries de Volterra de troisième ordre pour modéliser la fibre dans la partie récursive. L'INIC(3,3) compense les interférences linéaires et nonlinéaires. Pour évaluer les performances de l'INIC(3,3) et surtout pour évaluer les effets des interférences nonlinéaires, on introduit aussi deux autres approches l'INIC(3,1) et l'INIC(1,1).

L'INIC(3,1) utilise un égaliseur VNLE de troisième ordre pour compenser les effets nonlinéaires intra-bande/sous-porteuse. La sortie de cet égaliseur est donnée par l'équation. B.12.

Cependant, cette technique utilise un modèle linéaire de la fibre, et par conséquent elle considère uniquement les interférences linéaires. Donc, l'équation.B.13 devient:

$$W_{x/y,m}(\omega) = h_1(\omega)\widehat{X}_{x/y,m}(\omega). \tag{B.15}$$

L'INIC(1,1) est une approche qui ne considère que les effets linéaires. Donc, un égaliseur linéaire est utilisé dans la partie transverse donnée par:

$$Z_{x/y,m}(\omega) = k_1(\omega)Y_{x/y,m}(\omega). \tag{B.16}$$

Concernant la partie récursive, un modèle linéaire est aussi utilisé, donné par equation. B.15.

B.4.2 Simulations et résultats

B.4.2-a OFDM multi-bande

Pour évaluer les performances de l'annulateur des interférences nonlinéaires basé sur les séries de Volterra de troisième ordre INIC(3,3) dans le contexte de système OFDM multi-bande, on utilise la configuration du projet européen SASER dont l'objectif est de transmettre un signal OFDM multi-bande à $400Gbps$ pour une transmission longue distance. On garde la même configuration de la sectionB.3.2.

La distance de transmission est fixée à 800km. Concernant les résultats, on se concentre sur les bandes centrales puisque elles sont les plus affectées par les interférence nonlinéaires inter-bandes.

La Fig.B.21 montre le facteur Q en fonction de la puissance injectée par bande pour une transmission OFDM mono-polarisation et 4-bandes. Dans ce cas, le débit binaire est de 200Gbps. On constate que l'INIC(3,3) présente un gain de $0.9dB$ en comparaison avec le VNLE. Une augmentation de la puissance injectée de $1dB$ est aussi observée en utilisant l'INIC(3,3) au lieu du VNLE. Cette augmentation peut permettre l'utilisation d'une modulation multi-états plus élevée.

La Fig.B.22 montre la variation du facteur Q en fonction de la puissance injectée par bande pour une transmission OFDM double-polarisations et 4-bandes. Dans ce cas, le gain en facteur Q de l'INIC(3,3) en comparaison avec le VNLE est de $0.4dB$. Cette réduction du gain, par rapport au cas de transmission mono-polarisation, peut être expliqué par l'apparition des effets nonlinéaires inter-polarisations (XPolM). D'autre part les performances du VNLE sont très proches de celles de l'égalisation linéaire, qui compense uniquement la dispersion chromatique. Cela peut être expliqué par l'existence des interférences nonlinéaires qui réduisent significativement les performances de transmission.

B.4.2-b Nyquist WDM

On évalue aussi les performances de l'annulateur des interférences nonlinéaires dans le contexte de transmission Nyquist WDM. On génère 4 sous-porteuse WDM ayant une largeur de

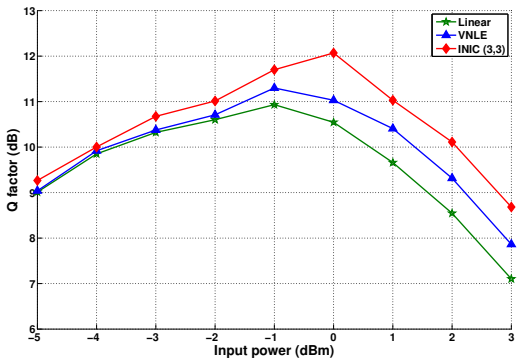

Figure B.21: Facteur Q vs. Puissance injectée pour une transmission mono-polarisation et 4-bandes 16QAM OFDM

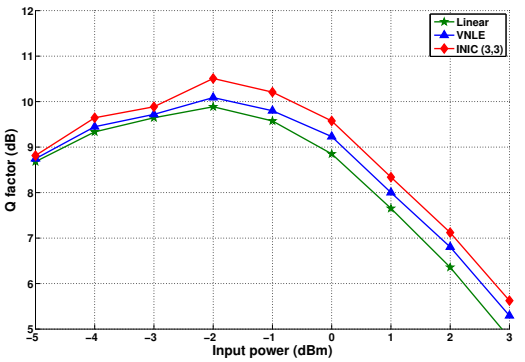

Figure B.22: Facteur Q vs. Puissance injectée pour une transmission double-polarisations et 4-bandes 16QAM OFDM

bande $R = 14GHz$ chacune. Chaque sous-porteuse optique est modulée en 16-QAM et le débit total est de 448Gbps. Concernant les paramètres de la fibre optique mono-mode utilisée pour la transmission, le coefficient d'atténuation est $\lambda = 0.2dB.km^1$, le paramètre de la dispersion est $D = 17ps.nm^{-1}.km^{-1}$ et le coefficient de la nonlinéarité est $\gamma = 0.0014m^{-1}.W^{-1}$. Un amplificateur EDFA, ayant un gain de $22dB$ et un facteur de bruit de $5.5dB$, est inséré après chaque $100km$ de distance.

Les paramètres à varier pour les simulations sont: le facteur de retombée (Roll-off) de filtre en racine de cosinus surélevé ρ, la distance de transmission, la puissance injectée par sous-porteuse optique et le facteur d'espacement de sous-porteuses δ. Ce dernier correspond au rapport de l'espacement de sous-porteuse par le débit symbole R. Pour les résultats, on se concentre sur les bandes centrales puisque elles sont les plus affectées par les interférences nonliniéares inter-bandes.

Dans la première partie de simulation, on fixe le facteur de retombée du filtre $\rho = 0.1$. Fig.B.23 montre la variation du facteur Q en fonction de la puissance injectée par sous-bande pour une transmission Nyquist WDM double-polarisations et 4-bandes. La distance de transmission est de 1000km et le facteur d'espacement de sous-porteuses $\delta = 1$. On observe que le DBP et le VNLE présentent des performances similaires à celles de l'égalisation linéaire à cause des interférences linéaires et nonlinéaires élevées. D'autre part, L'INIC(3,3), qui tient en compte les interférences nonlinéaires, montre un gain de $0.3dB$, $0.6dB$ et $1.5dB$ en comparaison avec l'INIC(3,1), l'INIC(1,1) et le DBP respectivement.

Fig.B.24 montre la variation du facteur Q en fonction du facteur d'espacement de sous-porteuses δ pour une distance de transmission de 1000km. Dans le cas d'une transmission super-Nyquist ($\delta < 1$), On constate que l'INIC(3,3), l'INIC(3,1) et l'INIC(1,1) sont beaucoup plus performants que les techniques de compensation nonlinéaires classiques DBP et VNLE. Par example, à $\delta = 0.95$, l'INIC(3,3) offre un gain de $2dB$ en comparaison avec le DBP and VNLE. Cela peut être expliqué par la présence des interférences très élevées. A cette même valeur du facteur d'espacement de sous-porteuses, l'INIC(3,3) présente un gain de $0.5dB$ en comparaison

avec l'INIC(3,1) qui ne prend pas en compte les interférences nonlinéaires. Cela montre que les interférences nonlinéaires sont importantes dans cette configuration. Cependant, lorsque $\delta = 1.1$, les interférences sont très faibles et donc les INICs donnent des résultats similaires à ceux des techniques classiques.

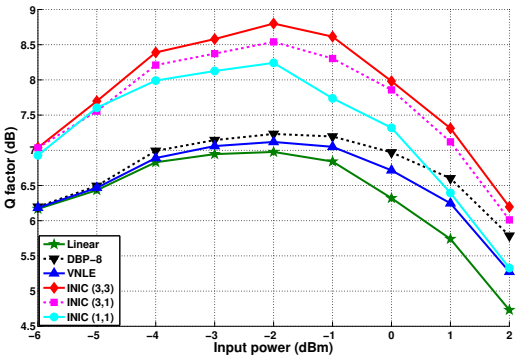

Figure B.23: Facteur Q vs. la puissance injectée ($\rho = 0.1$, $\delta = 1$)

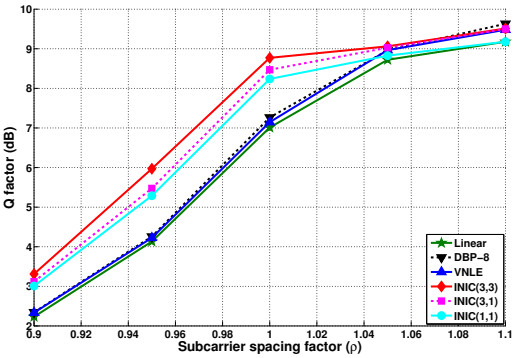

Figure B.24: Facteur Q vs. facteur d'espacement de sous-porteuses δ ($\rho = 0.1$)

La Fig.B.25 montre la variation de la puissance injectée par sous-porteuse en fonction de la distance de transmission pour un facteur d'espacement de sous-porteuses $\delta = 1$. L'INIC(3,3) présente un gain de 500km en distance en comparaison avec le DBP, le VNLE et l'INIC(1,1). Le gain de l'INIC(3,3) en comparaison avec l'INIC(3,1) est inférieure à 100km.

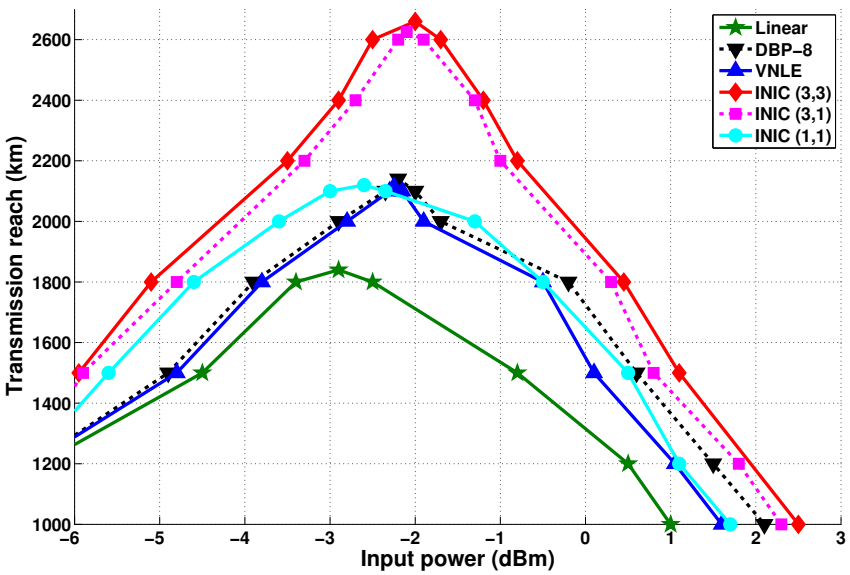

Figure B.25: Distance de transmission vs. la puissance injectée ($\rho = 0.1$)

Dans la deuxième partie de simulation, on réduit la valeur du facteur de retombée du filtre à $\rho = 0.01$ pour avoir un spectre plus rectangulaire. Fig.B.26 montre la variation du facteur Q en fonction de la puissance injectée par sous-bande pour une transmission double-polarisations et 4-bandes. La distance de transmission est de 1000km. On se met dans une

configuration super-Nyquist WDM avec un facteur d'espacement de sous-porteuses $\delta = 0.95$. Dans ce contexte, l'INIC(3,3) présente un gain de $0.5dB$ par rapport à l'INIC(3,1). La seule différence entre ces deux approches est la considération des interférences nonlinéaires. Ce qui montre que l'effet de ce type d'interférence est important dans cette configuration. D'autre part, les performances du DBP et du VNLE sont très proches de l'égalisation linéaire puisque ces deux techniques ne combattent pas les effets des interférences linéaires et nonlinéaires.

Fig.B.27 montre la variation du facteur Q en fonction du facteur d'espacement de sous-porteuses δ pour une distance de transmission de 1000km. Dans le cas d'une transmission super-Nyquist ($\delta < 1$), on constate que l'INIC(3,3), l'INIC(3,1) et l'INIC(1,1) sont beaucoup plus performants que le DBP et le VNLE. Cependant, dans les cas où les interférences sont très faibles ($\delta > 1$), des performances similaires sont observées.

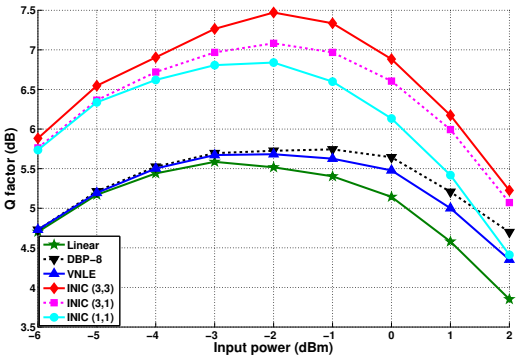

Figure B.26: facteur Q vs. la puissance injectée ($\rho = 0.1$, $\delta = 1$)

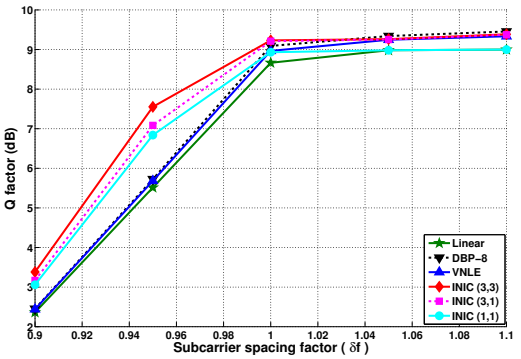

Figure B.27: facteur Q vs. facteur d'espacement de sous-porteuses δ ($\rho = 0.1$)

B.5 Conclusion et perspectives

B.5.1 Conclusion

Le travail effectué durant cette thèse consiste à compenser numériquement les effets non-linéaires de la fibre optique dans le contexte de systèmes de transmission à 400Gbps. On a proposé deux nouvelles méthodes pour combattre les effets nonlinéaires et on a évalué leurs performances dans les systèmes de transmission OFDM multi-bande et Nyquist WDM.

La première approche, nommée égaliseur nonlinéaire basé sur les séries de Volterra de cinquième ordre, consiste à compenser les effets nonlinéaires intra-bande. On a commencé par dériver mathématiquement le noyau de Volterra d'ordre cinq. Puis, on a proposé un schéma d'implémentation de cet égaliseur. L'évaluation des performance du VNLE de cinquième ordre a été fait dans le contexte de système OFDM multi-bande. Le VNLE de cinquième ordre a significativement amélioré les performances dans le cas de transmission OFDM mono-bande. En passant à une configuration multi-bande, une réduction de performance a été observée à cause des interférences inter-bandes.

Pour combattre les interférences inter-bandes, on a proposé une nouvelle méthode appelée annulateur des interférences nonlinéaires basé sur les séries de Volterra. Le principe de cette technique est basé sur l'égaliseur à retour de décision. L'annulateur des interférences nonlinéaires a significativement amélioré les performances dans le contexte de transmission OFDM multi-bande, Nyquist WDM et super-Nyquist WDM.

B.5.2 Perspectives

Comme perspectives du travail réalisé durant cette thèse, des autres études peuvent être réalisé en se basant sur les deux techniques proposées.

Pour améliorer les performances de l'égaliseur nonlinéaire basé sur les séries de Volterra de cinquième ordre, un passage à l'ordre cinq au niveau du modèle de la fibre basé sur les séries de Volterra peut être faire. Cependant, cela va rendre la technique beaucoup plus complexe.

En ce qui concerne l'annulateur des interférences nonlinéaires, une extension de cette approche pour combattre les effets nonlinéaires intra-bande/sous-porteuse peut être réalisée. La contrainte majeure de cette extension est l'existence des interférences causées par le symbole courant et les symboles pré-curseurs.

BIBLIOGRAPHY

[1] "Cisco visual networking index: Forecast and methodology, 2014–2019," *White paper*, 2015.

[2] G. P. Agrawal, *Fiber-Optic Communication systems*. John Wiley and Sons Inc, third edition ed., 2002.

[3] W. E. Shirbeeny, M. H. Aly, A. E. El-Samahy, and K. M. Emad, "Temperature dependence of zero dispersion wavelength in single-mode optical fibers for different materials," *International Journal of Pure and Applied Physics*, vol. 3, no. 1, pp. 122—-131, 2007.

[4] J. Tusuchiya and I. Hayakayama *J. Tusuchiya and I. Hayakayama, in Topical Meeting Optical Fiber Transmission II, Williamsburg, VA, 1977, PD1-1*.

[5] M.-J. Li and D. A. Nolan, "Optical transmission fiber design evolution," *Journal of Lightwave Technology*, vol. 26, no. 9, 2008.

[6] A. H. Gnauck, R. W. Tkach, A. R. Chraplyvy, and T. Li, "High-capacity optical transmission systems," *Journal of Lightwave Technology*, vol. 26, pp. 1032–1045, May 1 2008.

[7] R. J. Essiambre and R. W. Tkach, "Capacity trends and limits of optical communication networks," *Proceedings of the IEEE*, vol. 100, pp. 1035–1055, May 5 2012.

[8] M. A. Newhouse, L. J. Button, D. Q. Chowdhury, Y. Liu, and V. L. D. Silva, "Optical amplifiers and fibers for multiwavelength systems," *Proc. Lasers and Electro-Optics Soc. Annu. Meeting*, vol. 2, pp. 44–45, Feb 1995.

[9] A. J. Antos and D. K. Smith, "Design and characterization of dispersion compensating fiber based on the lp01 mode," *Journal of Lightwave Technology*, vol. 12, pp. 1739–1745, Oct 1994.

[10] K. Azadet and M. Yu, "Forward error correction (fec) techniques for optical communications," *IEEE 802.3 High-Speed Study Group Plenary meeting*, Jul 1999.

[11] V. Kamalov, B. Koley, X. Zhao, and C. F. Lam, "Field verification of 40 g qpsk upgrade in a legacy 10 g networks," 2010.

[12] O. E. DeLange, "Wide-band optical communication systems: Part ii—frequency-division multiplexing," *Proceedings of the IEEE*, vol. 58, no. 10, pp. 1683 – 1690, 1970.

[13] K. Kikuchi, "Fundamentals of coherent optical fiber communications," *Journal of Lightwave Technology*, vol. 34, Feb 2016.

[14] S. Gorshe, "A tutorial on itu-t g.709 optical transport networks (otn)," *Optical Transport Networks Technology*, 2010.

[15] E.Pincemin, M. Song, J. Karaki, O. Zia-Chahabi, T. Guillossou, D. Grot, G. Thouenon, C. Betoule, R. Clavier, A. Poudoulec, M. V. der Keur, Y. Jaouen, R. L. Bidan, T. L. Gall, P. Gravey, M. Morvan, B. Dumas-Feris, M. L. Moulinard, and G. Froc, "Multi-band ofdm transmission at 100 gbps with sub-band optical switching," *Journal of Lightwave Technology*, vol. 32, pp. 2202–2219, Jun 2014.

[16] G. P. Agrawal, *Nonlinear Fiber Optics*. Academic Press, third edition ed., 2001.

[17] R. Freund, C. Bunge, N. Ledentsov, D. Molin, and C. Caspar, "High-speed transmission in multimode fibers," *Journal of Lightwave Technology*, vol. 28, no. 4, 2010.

[18] G. Bosco, V. Curri, A. Carena, P. Poggiolini, and F. Forghieri, "On the performance of nyquist-wdm terabit superchannels based on pm-bpsk pm-qpsk pm-8qam or pm-16qam subcarriers," *Journal of Lightwave Technology*, vol. 29, pp. 53–61, Jan 2011.

[19] J. Aspnes and E. Ruppert, "Capacity limits of optical fiber networks," *Journal of Lightwave Technology*, vol. 24, pp. 662–701, 2010.

[20] L. Grüner-Nielsen, M. Wandel, P. Kristensen, C. Jorgensen, L. V. Jorgensen, B. Edvold, B. Pálsdóttir, and D. Jakobsen, "Dispersion-compensating fibers," *Journal of Lightwave Technology*, vol. 23, no. 11, 2005.

[21] A. O. D. Forno, A. Paradisi, R. Passy, and J. P. von der Weid, "Experimental and theoretical modeling of polarization-mode dispersion in single-mode fibers," *IEEE Photonics Technology Letters*, vol. 12, no. 3, 2000.

[22] S. J. Savory, "Digital filters for coherent optical receivers," *Optics Express*, vol. 16, no. 2, pp. 804—-817, 2008.

[23] F. corporation, "Introduction to edfa technology," Jun 2009.

[24] A. Abu-aisheh and S. Moslehpour, "Pre-amp edfa ase noise minimization for optical receiver transmission performance optimization," *Optics Communications*, pp. 2603—-2606, 2010.

[25] E. Desurvire, "Modeling erbium-doped fiber amplifiers," *Journal of Lightwave Technology*, vol. 9, pp. 271–283, Feb 1991.

[26] P. Poggiolini, “The gn model of nonlinear propagation in uncompensated coherent optical systems,” *Journal of Lightwave Technology*, vol. 30, no. 24, pp. 3857—-3877, 2012.

[27] S. P. Singh and N. Singh, “Cross-polarization modulation in polarization division multiplex transmission,” *Progress In Electromagnetics Research*, pp. 249—-275, 2007.

[28] M. Winter, D.Setti, and K. Petermann, “Cross-polarization modulation in polarization division multiplex transmission,” *IEEE Photonics Technology Letters*, vol. 22, no. 8, 2010.

[29] M. Winter, D. Kroushkov, and K. Petermann, “Polarization-multiplexed transmission system outage due to nonlinearity-induced depolarization,” 2010.

[30] P. J. Winzer, “High-spectral-efficiency optical modulation formats,” *Journal of Lightwave Technology*, vol. 30, no. 24, 2012.

[31] G.-W. Lu, T. Sakamoto, A. Chiba, T. Kawanishi, T. Miyazaki, K. Higuma, M. Sudo, and J. Ichikawa3, “Reconfigurable multilevel transmitter using monolithically integrated quad mach-zehnder iq modulator for optical 16-qam and 8-psk generation,” *Optics Express*, vol. 19, no. 6, 2011.

[32] S. Yan, X. Weng, Y. Gao, C. Lu, A. P. T. Lau, Y. Ji, L. Liu, and X. Xu, “Generation of square or hexagonal 16-qam signals using a dual-drive iq modulator driven by binary signals,” *Optics Express*, vol. 20, no. 27, 2012.

[33] W. Shieh, H. Bao, and Y. Tang, “Coherent optical ofdm: theory and design,” *Optics Express*, vol. 16, no. 2, 2008.

[34] W. Shieh and I. Djordjevic, *OFDM for Optical Communications*. Academic Press, 2010.

[35] E. Awwad, *Emerging space-time coding techniques for optical fiber transmission systems*. PhD thesis, Telecom ParisTech, 2015.

[36] M. Song, E. Pincemin, Y. Jaouen, and P. Ciblat, “Dimensioning of the 400gbps coherent multi-band ofdm transmitter/reciver,” *Deliverable 1.2.1. SASER-SIEGFRIED*, 2013.

[37] W. Shieh, X. Yi, Y. Ma, and Y. Tang, “Theoretical and experimental study on pmd-supported transmission using polarization diversity in coherent optical ofdm systems,” *Optics Express*, vol. 15, no. 16, 2007.

[38] M. Speth, S. Fechtel, G. Fock, and H. Meyr, “Optimum receiver design for wireless broadband systems using ofdm,” *Communications, IEEE Transactions*, vol. 47, no. 11, 1999.

[39] T. Schmidl and D. Cox, “Robust frequency and timing synchronization for ofdm,” *Communications IEEE Transactions*, vol. 45, no. 12, 1997.

[40] K. Shi and E. Serpedin, "Coarse frame and carrier synchronization of ofdm systems: a new metric and comparison," *Wireless Communications IEEE Transactions*, vol. 3, no. 4, 2004.

[41] S. L. Jansen, I. Morita, T. C. Schenk, and H. Tanaka, "Long-haul transmission of 16x52.5 gbits/s polarization-division- multiplexed ofdm enabled by mimo processing," *Journal of Optical Networking*, vol. 7, no. 2, 2008.

[42] X. Yi, W. Shieh, and Y. Ma, "Phase noise effects on high spectral efficiency coherent optical ofdm transmission," *Journal of Lightwave Technology*, vol. 26, no. 10, 2008.

[43] S. L. Jansen, I. Morita, T. C. W. Schenk, N. Takeda, and H. Tanaka, "Coherent optical 25.8-gb/s ofdm transmission over 4160-km ssmf," *Journal of Lightwave Technology*, vol. 26, no. 1, 2008.

[44] S. Kilmurray, T. Fehenberger, P. Bayvel, and R. I. Killey, "Comparison of the nonlinear transmission performance of quasi-nyquist wdm and reduced guard interval ofdm," *Journal of Lightwave Technology*, vol. 20, pp. 4198–4205, Feb 2012.

[45] Y. Jianjun, Z. Junwen, D. Ze, J. Zhensheng, C. Hung-Chang, C. Yi, X. Xin, and L. Xinying, "Transmission of 8 × 480-gb/s super-nyquist-filtering 9-qam-like signal at 100 ghz-grid over 5000-km smf-28 and twenty-five 100 ghz-grid roadms," *Optics Express*, vol. 21, no. 13, pp. 15686–15691, 2013.

[46] D. Godard, "Self-recovering equalization and carrier tracking in two-dimensional data communication systems," *Communications, IEEE Transactions*, vol. 28, pp. 1867—-1875,, 1980.

[47] H. Louchet, K. Kuzmin, and A. Richter, "Improved dsp algorithms for coherent 16-qam transmission," *ECOC*, vol. 2, pp. 57—58, Sep 2008.

[48] X. Xu, B. Châtelain, and D. V. Plant, "Decision directed least radius distance algorithm for blind equalization in a dual-polarization 16-qam system," *OFC*, pp. 1 – 3, Mars 2012.

[49] D.-S. Ly-Gagnon, S. Tsukamoto, K. Katoh, and K. Kikuchi, "Coherent detection of optical quadrature phase-shift keying signals with carrier phase estimation," *Journal of Lightwave Technology*, vol. 24, pp. 12—-21, Jan 2006.

[50] Y. Wang, E. Serpedin, and P. Ciblat, "Optimal blind nonlinear least-squares carrier phase and frequency offset estimation for burst qam modulations," *Asilomar*, vol. 2, pp. 1499 —-1503, 2001.

[51] D. Rafique, "Fiber nonlinearity compensation: commercial applications and complexity analysis," *Journal of Lightwave Technology*, vol. 34, no. 2, pp. 544—-552, 2016.

[52] S. L. Jansen, D. van den Borne, B. Spinnler, S. Calabrò, H. Suche, P. M. Krummrich, G.-D. K. W. Sohler, and H. de Waardt, "Optical phase conjugation for ultra long-haul phase-shift-keyed transmission," *Journal of Lightwave Technology*, vol. 24, pp. 54—-64, Jan 2006.

[53] E. Ip and J. M. Kahn, "Compensation of dispersion and nonlinear impairments using digital back propagation," *Journal of Lightwave Technology*, vol. 26, no. 20, pp. 3416 – 3425, 2008.

[54] D. Rafique, M. Mussolin, M. Forzati, J. Mårtensson, M. N. Chugtai, and A. D. Ellis, "Compensation of intra-channel nonlinear fibre impairments using simplified digital back-propagation algorithm," *Optics Express*, vol. 19, no. 10, pp. 9453–9460, 2011.

[55] D. Rafique, M. Mussolin, M. Forzati, J. Mårtensson, M. N. Chugtai, and A. D. Ellis, "Modified split-step fourier method for compensation of nonlinear fibre impairments," *ITCON*, 2011.

[56] K. V. Peddanarappagari and M. Brandt-Pearce, "Volterra series transfer function of single-mode fibers," *Journal of Lightwave Technology*, vol. 15, no. 12, pp. 2232—-2241, 1997.

[57] M. Schetzen, "Theory of pth-order inverse of nonlinear systems," *Trans. Circuits Syst*, vol. 23, no. 5, pp. 285—-291, 1976.

[58] M. Schetzen, *The volterra and Wiener theories of nonlinear systems*. Krieger Publishing Company, 2006.

[59] L. Lui, L. Li, Y. Huang, K. Cui, Q. Xiong, F. N. Hauske, C. Xie, and Y. Cai, "Intrachannel nonlinearity compensation by inverse volterra series transfer function," *Journal of Lightwave Technology*, vol. 30, no. 3, pp. 310–316, 2012.

[60] J. D. Reis and A. L. Teixeira, "Unveiling nonlinear effects in dense coherent optical wdm systems with volterra series," *Optics Express*, vol. 18, no. 8, pp. 8660—-8670, 2010.

[61] Z. Pan, B. Châtelain, M. Chagnon, and D. V. Plant, "Volterra filtering for nonlinearity impairment mitigation in dp-16qam and dp-qpsk fiber optic communication systems," *OFC*, 2011.

[62] S. B. Amado, F. P. Guiomar, N. J. Muga, J. D. Reis, S. M. Rossi, A. Chiuchiarelli, J. R. F. Oliveira, A. L. Teixeira, and A. N. Pinto, "Experimental demonstration of the parallel split-step method in ultra-long-haul 400g transmission," *ECOC*, 2015.

[63] J. Tsimbinos, *Identification and compensation of nonlinear distortion*. PhD thesis, University of South Australia, Feb. 1995.

[64] D. D. Falconer, "Adaptive equalization of channel nonlinearities in qam data transmission systems," *Bell System Technical Journal*, vol. 57, no. 7, 1978.

[65] K. Shibahara, A. Masuda, S. Kawai, and M. Fukutoku, "Multi-stage successive interference cancellation for spectrally-efficient super-nyquist transmission," *ECOC*, 2015.

Nonlinear effects compensation for long-haul superchannel transmission system

Abdlkerim AMARI

RESUME : Les systèmes de communications optiques jouent un role important pour satisfaire la demande incessante de trafics de données. Cette demande, induite par des applications gourmandes en termes de bande passante et débit, necéssite une augmentation de la capacité des réseaux optiques d'accès et par conséquent une augmentation des capacités de réseaux de transports métropolitains et longues distances. La prochaine génération de systèmes WDM longue distance devrait opérée à des débits de 400Gbps ou 1Tbps. Cette montée en débit s'appuiera sur des nouvelles formes d'ondes avancées de type mono-porteuse (Nyquist-WDM) ou multi-porteuse (OFDM multi-bande). Ces approches sont basées sur le multipléxage de plusieurs porteuses espacées par des intervalles de garde réduits. D'autre part, pour générer ces très haut débits, des modulations multi-états sont utilisées pour chaque porteuse grâce à leur efficacité spectrale élevée. Ces types de systèmes, qui combinent à la fois les approches multi-bande et les modulations multi-états, sont extremement vulnérables aux effets nonlinéaires de la fibre optique. En fait, les effets nonlinéaires sont dépendants de la puissance de transmission et inversement proportionels à l'intervalle de garde. Cela rend leur compensation indispensable pour maintenir des bonnes performances des systèmes en terme de distance de transmission. Grâce à l'emploi de récepteurs à détection cohérente, des techniques de traitement du signal numérique sont utlisées pour combattre les effets nonlinéaires.

Dans cette thèse, nous avons proposé des nouvelles techniques basées sur les séries de Volterra et les égaliseurs à retour de decision pour compenser respectivement les effets nonlinéaires intra-bande et les interférences nonlinéaires inter-bande.

MOTS-CLEFS : Transmission optique cohérent, 400Gbps/1Tbps, effets nonlinéaires, séries de Volterra, traitement numérique du signal, interférences nonlinéaires, transmissions longues distances

ABSTRACT : Optical communication systems have evolved since their deployment to meet the growing demand for high-speed communications. Over the past decades, the global demand for communication capacity has increased exponentially and the most of the growth has occurred in the last few years when data started dominating network traffic. In order to meet the increase of traffic demands fueled by the growth of internet services, an increase of access network capacity and consequently metro and long-haul network capacities is required. Next generation of long-haul WDM transmission systems is expected to operate at 400Gbps or 1Tbps bit rate. Superchannel approaches, such as Nyquist WDM and multi-band OFDM, allow both high spectral efficiency and small guard-band which makes them promising candidates to generate these high bit rates in combination with multi-level modulations formats. Such transmission systems are strongly disturbed by fiber nonlinear effects which increase with the data rate and the small guard band. Therefore, fiber nonlinearities compensation is required to get the desired performance in terms of transmission reach. DSP based approaches such as digital back propagation and third-order Volterra based nonlinear equalizer have been already proposed to deal with intra-channel or intra-band nonlinear effects.

In the context of superchannel systems, we have proposed two new compensation techniques to deal with fiber nonlinear effects. The first one, called fifth-order inverse Volterra based nonlinear equalizer, compensate for intra-band nonlinear effects. The second approach, which is the inter-band/subcarrier nonlinear interference canceler, is proposed to combat the nonlinear interference in superchannel systems.

KEY-WORDS : Optical fiber communications, Superchannel, MB-OFDM, Nyquist WDM, Volterra series, Nonlinear effects, Nonlinear interference, Digital signal processing

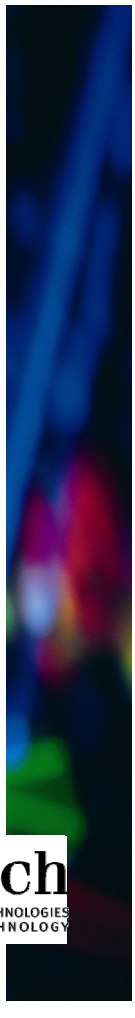

TELECOM ParisTech

EDiTE

ParisTech
INSTITUT DES SCIENCES ET TECHNOLOGIES
PARIS INSTITUTE OF TECHNOLOGY